DOKUZ EYLÜL UNIVERSITY
GRADUATE SCHOOL OF NATURAL AND APPLIED SCIENCES

MANUFACTURING AND TESTING OF DIRECT METHANOL FUEL CELLS BASED ON ALTERNATIVE MATERIALS

by
Mustafa ERÇELİK

July, 2017
İZMİR

MANUFACTURING AND TESTING OF DIRECT METHANOL FUEL CELLS BASED ON ALTERNATIVE MATERIALS

A Thesis Submitted to the
Graduate School of Natural and Applied Sciences of Dokuz Eylül University
In Partial Fulfillment of the Requirements for the Master of Science of
Department of Mechanical Engineering

by
Mustafa ERÇELİK

July, 2017
İZMİR

M.Sc THESIS EXAMINATION RESULT FORM

We have read the thesis entitled **"MANUFACTURING AND TESTING OF DIRECT METHANOL FUEL CELLS BASED ON ALTERNATIVE MATERIALS"** completed by **MUSTAFA ERÇELİK** under supervision of **ASSOC. PROF. DR. CAN ÖZGÜR ÇOLPAN** and we certify that in our opinion it is fully adequate, in scope and in quality, as a thesis for the degree of Master of Science.

Assoc. Prof. Dr. Can Özgür ÇOLPAN

Supervisor

Assoc. Prof. Dr. Yılser Devrim

(Jury Member)

Asst. Prof. Dr. Hadi Ganjehsarabi

(Jury Member)

Prof.Dr. Emine İlknur CÖCEN
Director
Graduate School of Natural and Applied Sciences

ACKNOWLEDGMENT

First and foremost, I gratefully thank my supervisor Assoc. Prof. Dr. Can Özgür ÇOLPAN for his endless support and patience. He contributed to my graduate school experience by giving me intellectual freedom in my studies, supporting my attendance at various conferences, and demanding a high quality of work in all my endeavors.

I would like to thank dear friend Mr. Adnan ÖZDEN, who contributed significantly to this thesis.

In addition, I wish to express my special thanks to Dr. David OUELLETTE, who is my friend and also my advisor, for his valuable contributions and supports in this study.

I would also like to express sincere thanks to Assoc. Prof. Dr. Yılser DEVRİM for her technical supports and review of this thesis. I would like to thank Prof. Aytunç EREK for reviewing my thesis. I would like to thank Prof. Dr. Erol ŞEKER for his technical supports. In addition, I thank Asst. Prof. Dr. Hadi GANJEHSARABI for his endless support.

Finally, I want to thank all faculty members of the Dokuz Eylül University Mechanical Engineering Department for their instructions during my graduate studies.

Mustafa ERÇELİK

MANUFACTURING AND TESTING OF DIRECT METHANOL FUEL CELLS BASED ON ALTERNATIVE MATERIALS

ABSTRACT

In this thesis, the performances and stabilities of Direct Methanol Fuel Cells (DMFCs) produced with alternative Membrane Electrode Assembly (MEA) materials are investigated through experimental methods. Furthermore, the operating conditions that yield the highest performance for DMFC are determined with single cell experiments. In these experiments, Nafion based composite membranes, which are Nafion/SiO2, Nafion/TiO2, and Nafion/ZrP, were prepared with recasting method. The structures of these composite membranes were investigated by Scanning Electron Microscopy (SEM), proton conductivity measurement, Thermogravimetric Analysis (TGA), X-ray Diffraction (XRD) and water uptake measurement. Performance testings of the DMFCs based on these composite membranes as well as commercial Nafion® 115 membrane were performed using a computer aided fuel cell test station for different values of cell temperature and methanol concentration. Apart from the membrane studies, the effect of introduction of titania (TiO2) material into Pt-Ru/C anode electrocatalyst and introduction of zirconium hydrogen phosphate (ZrP) material into Pt/C cathode electrocatalyst on the performance of DMFCs were investigated in different studies. TiO2 materials were first synthesized applying a sol-gel method and then incorporated directly into commercial Pt-Ru/C anode electrocatalyst with different TiO2 weight ratios to improve the performance of the DMFC. For comparison, the anode electrocatalysts with the same TiO2 weight ratios were also prepared using commercial TiO2 materials.

Keywords: Direct methanol fuel cell, membrane electrode assembly, Nafion/SiO2 composite membrane, Nafion/TiO2 composite membrane, Nafion/ZrP composite membrane, Pt-Ru/C-TiO2 anode electrocatalyst, Pt/C-ZrP cathode electrocatalyst, experimental.

ALTERNATİF MALZEMELERE DAYALI DOĞRUDAN METANOLLÜ YAKIT PİLİ ÜRETİMİ VE TEST EDİLMESİ

ÖZ

Bu tezde alternatif malzemeler kullanılarak üretilmiş olan Membran Elektrot Atacı (MEA) içeren Doğrudan Metanollü Yakıt Pillerinin (DMYP) performansları ve kararlılıkları incelenmiştir. Ayrıca tek hücre deneyleriyle DMYP için en iyi çalışma koşulları belirlenmiştir. Bu deneylerde kullanmak için Nafion bazlı Nafion/SiO2, Nafion/TiO2 ve Nafion/ZrP kompozit membranlar döküm yöntemiyle hazırlanmıştır. Bu kompozit membranların yapısı taramalı elektron mikroskobu (SEM), proton iletkenlik ölçümü, Termogravimetrik Analiz (TGA), X-ışını kırılım yöntemi (XRD) ve su tutma ölçümü ile incelenmiştir. Kompozit membran bazlı DMYP'ler ile ticari Nafion® 115 membran bazlı DMYP'ler farklı hücre sıcaklıklarında ve metanol derişimlerinde bilgisayar destekli yakıt pili test istasyonu kullanılarak performans testleri gerçekleştirilmiştir. Membran çalışmalarına ek olarak, Pt-Ru/C anot elektrokatalizörüne titanyum dioksit (TiO2) ve Pt/C katot elektrokatalizörüne zirkonyum hidrojen fosfat (ZrP) eklenmesinin DMYP performansına olan etkisi ayrı ayrı ele alınmıştır. TiO2 malzemesi öncelikle sol-gel metoduyla sentezlenmiştir ve direkt olarak ticari Pt-Ru/C anot elektrokatalizörüne farklı kütlesel oranlarda eklenerek DMYP performansını arttırmayı amaçlamaktadır. Karşılaştırmak amacıyla, aynı kütlesel oranlarda ticari TiO2 içeren anot elektrokatalizörleri hazırlanmıştır.

Anahtar kelimeler: Doğrudan metanollü yakıt pili, membran elektrot atacı, Nafion/SiO2 kompozit membran, Nafion/TiO2 kompozit membran, Nafion/ZrP kompozit membran, Pt-Ru/C-TiO2 anot elektrokatalizörü, Pt/C-ZrP katot elektrokatalizörü, deneysel.

CONTENTS

LIST OF FIGURES

Page

LIST OF TABLES

Page

CHAPTER ONE
INTRODUCTION

1.1 Introduction

Fuel cells are electrochemical devices that convert the chemical energy of the fuel to electrical energy directly. In the last years, fuel cell technology has received remarkable attention in many areas from small portable applications (e.g. mobile phones and laptops) to larger applications (e.g. vehicles and stationary power generation) (Beydaghi et al., 2015; Yuan et al., 2014; Zhang et al., 2006). Although Proton Exchange Membrane Fuel Cell (PEMFC) is one of the most popular fuel cell types, there are still some challenges, especially associated with the storage and delivery of the hydrogen. In this regard, Direct Methanol Fuel Cells (DMFCs) are seem more feasible for portable power applications due to their following advantages such as high energy density of methanol, easy storage as the methanol is in liquid form, and easier using and handling of methanol. However, low reaction kinetics at the anode, high cost of platinum electrocatalyst, low durability and stability, methanol crossover problem, poisoning of precious platinum electrocatalyst via carbon monoxide (CO) and the two-phase flow management are the main obstacles towards the commercialization of DMFCs. A various number of experimental and numerical studies, including re-designing the architecture of the Membrane Electrode Assembly (MEA) and its components and developing alternative materials and manufacturing techniques have been carried out to mitigate the negative effects of the above-mentioned problems as well as to achieve and improved DMFC performance (Liu et al., 2013; Chen et al., 2005; Hobson et al., 2002; Kamarudin & Hashim, 2012; Wei et al., 2002; Cui et al., 2015; Chu et al., 2014; Osmieri et al., 2017; Shu et al., 2016; Sebastián et al., 2016; Hu et al., 2015; Sebastián, Serov, Artyushkova, Atanassov, et al., 2016; Patel et al., 2005).

1.2 Motivation

As mentioned in Section 1.1, the performance of DMFCs can be increased by using alternative materials and optimizing operating conditions. Because of these reasons, this thesis is focused on the development of alternative MEA materials for DMFCs and the finding of the best operation conditions that yield the highest performance. The motivation of this thesis can be listed as follows;

- According to the findings of the literature survey, Nafion based composite membranes (e.g. Nafion/SiO_2 and Nafion/TiO_2) are very promising in terms of increasing the proton conductivity and mechanical stability at high temperatures. Therefore, the single cell performance of DMFCs with Nafion/SiO_2 and Nafion/TiO_2 composite membranes can be determined under various operating cell conditions.
- The literature survey discussed above indicates that introduction of TiO_2 materials into Pt-Ru/C anode electrocatalyst could be useful for achieving an improved DMFC performance.
- The literature survey discussed above demonstrates that Nafion/ZrP composite membranes may have a great potential for being used as a state-of-the-art material for DMFCs, notably at elevated operating temperatures (>80°C).

1.3 Objectives

The main aim of this thesis is to compare the performance of DMFCs based on alternative materials with those based on conventional materials. By this means, the materials that yield better DMFC performance and stability are identified. In order to achieve this goal, in addition to the performance tests, characterization studies of membranes, anode catalyst layers and cathode catalyst layers that are made of alternative materials were also carried out. The main objectives of this thesis are listed below;

- No works can be found related to the performance comparison of Nafion/SiO_2 and Nafion/TiO_2 composite membranes for DMFCs. For this reason, Nafion/SiO_2 and Nafion/TiO_2 composite membranes were synthesized by applying solvent casting method as to investigate the effect of usage of these membranes on the performance of DMFCs. In addition, the preparation and characterization of Nafion based nanocomposite membranes to improve the DMFC performance were reported.

- There is no work in the literature related to the performance comparison of DMFCs based on Pt-Ru/C-TiO_2 anode hybrid catalyst containing commercial and in-house synthesized TiO_2. In this thesis, a simple preparation procedure of a composite anode hybrid catalyst was carried out, and the performances of the DMFCs based on Pt-Ru/C-TiO_2 anode hybrid catalyst were investigated. Towards this direction, TiO_2 nanoparticles were synthesized by a sol-gel method and Pt-Ru/C-TiO_2 anode hybrid catalyst containing 5, 15, and 25 wt.% of in-house synthesized TiO_2 with respect to the amount of commercial Pt-Ru/C anode hybrid catalyst were prepared. Then, Pt-Ru/C-TiO_2 anode hybrid catalyst with the same weight ratios were also prepared using commercial TiO_2 materials.
- There is no significant study comparing the performance of DMFCs having Nafion/ZrP composite membranes (made of different ZrP weight ratios) with that of DMFCs having Nafion® membranes. In addition, to the best of knowledge, there is also no work related to the performance comparison of DMFCs having both Pt/C-ZrP cathode catalyst and Nafion/ZrP composite membrane with DMFC made of conventional materials.

1.4 Thesis Outline

The next chapter is devoted to the introduction of fuel cell technologies, especially Direct Methanol Fuel Cells (DMFCs). This chapter includes an overview of performance characterization of DMFCs, characterization of fuel cell materials, and literature review on the experimental studies for DMFCs.

The third chapter covers the methodology of the experimental studies which comprise the Nafion/TiO_2 and Nafion/SiO_2 composite membrane based DMFCs, Pt-Ru/C-TiO_2 anode catalyst based DMFCs, Nafion/ZrP composite membrane and Pt/C-ZrP cathode catalyst based DMFCs. In this section, firstly Nafion/TiO_2 and

Nafion/SiO_2 composite membrane preparation and characterization are mentioned. Here, MEA manufacturing process and performance testing method are also discussed. Secondly, preparation of in-house TiO_2 nanoparticles and membrane activation, MEA manufacturing process, and performance testing are examined, respectively. As the last step of the third chapter, Nafion/ZrP composite membrane preparation, characterization, MEA manufacturing and performance testing are given.

In the fourth chapter, the results of DMFCs produced and tested in the previous section are given and discussed in detail.

The fifth chapter includes conclusions related to the studies in this thesis.

CHAPTER TWO
BACKGROUND AND LITERATURE REVIEW

2.1 Fuel Cells

Fuel cells can be defined as electrochemical devices that convert the chemical energy of the fuel to electrical energy directly. The fuel and oxidant (oxygen or air) are fed to anode and cathode sides of the fuel cell, respectively. After the electrochemical reaction occurs in the anode and cathode catalyst layers of the fuel cell, the ions that are released are transported through the membrane to the other electrode. As a result of these electrochemical reactions, the electrons reach the load via an external circuit. The circulation of the electrons creates electrical power. Fuel cells are generally named according to the fuel and material used. Figure 2.1 shows the commonly used fuel cell types and their associated fuels, products and operating temperatures.

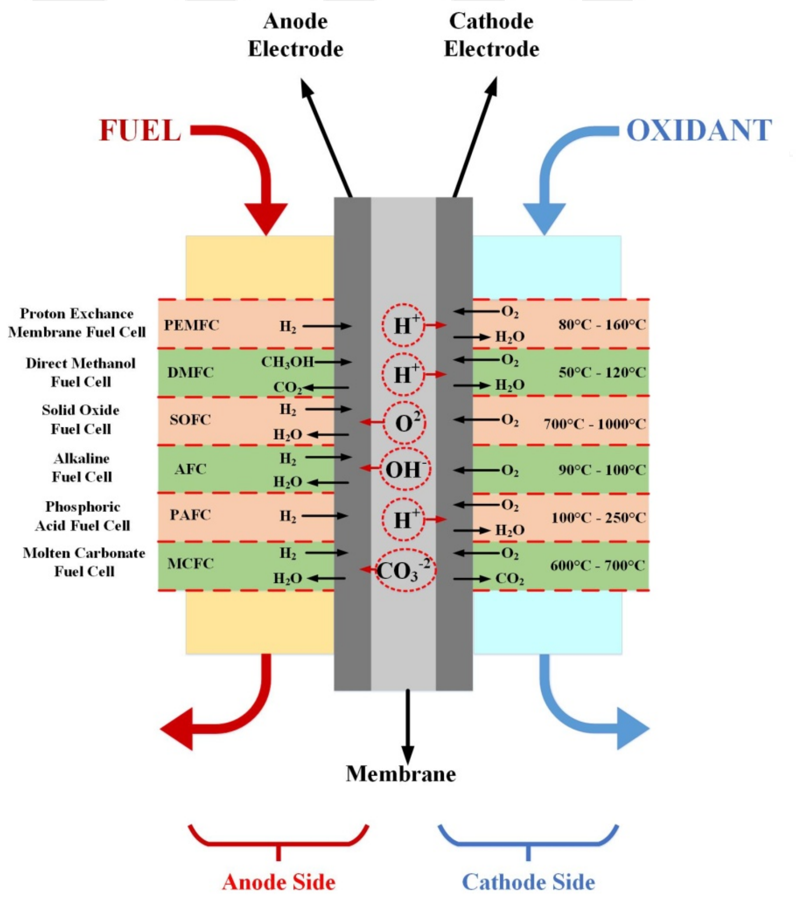

Figure 2.1 The fuel cell types and operating temperatures

2.2 Direct Methanol Fuel Cell (DMFC)

Direct methanol fuel cell (DMFC), which generally uses liquid phase methanol as fuel and oxygen or air as oxidant, is a subcategory of the proton exchange membrane fuel cells (PEMFCs). DMFCs have been used in a large number of applications ranging from portable power to vehicle applications (Thiam et al., 2011; Karim & Kamarudin, 2013). The direct methanol fuel cells are seemed more feasible for portable power applications due to their following advantages;

- lower emission values (Basri et al., 2010)
- high energy density of methanol (3800 kcal/L) (Patel et al., 2015)
- easy storage as the methanol as it is in liquid form
- ability to operate without a reformer
- easy handling of methanol

Despite the many advantages of DMFCs, there are still some constraints to be overcomed, including high cost of platinum electrocatalyst, low durability and stability, relatively low electrical efficiency due to the sluggish reaction kinetics at the anode and cathode, methanol crossover problem, and poisoning of precious platinum electrocatalyst via carbon monoxide (CO) (Cui et al., 2015; Chu et al., 2014; Osmieri et al., 2017; Shu et al., 2016). To overcome these challenges, there has been an active ongoing research done by many research institutes that includes the development and testing of DMFCs with different materials and manufacturing techniques (e.g., Yang & Manthiram, 2003; Wang et al., 2005; Basri et al., 2010). The main component of a DMFC is illustrated in Figure 2.2. As can be seen in this figure, a DMFC is composed of current collectors, flow field plates, and membrane electrode assembly (MEA).

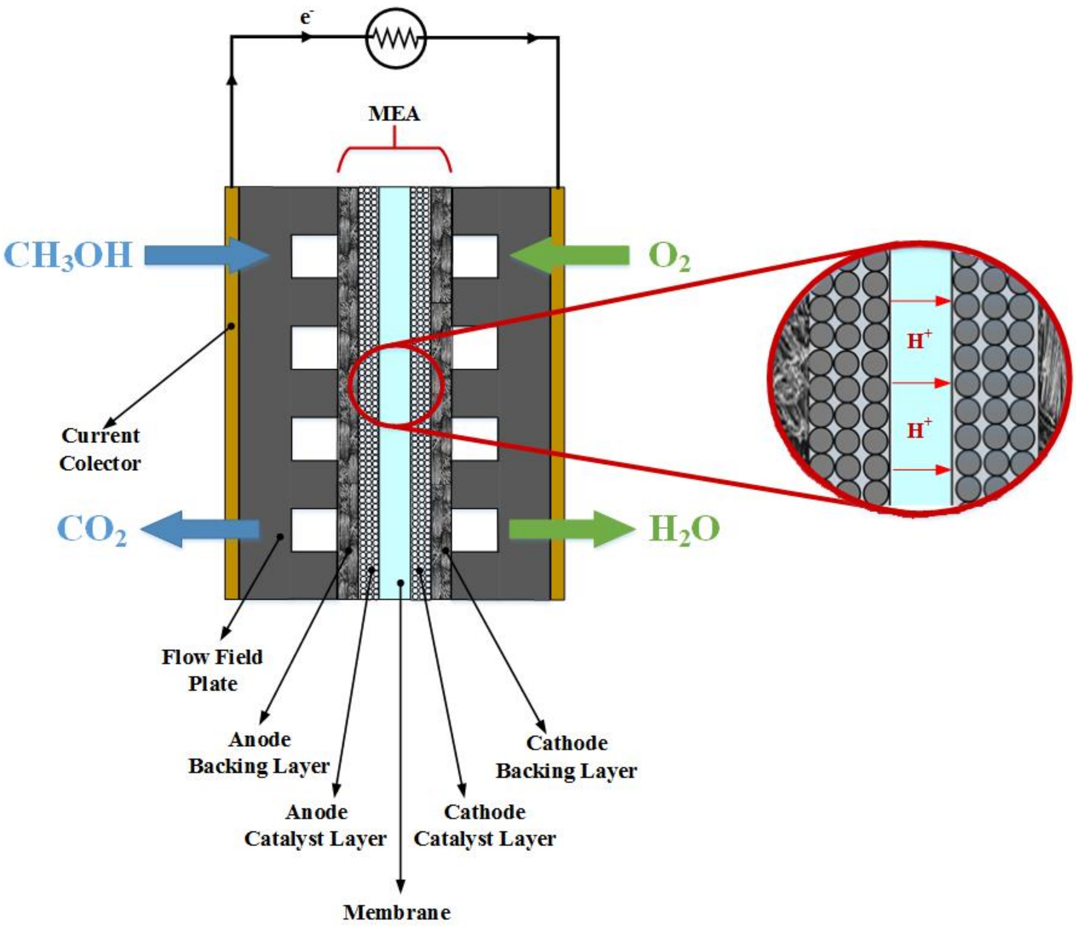

Figure 2.2 The main components of Direct Methanol Fuel Cell (DMFC)

As can be exhibited in the Eq. (2.1), Methanol Oxidation Reaction (MOR) occurs on the anode catalyst layer and protons and electrons are released. Protons generated transport from the anode side to the cathode side through a proton conducting membrane. In the cathode catalyst layer, Oxygen Reduction Reaction (ORR) occurs as showin in Eq. (2.2). In this reaction, protons and electrons are consumed and water is produced. The overall reaction is given in Eq. (2.3).

$$CH_3OH + H_2O \rightarrow CO_2 + 6H^+ + 6e^- \quad (2.1)$$

$$6H^+ + 6e^- + 1.5O_2 \rightarrow 3H_2O \quad (2.2)$$

$$CH_3OH + 1.5O_2 \rightarrow CO_2 + 2H_2O \quad (2.3)$$

The MEA is defined by authorities as the “heart” of a DMFC. Each component of the MEA is examined from Section 2.2.1 to Section 2.2.4.

2.2.1 Membrane

Membranes are selectively permeable materials that allow hydrogen ions (i.e. protons) formed during the electrochemical reactions in the anode catalyst layer to pass to the cathode side. The properties expected from a DMFC membrane can be listed as follows:

- high proton conductivity
- electrical isolation
- to prevent the oxygen/air pass from the cathode side to the anode side
- to minimize the passage of methanol solution from anode side to cathode side
- mechanical stability under the DMFC operation conditions
- chemical stability under the DMFC operation conditions

The most widely used membranes in DMFCs are Nafion® membranes which are perfluorosulfononic acid type membranes. In Figure 2.3, Nafion® membrane's chemical structure is shown.

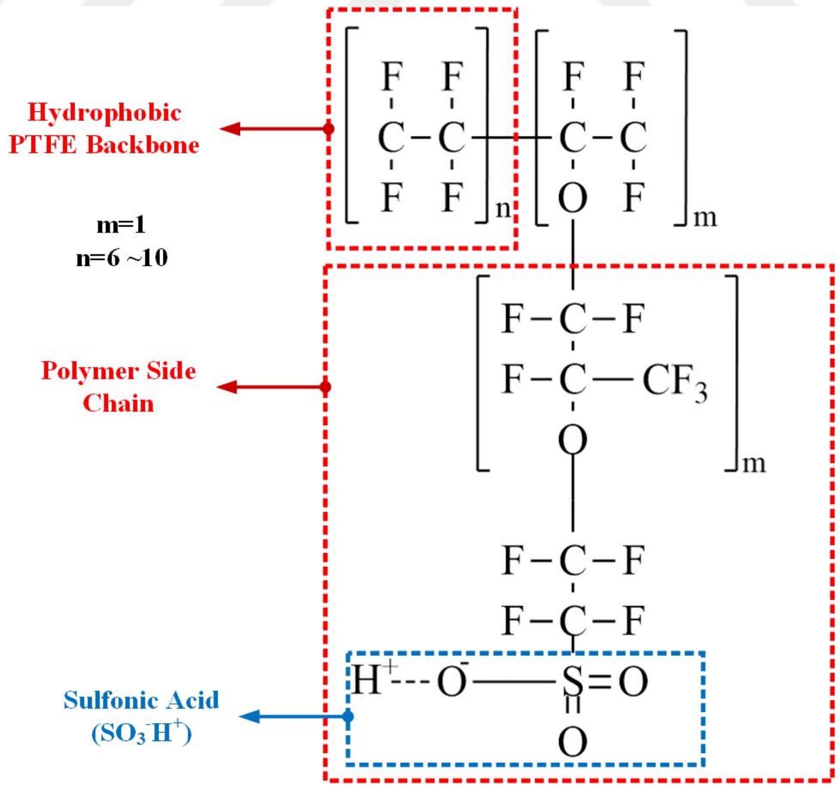

Figure 2.3 Chemical structure of Nafion® membrane (adapted from Ouellette, 2015)

As can be seen in Figure 2.3, although the Teflon (PTFE) backbone shows majorly hydrophobic characteristic, sulfonic acid (SO_3H^+) at the end of the side chain shows highly hydrophilic. Thus, the membranes can absorb a large amount of water. Hydrogen ions transport within the well-hydrated areas and therefore these materials can be defined as “proton conductive” (Barbir, 2012).

The proton transport mechanism for hydrated membranes is usually described as either a hopping mechanism (e.g. Grotthuss transport) or as a diffusion mechanism (e.g. vehicular mechanism) (Peighambardoust et al., 2010). In the hopping mechanism, protons hop from one hydrolyzed ionic site (SO_3^- $H3O^+$) to another hydrolyzed ionic site across the membrane. It is well known that the hopping mechanism has not a significant effect for perflourinated sulfonic acid membranes like Nafion. The scheme of the hopping mechanism is illustrated in the Figure 2.4.

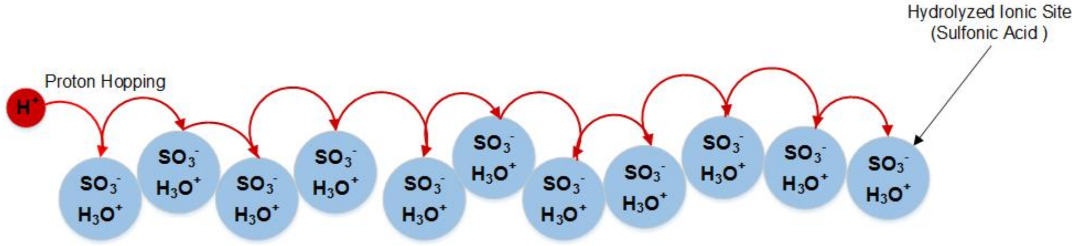

Figure 2.4 The hopping mechanism (adapted from DeLuca et al., 2006)

In the vehicular mechanism, hydrated protons (H_3O^+) diffuse via the aqueous medium in response to the electrochemical difference. In this mechanism, water connected protons (H^+ $(H_2O)_x$) carry the water molecules inward the membrane as a result of electroosmotic drag. The protons attach themselves to a vehicle site (e.g., water) and in this way carry the protons. The main function of the formation of the vehicular mechanism is the existence of the free volumes within polymeric chains in the membrane (Peighambardoust et al., 2010).

The proton transport mechanism within composite membranes is a more complex process as it involves both the surface and chemical properties of the inorganic and organic phases. Although the precise role of inorganic components in stabilizing the proton transport properties of composite based Nafion is still not well understood, it may be presumed that the primary function of the nanoparticles is to stabilize the polymer morphology with increasing temperature. Proton conductivity improvements would depend upon whether the fraction of bulk water and the bulk proton concentrations are increased as a result of the inorganic additives or not (Peighambardoust et al., 2010). The Vehicular mechanism in pristine membranes and polymer/nano-particle composite membranes are shown in Figure 2.5.

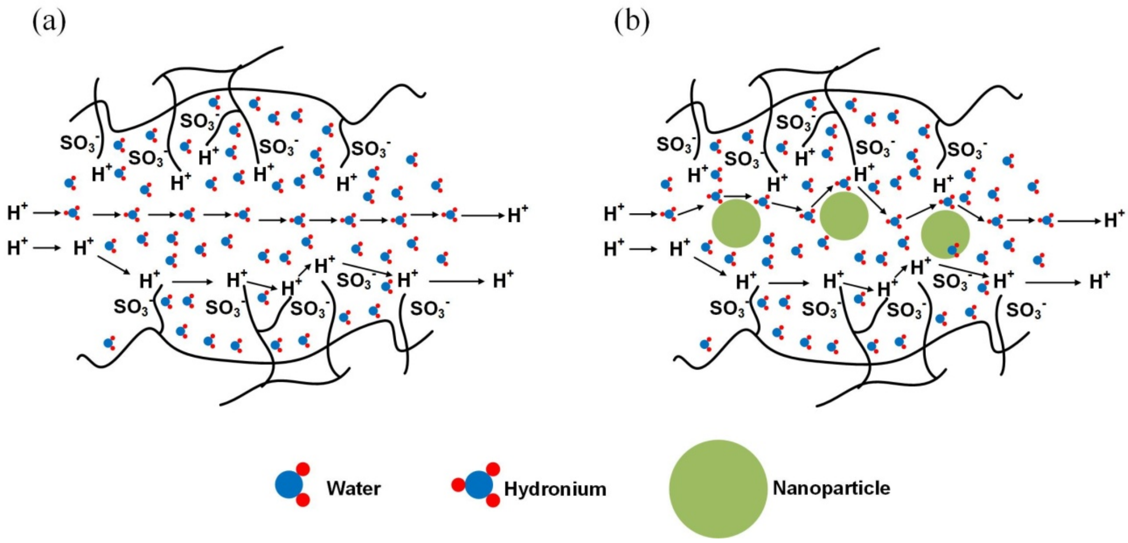

Figure 2.5 The Vehicular Mechanism in (a) pristine membranes and (b) polymer/nano-particle composite membranes (adapted from DeLuca et al., 2006)

2.2.2 Anode Catalyst Layer

Anode catalyst layer is the layer where the methanol oxidation reaction (MOR) occurs. The use of methanol in DMFCs has many advantages; however, it exhibits poor electrochemical activity in the acidic medium. Using the alloys of Platinum (Pt) with other metals to overcome this problem is the most common solution. In this case, carbon supported or unsupported bimetallic platinum based catalysts such as Platinum-Ruthenium (Pt-Ru) has been considered as the most promising material for the oxidation of methanol. Conventionally, carbon supported or unsupported Pt-Ru has been used as the anode electrocatalyst for DMFCs instead of bare platinum since incorporation of second substrate (e.g., Ru) aids in removing the intermediates from the surface which thus hampers poisoning of precious metal (Das et al., 2015).

2.2.3 Cathode Catalyst Layer

Cathode catalyst layer is the layer where the oxygen reduction reaction (ORR) occurs. Generally, in DMFCs, carbon supported or unsupported Platinum (Pt) is used as the cathode catalyst. However, Pt cathode catalyst causes some problems (e.g., performance loss due to CO poisoning and sluggish reaction kinetics at the cathode and an increase in the material cost) for DMFCs.

2.2.4 Backing Layer

The layer which is located between the catalyst layer and flow field plate is called backing layer. In DMFCs, carbon cloth or carbon paper is used widely as the anode backing layer and cathode backing layer. The main functions of the backing layers can be listed as follows;

- to prevent the diffusion of the methanol solution and oxygen/air through the catalyst layers
- to remove the gases and water which are produced during the electrochemical reactions from the reaction areas
- to supply the electrical connection between catalyst layers and flow field plates
- to provide the mechanical support to the MEA

2.3 Performance Characterization of DMFC

The simplest and therefore often used practice for examining the performance of the DMFC is to examine the polarization curves. The cell potential is much lower than the theoretical potential of a fuel cell in the real working state. The reason of this situation is the potential losses in the fuel cell. In Figure 2.6, typical polarization curve for a DMFC is shown together with the theoretical potential and the locations that the main potential losses dominate.

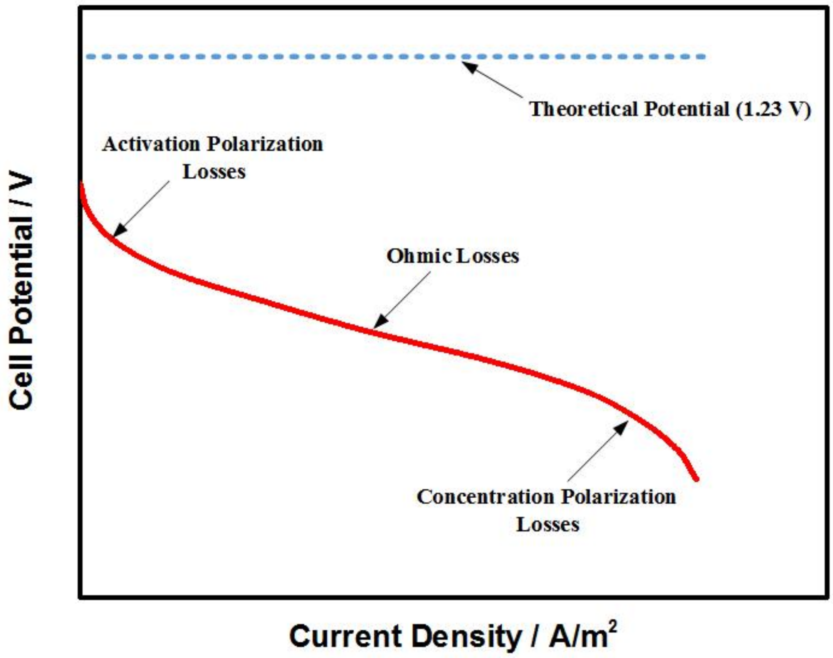

Figure 2.6 Typical polarization curve for a DMFC

The main sources for the low potential of actual fuel cell applications are as follows;

- activation polarization losses
- ohmic losses
- concentration polarization losses
- other losses (e.g. internal current leakage, species crossover)

Activation polarization losses are dominated by the catalyst material on the catalyst layers. Ohmic losses are sourced to ionic and electrical conductivity losses through the membrane, catalyst layers, and other fuel cell components. Concentration polarization losses occurred when the mass transport limitations of the reactants to the electrodes. Other losses include potential losses due to internal current leakage, species crossover, etc.

2.4 Characterization of Fuel Cell Materials

2.4.1 Water Uptake

Water uptake property plays a significant role in proton exchange membrane characterization. The hydration of the membrane is closely related to the proton conductivity. For the water uptake measurements, a typical procedure is as follows (Zhang et al., 2011). The membranes are immersed into deionized water overnight at 80°C. The excess water is wiped off with a foam filter and they are then weighed immediately. Subsequently, the membranes are dried at 100°C in an oven to constant weight. The water uptake can be calculated using the Eq. (2.4);

$$\text{Water Uptake} = \frac{W_{wet} - W_{dry}}{W_{wet}} \times 100\ (\%) \qquad (2.4)$$

where, W_{wet} and W_{dry} are the weights of the water-swollen and dry membrane sample, respectively.

2.4.2 Proton Conductivity

Proton conductivity is one of the important properties of proton exchange membranes, which can directly affect the performance. A common way of measuring proton conductivity is 4 probe Electrochemical Impedance Spectroscopy (EIS). In this method, measurements can be performed in longitudinal direction in air/water vapour atmosphere at 100% relative humidity as a function of temperature. The proton conductivity [σ, $(\Omega\cdot cm)^{-1}$] can be calculated on the basis of the measured resistance according to the Eq. (3.2) (Hasegawa et al., 2013);

$$\sigma = \left(\frac{1}{R}\right) \times \left(\frac{l}{A}\right) \qquad (2.5)$$

where l is the distance between the two electrodes (cm), R is the membrane resistance (Ω) and A is the cross-sectional area of the membrane (cm^2). Proton conductivity experiments should be repeated several times to confirm reproducibility in results.

2.4.3 Thermogravimetric Analysis (TGA)

Thermogravimetric Analysis (TGA) is a method in which the mass of a substance is monitored as a function of time or temperature as the sample specimen is subjected to a controlled temperature program in a controlled atmosphere. The mass of the sample is monitored during the TGA analysis. Thermal stability of the samples (e.g. membranes) could be determined by TGA method (Coats & Redfern, 1963).

2.4.4 Scanning Electron Microscopy (SEM)

Scanning electron microscopy (SEM) is an electron microscope type that acquires images by scanning the surface of the sample with a focused electron beam. In the most SEM applications, data are collected over a selected area of the sample surface and a two-dimensional (2D) image is generated. SEM could be used to investigate the microstructure of the bare Nafion membrane as well as those of the composite membranes with different contents of additives.

2.4.5 Energy Dispersive X-ray Spectroscopy (EDX)

Energy Dispersive X-ray spectroscopy (EDX) is an analytical method for analytical or chemical characterization of materials. EDX systems are generally attached an Electron Microscopy instruments such as Transmission Electron Microscopy (TEM) or Scanning Electron Microscopy (SEM). EDX is based on the detection of characteristic X-rays effused of an element in consequence of the de-excitation of core electron holes created by a high energy electron beam. An electron from a higher binding energy electron level falls into the core hole and an X-ray with the energy of the difference of the electron level binding energies is emitted.

2.4.6 X-ray Diffraction (XRD)

X-ray Diffraction (XRD) is based on the principle of breaking X-rays characteristic of each crystal depending on its specific atomic arrangement. The X-rays sent to a crystal are scattered by the crystal structure. The working principle of XRD measurements can be expressed as the sum of the data of the refraction or scattered ray. For the aim of this analysis, the analyzed materials are firstly finely ground, homogenized. After then average bulk composition can be examined.

2.5 Literature Review

2.5.1 Literature Review Nafion/TiO_2 and Nafion/SiO_2 Composite Membrane Based DMFCs

In the most of the DMFC applications, Perfluorosulfononic acid type membranes (e.g. Nafion®) are commonly used. Nafion® membranes have attracted much attention due to their high proton conductivity, flexibility, and excellent chemical and mechanical stability in the soaked state (Yuan et al., 2014; Salarizadeh et al., 2013). In spite of the fact that Nafion® has all these advantages, bare Nafion® has dehydration problem at higher temperatures (>80°C) that result in low cell performance. Because of this problem, the methanol permeability increases; whereas proton conductivity decreases at these temperatures (Devrim et al., 2012; Xu et al., 2015; Ye et al., 2007). In order to overcome this problem, researchers have started to pay more attention to the alternative membranes which can provide better performance especially at high temperatures.

Latest studies have shown that composite membranes are very promising due to their ability to maintain high proton conductivity at relatively high temperatures. The introduction of inorganic particles into the Nafion matrix helps to improve the proton conductivity and thermal stability of the nanocomposite membranes as compared to the bare Nafion® membrane (Devrim et al., 2012). There are some studies on the investigation of the effects of composite membranes on the performance of fuel cells. For instance, Kim et al. (2003) have investigated heteropolyacid/directly polymerized sulfonated poly copolymer composite membranes. According to their results, HPA/BPSH copolymer composite membranes are very promising especially at high temperatures (>100°C) in a PEMFC. Shao et al. (2006) have investigated the effect of Nafion membranes having SiO_2, TiO_2, WO_3, and SiO_2/PWA inorganic materials on the performance of PEMFCs, experimentally. As a result of these experiments, Nafion/SiO_2, Nafion/TiO_2, Nafion/WO_3, and Nafion/SiO_2/PWA composite membranes provided higher power density in comparison to the commercial Nafion® 115 membrane. Other types of Nafion based composite membranes that have been synthesized for fuel cell applications include but not limited to Nafion/ZrP (Rodgers et al., 2009; Vaivars et al., 2004; Yang et al., 2011), Nafion/Diphenylsilicate (Liang et al., 2006), Nafion/Teflon (Lin et al., 2003; Chen et al., 2008; Park et al., 2012; Lin et al., 2005; Liu et al., 2013), disopropyl phosphite/Nafion (Park et al., 2000), and Nafion/clay-SO_3 (Bébin et al., 2006).

According to the findings of this literature survey, Nafion based composite membranes (e.g. Nafion/SiO_2 and Nafion/TiO_2) are very promising in terms of increasing the proton conductivity and mechanical stability at high temperatures. For instance, Adjemian et al. (2002) studied Silicon oxide/Nafion composite membranes for operation in PEMFCs. They reported that the silicon oxide was very useful for improving the water retention and increasing proton conductivity at elevated temperatures (from 80°C to 140°C). They also emphasized the fact that silicon oxide based membrane was more durable as compared to Nafion® 115 at high operation temperatures. Ke et al. (2012) conducted research on the performance of PEMFCs having Nafion/SiO_2 and bare Nafion membranes, and found that the PEMFCs having Nafion/SiO_2 membrane provides better performance as compared to the PEMFC having bare Nafion membrane. They concluded that Nafion/SiO_2 membranes are very promising for PEMFCs at high operation temperatures. Jian-hua et al. (2008) used both humidified and dry reactants in their experiments to evaluate the water retention ability and electrochemical performance of Nafion/TiO_2 composite membranes via a single PEMFC. The results of their study showed that the MEA having Nafion/TiO_2 membrane provides better performance in comparison to the MEA having bare Nafion.

Although Nafion® has been used as the membrane in DMFCs due to its chemical and thermal stability, and very high proton conductivity especially in the soaked state, it dehydrates when the operating temperature gets higher than 80°C. Because of this dehydration problem, the performance of the DMFC deteriorates after this temperature.

2.5.2 Literature Review of Pt-Ru/C-TiO_2 Anode Catalyst Based DMFCs

A various number of experimental and numerical studies, including re-designing the architecture of the Membrane Electrode Assembly (MEA) and its components and developing alternative materials and manufacturing techniques have been carried out to mitigate the negative effects of the above-mentioned problems as well as to achieve an improved DMFC performance (Sebastián et al., 2016; Hu et al., 2015; Sebastián, Serov, Artyushkova, Atanassov, et al., 2016; Patel et al., 2015). As one of the most important components of a DMFC, significant research efforts have focused on the synthesis of robust anode electrocatalyst with higher electrocatalytic activity so as to improve the methanol oxidation reaction (MOR) kinetics as well as to achieve an enhanced DMFC performance (Dawoud et al., 2007; Ghouri et al., 2015; Das et al., 2015). Conventionally, carbon supported or unsupported Pt-Ru has been used as the anode electrocatalyst for DMFCs instead of bare platinum since incorporation of second substrate (e.g., Ru) aids in removing the intermediates from the surface which thus hampers poisoning of precious metal (Liu et al., 2015). Otherwise, the absorbed intermediates (e.g., CO) bring about a kinetic obstacle by transforming electrochemically active areas into inactive areas through occupying the available spaces. In other words, alloying Pt and Ru as an anode electrocatalyst promotes the oxidation of CO to carbon dioxide (CO_2) and mitigates the problem of Pt poisoning (Narischat et al., 2014). However, using this anode electrocatalyst still does not yield the desired performance, electrocatalytic activity, and durability goals, especially when the lifetime of DMFC is considered. To achieve an improved MOR kinetics, Pt-Ru anode electrocatalyst has been modified by dispersing them on highly conductive nanoparticles with high surface area or by incorporating non-noble metals into the anode electrocatalyst (Narischat et al., 2014; Xiong et al., 2013; Huang & Wang, 2014; Veizaga et al., 2014; Tokarz et al., 2013).

Suitability of an anode electrocatalyst support is highly dependent on several performance-enhancing properties: an acceptable stability and durability in acidic porous media, a sufficient surface area for well-proportioned dispersion of fine particles of anode electrocatalyst, and a proper electrical conductivity (Patel et al., 2015). However, the electrocatalytic activity of Pt-Ru anode electrocatalyst markedly depends on the structure, particle size, and Pt or Ru content in it. Many research studies have been conducted to optimize the Pt-Ru anode electrocatalyst towards previously-mentioned properties (e.g., Arico et al., 2001; Li et al., 2003). These studies showed that either a high anode electrocatalyst loading (~2.0-8.0 mg•cm^{-2}) or highly-pure methanol based diluted solution is required when Pt-Ru is used as the anode electrocatalyst. However, higher electrocatalyst loading or usage of highly-pure methanol based diluted solution results in relatively high material costs, creating constraints towards the widely-usage of DMFCs in the commercial market (Scibioh et al., 2008). Seeing that reduction of the electrocatalyst loading from the present 2.0-8.0 mg•cm^{-2} to <1.0 mg•cm^{-2} without performance compromise and optimization of catalytic activity via appropriate supporting materials are matters of vital importance (Liu et al., 2006).

As previously emphasized, there have been significant research efforts on re-designing the architecture of the anode electrocatalyst to address Pt poisoning problem and to achieve a higher activity for the MOR by making further modifications. Another widely-accepted approach is to incorporate non-noble metals or metal oxides into the anode electrocatalyst to make it more capable of absorbing oxygenated species, to improve its CO tolerance, and ultimately to enhance the MOR (Shan et al., 2007). The main aim for incorporating non-noble metals or metal oxides into anode electrocatalyst is to oxidize the intermediates thoroughly to CO_2 and to facilitate the breaking of carbon-carbon bonds in methanol (Long et al., 2000). Recent studies showed that several metal oxides including IrO_2, V_2O_5, CeO_2, WO_3, MO_3, and TiO_2 have been extensively used as a support for Pt-based electrocatalysts to improve their catalytic activity for the MOR (Scibioh et al., 2008; Zhang et al., 2010; Maiyalagan & Khan; 2009; Micoud et al., 2009; Justin & Rao, 2011; Drew et al., 2005; Abdelkareem et al., 2013).

Among all the metal oxides, titania (TiO_2) is one of the most promising promoters due mainly to its ability to remain stable under acidic environments and reduce the adsorption energy of CO. Hence, when Pt-Ru/C anode electrocatalyst is supported on TiO_2, Pt becomes more effective in terms of activity for the same oxidation reactions and thus leads to a decrease in the adsorption energy of CO. With the existence of

TiO_2, the reduction of Ti^{3+} takes place and thus brings about an increase in electronic density on Pt. The bonds between the Pt and CO become weaker, leading to an increase in the mobility of CO groups on Pt (Macak et al., 2005). In addition, during the MOR, TiO_2 facilitates the adsorption of hydroxide (OH) species, leading to an increase in the rate of conversion of the catalytically poisonous intermediates (e.g., CO) into CO_2. Several studies were conducted to investigate the performance of Pt-Ru/C-TiO_2 as anode electrocatalyst used to promote the MOR. The results of the conducted studies revealed that mixing TiO_2 materials with Pt-Ru/C could improve the electrocatalytic properties of Pt-Ru/C especially for methanol electro-oxidation. For instance, Wang et al. (2013) prepared TiO_2-promoted Pt-Ru/C anode electrocatalysts adding TiO_2 nanoparticles directly to Pt-Ru/C and investigated electrocatalytic activity and stability properties of the anode electrocatalyst in the MOR through cyclic voltammetry. Their study results clearly demonstrated that the introduction of TiO_2 materials into Pt-Ru/C anode electrocatalyst provides an improved electrocatalytic performance during the MOR.

2.5.3 Literature Review of Nafion/ZrP Composite Membrane and Pt/C-ZrP Cathode Catalyst Based DMFCs

One of the important components of MEA is the membrane, which acts as an electrolyte to carry the protons from the anode to cathode. The membrane also creates a barrier by preventing the transport of electrons from one electrode to the other (Mauritz & Moore, 2004). Conventionally, DuPont's Nafion® 117, 115 or 212 has been used as the membrane for this type of fuel cell due to its chemical features, such as high proton conductivity and chemical stability at relatively low operating temperatures (up to 80°C). The proton conduction mechanism through this membrane depends markedly on the movement of protons with the help of sulfonic acid (SO_3H) groups as long as water exists. The membrane therefore should be well-hydrated to maintain an appropriate hydration level (Sridhar et al., 2001). Although Nafion® membranes provide these aforementioned desirable properties at low operating temperatures (<80°C), as the temperature becomes higher than 80°C, the membrane starts to dehydrate and becomes less effective in reference to proton conductivity (Ercelik et al., 2017). As a result of this dehydration problem, the performance of DMFC deteriorates due mainly to decrease in the proton conductivity of the membrane especially at elevated temperatures (>80°C) (Devrim et al., 2012; Rosenthal et al., 2012). Moreover, the single cell operating at relatively low temperatures (<80°C) faces with some other challenges, including sluggish kinetics of oxygen reduction and methanol oxidation reactions and less catalyst contamination (CO poisoning) tolerance (Wu et al., 2008). When the operating temperature reaches elevated levels (>80°C), the reaction kinetics increase and the risk of CO poisoning decreases (Yang et al., 2001). Considering these facts, it is expected that operating at elevated temperatures (>80°C) would increase DMFC performance significantly, if suitable MEA materials could be used. Therefore, in order to take advantage of high temperature operation, the membrane needs to fulfill some desired properties, including high proton conductivity, thermal and chemical stability, and low fuel permeability even at elevated operating temperatures (Wannek et al., 2010).

There has been an ongoing research in the area of development of alternative membranes to circumvent the problem of membrane dehydration. Some alternative membranes, which possess an improved water retention ability and thermal stability at elevated temperatures (>80°C), have been developed and investigated (Staiti et al., 2001; Chalkova et al., 2005). Several approaches have been extensively used in the manufacturing process of these alternative membranes, including incorporation of some metal-oxide particles (e.g., TiO_2, SiO_2, $TiSiO_4$, and ZrP) into the Nafion® matrix to improve the proton conductivity, water retention properties, and thermal and chemical stability of the bare Nafion® membrane. For instance, Devrim et al. (2012) manufactured Nafion/TiO_2, Nafion/SiO_2, and Nafion/nanosize titanium silicon oxide ($TiSiO_4$) composite membranes using ultrasonic spraying technique and conducted some experimental studies to determine the performances of these composite membranes in the proton exchange membrane fuel cells (PEMFCs). The results of their study showed that Nafion/$TiSiO_4$ composite membrane yields better performance as compared to Nafion®, Nafion/TiO_2, and Nafion/SiO_2 membranes. They also reported that the composite membranes are very promising for PEMFCs due to their superior water retention and uptake abilities at elevated operating temperatures. Jalani et al. (2005) synthesized Nafion/ZrO_2, Nafion/SiO_2, and

Nafion/TiO_2 nanocomposite membranes by sol-gel method for high temperature PEMFCs and characterized them using Thermogravimetric Analysis (TGA) and Dynamic Mechanical Analysis (DMA). Their goal for synthesizing these composite membranes was to develop membranes, which have high proton conductivity and appropriate water retention and thermo-mechanical properties. The results of their TGA and DMA showed that the nanocomposite membranes have superiority as regards degradation and glass transition temperature over bare Nafion®. Other types of Nafion® based composite membranes which have been synthesized for fuel cell applications include but not limited to Nafion/ PTFE (Yu et al., 2007; Lin et al., 2005; Lin et al., 2009), Nafion/PVA (Mollá & Compañ, 2011), and disopropyl phosphite/Nafion (Park et al., 2000).

According to literature survey, Nafion® based composite membranes, especially Nafion/ZrP composite membranes, are considered to be of "highly promising", particularly for overcoming the problem of dehydration and increasing the proton conductivity of the membrane at relatively high operating temperatures. For example, Yang et al. (2001) prepared Nafion/ZrP composite membrane and investigated the performance of the PEMFC based on this membrane. They also made performance comparison between the PEMFC having a Nafion/ZrP composite membrane and PEMFC having an unmodified Nafion® membrane under various operating conditions. They reported that the Ohmic resistance of the Nafion/ZrP composite membrane at elevated temperatures (130°C-140°C) was dramatically less than that of unmodified Nafion® membrane. The PEMFC with a Nafion/ZrP composite membrane showed much higher current density in comparison to PEMFC having unmodified Nafion® membrane at temperatures above 100°C. It was also reported that the performance values of both of the PEMFCs at 80°C were almost same. Costamagna et al. (2002) investigated the composite Nafion/ZrP composite membranes for high temperature PEMFCs. The results of their study demonstrated that the PEMFC having Nafion/ZrP composite membrane gave 1500 mA/cm^2 at the operating conditions of 130°C and 3 bar. It was also stated that the Nafion/ZrP composite membrane exhibited highly stable behavior at 130°C.

Another important component of MEA is the catalyst, which has a significant effect on the performance of a fuel cell. Conventionally, carbon supported or unsupported Pt-Ru and Pt have been used as the catalyst for the anode and cathode sides of DMFC, respectively. However, Pt cathode catalyst causes some problems (e.g., performance loss due to CO poisoning and sluggish reaction kinetics at the cathode and an increase in the material cost) for DMFCs. Recently, researchers have started to pay more attention to the investigation of some Pt-based alternative cathode catalysts, such as Pt-Co, Pt-Pd, Pt-Fe, and Pt-Au to alleviate the negative effects associated with these problems. These Pt-based alternative cathode catalysts have been proven to be effective and are considered to be state-of-the-art catalysts due to their significant characteristics, including the ability to decrease the active areas for methanol adsorption at the cathode side, to reduce undesired methanol oxidation at the cathode, and to achieve relatively higher catalytic activity for oxygen reduction (Starr et al., 2013; Shukla & Raman, 2003; Wang et al., 2008; Antolini et al., 2006). For instance, Xu et al. (2010) and Selvarani et al. (2009) investigated the effect of Pt-Au alloy cathode catalyst on the performance of DMFCs and they reported that the power density of the DMFC having Pt-Au/C cathode catalyst is almost twice as much as the MEA having conventional Pt/C cathode catalyst. Shukla and Raman (2003) investigated the effect of different methanol resistant oxygen reduction catalysts, including Pt-Fe/C and Pt-Co/C on the performance of DMFCs. They reported that these catalysts could be a good solution for mitigating the performance losses in the DMFCs that take place through methanol crossover from the anode to cathode. Owing to these composite cathode catalysts, significant progress in improving the performance of DMFCs has been achieved; however, there are still some challenges as regards improving the rate of oxygen reduction reaction (ORR) at the cathode. This challenge could be ironed out incorporating additives (e.g., zirconium hydrogen phosphate (ZrP)) into the cathode catalyst. Due to its layered structure, high proton conductivity arising from high proton mobility notably on the surface of ZrP (Alberti et al., 1978), comparatively high hygroscopicity at elevated temperature operation, and cation exchange features (Barron et al., 2015), ZrP could be used as a temperature-proof solid electrolyte to maintain proper proton conductivity at elevated operating temperatures (Xie et al., 2006).

CHAPTER THREE
EXPERIMENTAL STUDY

3.1 Introduction

In this chapter, Nafion/TiO_2 composite membrane, Nafion/SiO_2 composite membrane, PtRu/C-TiO_2 anode catalyst, Nafion/ZrP composite membrane, and Pt/C-ZrP cathode catalyst based DMFC's manufacturing and experimental investigation steps are presented. For this aim, each alternative material based DMFCs is discussed on different subsections in this chapter.

3.2 Nafion/TiO_2 and Nafion/SiO_2 Composite Membrane Based DMFCs

The literature survey discussed above shows that Nafion/SiO_2 and Nafion/TiO_2 composite membranes have been proven to be very effective to overcome this problem in proton exchange membrane fuel cells (PEMFCs) operating with hydrogen. However, no works can be found related to the performance comparison of Nafion/SiO_2 and Nafion/TiO_2 composite membranes for DMFCs. For this reason, Nafion/SiO_2 and Nafion/TiO_2 composite membranes were synthesized by applying solvent casting method as to investigate the effect of usage of these membranes on the performance of DMFCs. In addition, I report the preparation and characterization of Nafion based nanocomposite membranes to improve the DMFC performance. Three different MEAs with Nafion/SiO_2, Nafion/TiO_2, and Nafion® 115 membranes were fabricated using the ultrasonic coating method. The effect of these Nafion based composite membranes on the performance of DMFCs was compared with that of DMFC having Nafion® 115 membrane. The comparison studies of these MEAs were performed at different temperatures, which are 60°C, 80°C, and 95°C.

3.2.1 Materials

The commercially available Hydrogen peroxide (Emsure®, chemical purity 30 wt%) and Sulfuric acid (Emsure®, chemical purity 95-97 wt%) were obtained from Merck (Darmstadt, Germany). Teflon treated carbon cloth (ELAT LT1400W) used as anode backing layer was obtained from Nuvant Systems Inc. (Crown Point, IN, USA). Anode catalyst powder (HP 60 wt% Pt-Ru on Vulcan XC-72) and cathode catalyst powder (HP 60 wt% Pt on Vulcan XC-72) were used as anode and cathode catalyst, respectively. Nafion® 115 membrane purchased from DuPont Corp. (Delaware, USA). 15 wt% Nafion solution (LIQUION™ Solution LQ-1115 1100EW 15 wt%) was obtained from Ion Power Inc. (Delaware, USA). TiO_2 (Anatase) was obtained from Degussa (P25) and SiO_2 was obtained from Aldrich and used as received. N,N-dimethylacetamide ($CH_3C(O)N(CH_3)_2$, DMAc) were used as received. All solvents including isopropyl alcohol (Aldrich), methanol (Aldrich) and sulfuric acid (H_2SO_4, 97%, Aldrich) were of reagent grade and were used without further purification.

3.2.2 Membrane Preparation and Characterization

Nafion based composite membranes were prepared using the recasting method (Devrim et al., 2012). 15 wt% Nafion solution was evaporated at 60°C until a dry residue was obtained. The residual Nafion resin was redissolved in a desired amount of DMAc to form a solution containing 10 wt% of Nafion. An appropriate amount of 5 wt% Nafion solution was mixed with 2.5 wt% inorganic particles in an ultrasonic bath for 1 h. The resulting mixture was cast onto glass surface and was slowly evaporated at 80°C to remove most of the DMAc solvent. The membrane was removed from the glass surface by wetting with water. All membranes were stored in water before any test was performed. The composite membrane thickness around 70±5 µm was obtained from 2.5 wt% nanoparticle loading. Inorganic particle content was selected as 2.5 wt% according to Devrim et al. (2014). Inorganic particle content was optimized and 2.5 wt% was found as optimum inorganic particle content to maintain homogenous particle distribution in polymer matrices.

All membranes were pretreated by heating to 80°C in 3 wt% H_2O_2 for 1 h, followed rinsing in doubly deionized water. The membranes were then boiled in deionized water for 1 h. Then, those membranes were put into the 5 wt% H_2SO_4 and boiled for 1 h. After further rinsing in doubly deionized water to remove the final traces of acid, the membranes were stored in doubly deionized water until required

(Liu et al., 2016; Sabet-Sharghi et al., 2013; Cho et al., 2009). Figure 3.1 illustrates the membrane activation process steps.

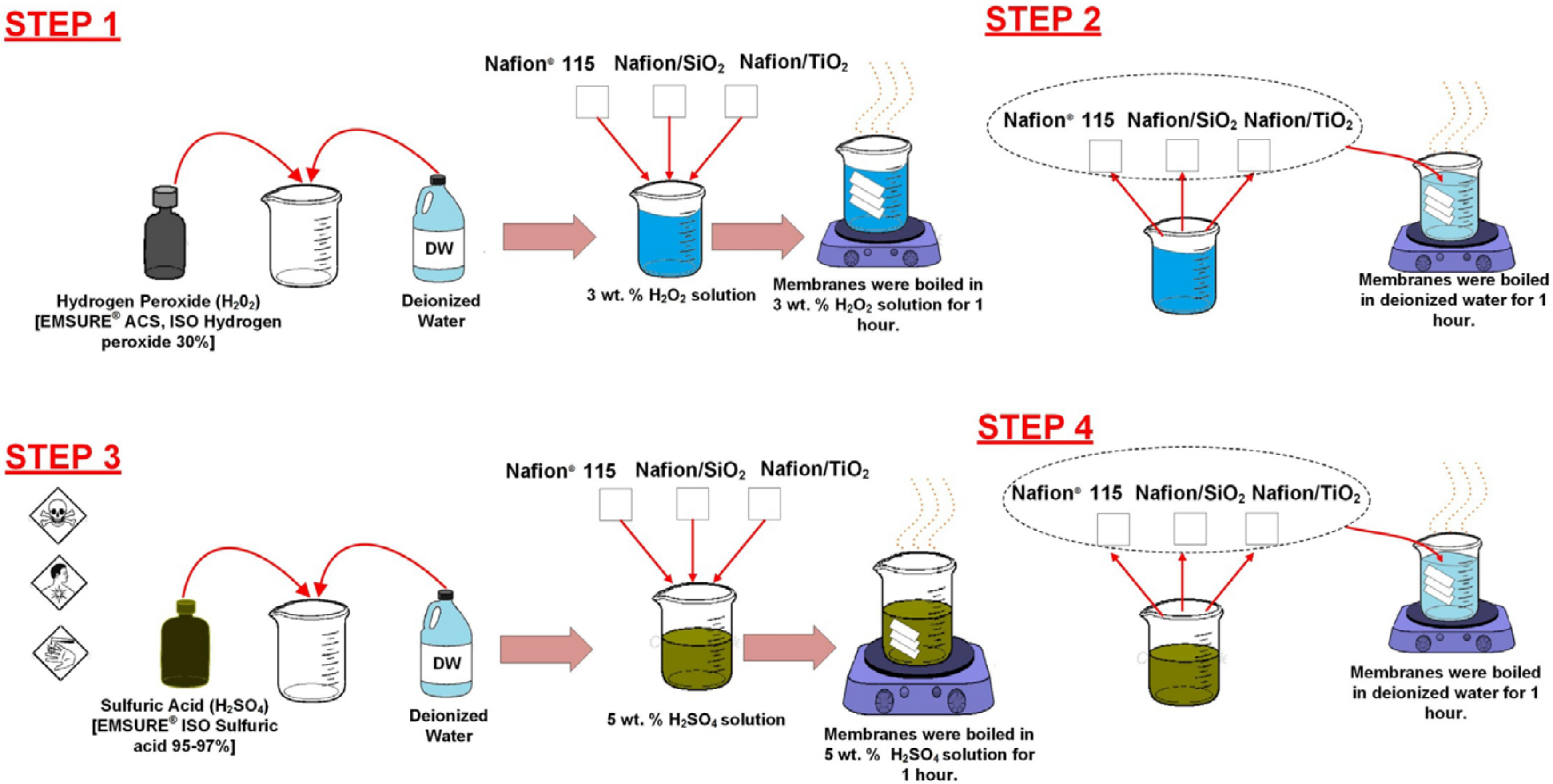

Figure 3.1 Membrane activation process steps

26

For water uptake measurements, the membranes were immersed into deionized water overnight at 80°C. The excess water was wiped off with a foam filter and they were then weighed immediately. Subsequently, the membranes were dried at 100°C in an oven to constant weight. The water uptake was calculated using the Eq. (3.1) (Zhang et al., 2011; Kim et al., 2000);

$$\text{Water Uptake} = \frac{W_{wet} - W_{dry}}{W_{wet}} \times 100\ (\%) \tag{3.1}$$

where, W_{wet} and W_{dry} are the weights of the water-swollen and dry membrane sample, respectively.

The surface morphology of nanocomposite membranes were examined in QUANTA 400F Field Emission Scanning Electron Microscope (SEM) equipped with an energy dispersive X-ray (EDX) spectrometer. Before measurements, the samples were coated with a layer of gold to enhance electrical conduction.

Proton conductivity is one of the important properties of proton exchange membranes, which can directly affect the performance. The proton conductivity of the membranes was observed using a ZIVE SP2 Electrochemical Workstation (WonA-Tech, Korea). All measurements were performed in longitudinal direction; in air/water vapor atmosphere at 100% relative humidity with 4 probe EIS as a function of temperature. The proton conductivity [σ, $(\Omega\cdot\text{cm})^{-1}$] was calculated on the basis of the measured resistance according to the Eq. (3.2) (Hasegawa et al., 2013);

$$\sigma = \left(\frac{1}{R}\right) \times \left(\frac{l}{A}\right) \tag{3.2}$$

where, l is the distance between the two electrodes (cm), R is the membrane resistance (Ω) and A is the cross-sectional area of the membrane (cm^2). Proton conductivity experiments were repeated five times to confirm reproducibility in results

3.2.3 MEA Manufacturing Process

3.2.3.1 The Preparation of Anode and Cathode Catalyst Inks

The first step in the MEA manufacturing is the preparation of the catalyst inks. The amounts of cathode and anode catalyst powders were determined using Eq. (3.3). In this equation, the catalyst loadings were chosen as 4 mg_{PtRu}/cm^2 and 4 mg_{Pt}/cm^2 for the anode and cathode sides, respectively. The wt. % of metal was taken as 60 wt. % of Pt-Ru and 60 wt. % of Pt, for the anode and cathode sides, respectively. In this study, the active area was selected as 25 cm^2. C is the catalyst loss ratio, which changes between 0 and 1 and depends on the catalyst coating technique. In this study, this parameter was considered as 0.03 due to the high catalyst coating efficiency of the ultrasonic coating technique. The amount of catalyst powder calculated from Eq. (3.3) was mixed with appropriate amounts of deionized water, Nafion® solution, and isopropyl alcohol. To make the catalyst ink homogeneous, this ink was first mixed by magnetic stirrer for 30 min and then ultrasonic stirrer for 2 h. The same method was applied for preparation of both the anode and cathode catalyst inks.

$$\text{Amount of Catalyst Powder} = \left(\frac{\text{Catalyst loading}}{\text{wt\% of Metal}} \times \text{Active Area}\right) \times (1 + \mathrm{C}) \qquad (3.3)$$

3.2.3.2 Coating of the Catalyst Ink

In this study, ultrasonic coating technique was used with an ultrasonic coating machine (SONO-TEK). After preparing and homogenizing the catalyst inks, they were put into the injector of ultrasonic coating machine. During the coating process, backing layers (carbon cloth for the anode side and carbon paper for the cathode side) were placed on the vacuum table; the flow rate of the catalyst ink was set to 3 ml/min, and the temperature of the vacuum table was kept at 50°C. After the coating process was completed, the backing layers were kept at the room temperature to make them fully dried. The preparation of catalyst ink and coating of the catalyst ink on a backing layer surface are illustrated in Figure 3.2. Ultrasonic coating machine (SONO-TEK) is shown in Figure 3.3.

29

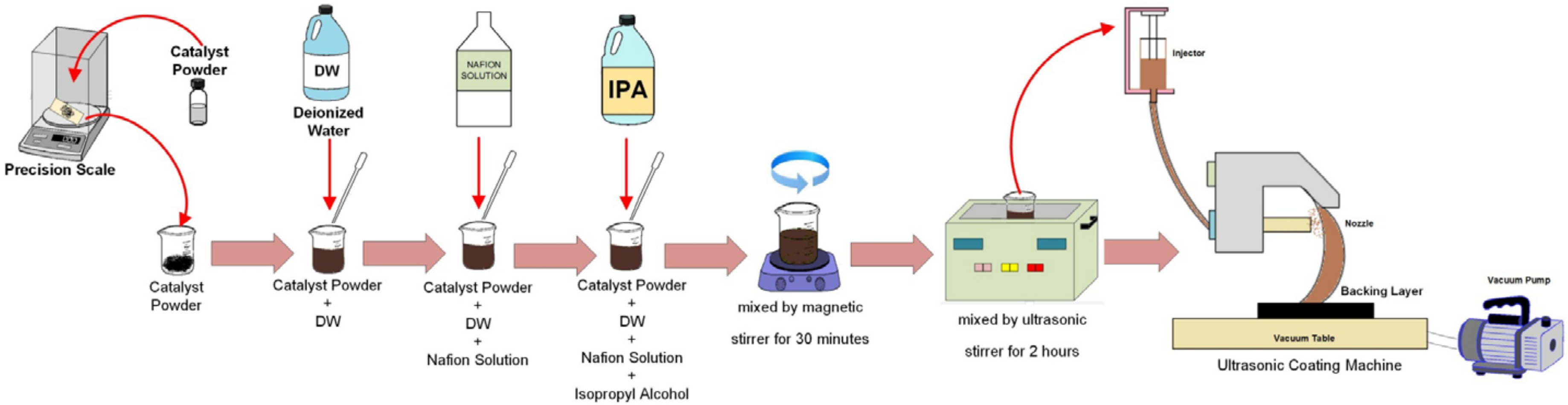

Figure 3.2 The preparation catalyst ink and coating of the catalyst ink on a backing layer surface

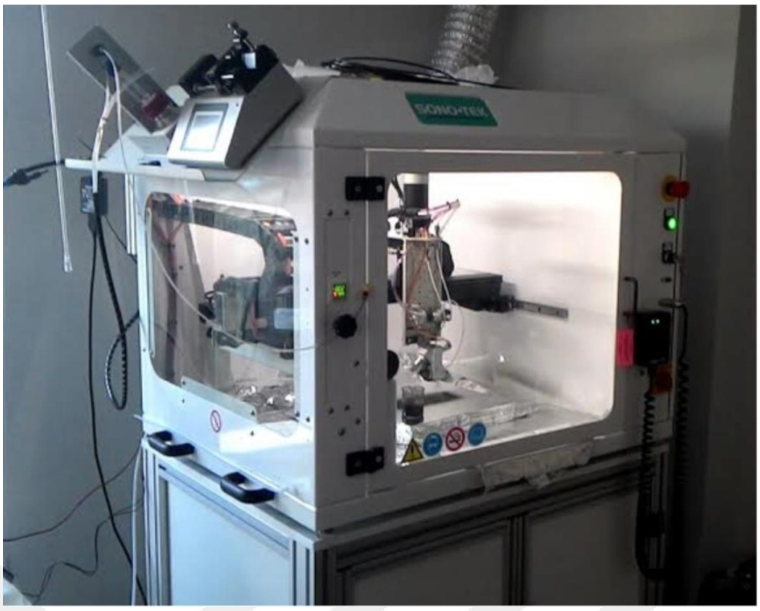

Figure 3.3 Ultrasonic coating machine (SONO-TEK)

3.2.3.3 Hot Press Process

The last step of the MEA manufacturing is the hot press process. In this process, the membrane was placed between the anode and cathode catalyst coated backing layers and pressed at 120°C and 6.89 MPa for 4 min (Tamaki et al., 2011; Zhao et al., 2005; Chen et al., 2006; Tang et al., 2007). The same procedure was repeated for each membrane type (Nafion/SiO_2, Nafion/TiO_2, and Nafion® 115) to manufacture three MEAs. The illustration of the hot press process was shown in Figure 3.4.

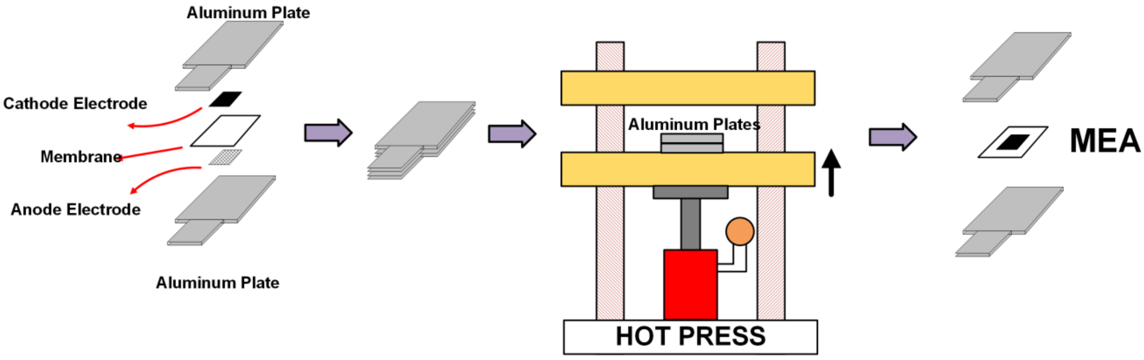

Figure 3.4 Hot press process

3.2.4 Performance Testing

The performances of the MEAs manufactured using the ultrasonic coating technique, as discussed in Section 3.2.3, were investigated experimentally for different temperature values. In the experiments, the current and power values of the MEAs were measured as the voltage changes from 0.6 V to 0.2 V. The experiments were conducted using the following procedure. First, the flow channels were cleaned up using a soft brush to protect them against non-uniform flow distribution and physical damage, which could originate from the abrasive structures of the inorganic particles. Second, two gaskets with the thickness of 0.1 mm were placed at the anode and cathode sides of the single cell in order to prevent the leakage problem. The single cell was tightened with a compression torque value of 3.6 N•m after the MEA was placed between the gaskets. This value was determined in order to keep the compression ratio of the MEA in the range of 20±5 %, which is suggested as the optimum value in the literature (User instructions for DMFC electrodes & MEAs prior to installation, n.d.). Keeping the compression ratio in this range is critical not to cause any leakage problems and damage to the components of the fuel cell and also to provide sufficient contact between the MEA and the bipolar plates. In this regard, before starting the tightening process, the thickness of the MEAs was measured at 9 different points on the active areas of the MEAs. The average thickness of the MEA was then calculated taking the average of the measured thicknesses. The locations of the points for each MEA are shown in Figure 3.5, and the measured values of the thickness of each point and the average thicknesses of the MEAs are given in Table 3.1.

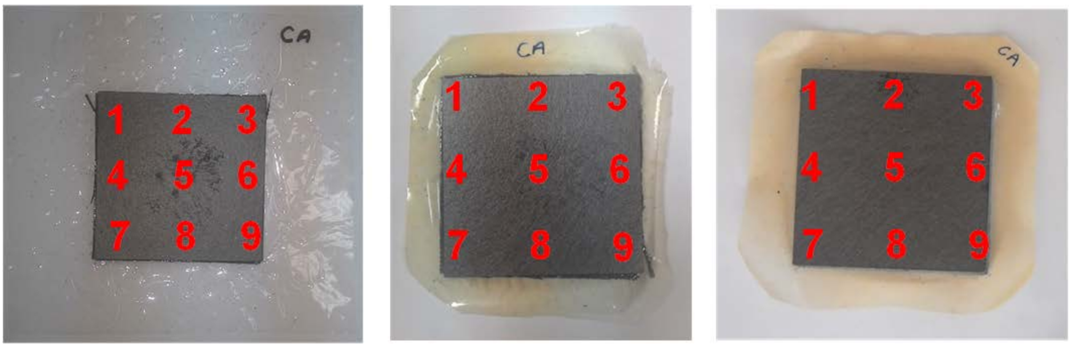

(a) (b) (c)

Figure 3.5 Location of the measurement points for (a) Nafion® 115 membrane based MEA, (b) Nafion/SiO_2 membrane based MEA, and (c) Nafion/TiO_2 membrane based MEA (Ercelik et al., 2017)

Table 3.1 Measured values of the thickness of each point and the average thicknesses of the MEAs

Average MEA Thickness (mm)*	**1**	**2**	**3**	**4**	**5**	**6**	**7**	**8**	**9**	**$t_{average}$**
Nafion® 115	0.948	0.945	0.957	0.952	0.938	0.940	0.936	0.945	0.958	0.947
Nafion/SiO_2	0.860	0.856	0.842	0.861	0.864	0.842	0.854	0.841	0.829	0.850
Nafion/TiO_2	0.825	0.824	0.839	0.815	0.836	0.856	0.831	0.842	0.838	0.834

After the MEAs were placed to the single cell, an pretreatment procedure was applied to make the membrane fully soaked. In this procedure, deionized water and humidified oxygen with very high stoichiometric flow ratios were fed into the anode and cathode flow channels, respectively. In addition, the temperature of the single cell was increased gradually to the desired operating temperature which the experiments were carried out. The pretreatment procedure took around 3 h. `

As the MEA was fully soaked, a test procedure was applied to get the current density for a given voltage, and thus to generate the polarization curve. A computer aided DMFC test station, which is shown in Figure 3.6 and Figure 3.7, was used to obtain the necessary data to generate this curve. During the experiments, the outlet pressure of the oxygen tank was set to 1.50 bar and the pressure at the inlet of the cathode side of the cell was kept at 1.35 bar. The flow rates of the humidified oxygen and methanol solution were set to 200 ml/min and 1.94 ml/min, respectively. The methanol concentration was varied between 0.75 M and 1.50 M (for only the experiments with Nafion® 115 membrane) and the temperature of the cell was changed from 60°C to 95°C. In the experiments, the methanol solution and oxygen were passed through the flow channels. The methanol solution was fed to the cell with the help of a magnetic drive gear pump at a temperature value which is 5°C above the cell temperature. On the other hand, oxygen gas was passed through a mass flow controller and a humidifier before entering the cathode side of the fuel cell. The main reason of using humidifier is to help maintain well-hydrated membrane. In addition, the oxygen gas was also heated at this stage to keep the temperature level of the oxygen gas same with the operating temperature of the fuel cell in order to provide uniform temperature distribution within the cell. Once the fuel cell reached to the steady state condition at the open circuit voltage (OCV), the break-in procedure, in which several voltage steps interrupted by OCV steps were applied, was begun. These steps were applied until the voltage value reached to 0.2 V; and then the same procedure was repeated until the difference between two consecutive polarization curves became negligible. When the measurements were completed, the flow rates of the humidified oxygen and methanol solution were set to zero and nitrogen gas was started to send through the cathode flow channels to throw away the liquid droplets trapped inside the channels.

34

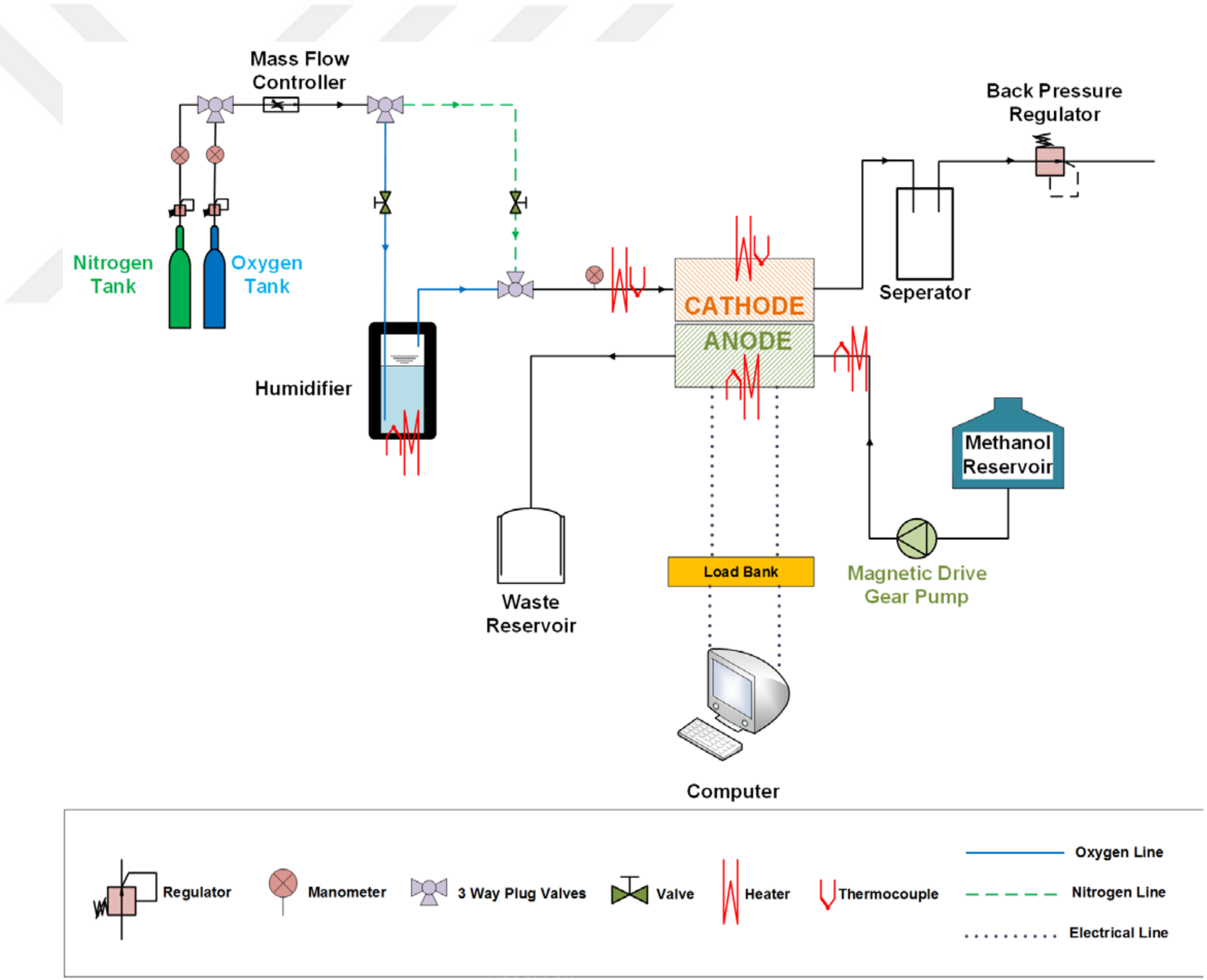

Figure 3.6 Schematic of the computer aided DMFC test station (Ercelik et al., 2017)

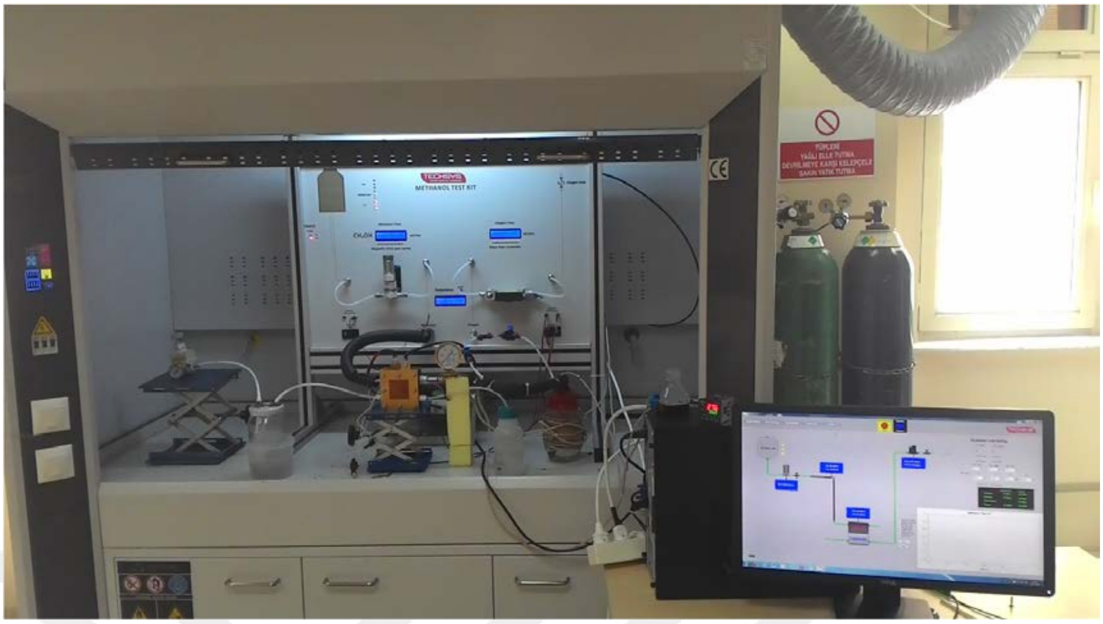

Figure 3.7 The computer aided DMFC test station

3.3 Pt-Ru/C-TiO_2 Anode Catalyst Based DMFCs

The literature survey discussed above indicates that introduction of TiO_2 materials into Pt-Ru/C anode electrocatalyst could be useful for achieving an improved DMFC performance. As already discussed, although some studies have been conducted to investigate the electrochemical, catalytic, stability, and methanol tolerance characteristics of Pt-Ru/C-TiO_2 as a potential anode hybrid catalyst, there is no work in the literature related to the performance comparison of DMFCs based on Pt-Ru/C-TiO_2 anode hybrid catalyst containing commercial and in-house synthesized TiO_2. In this study, a simple preparation procedure of a composite anode hybrid catalyst was carried out, and the performances of the DMFCs based on Pt-Ru/C-TiO_2 anode hybrid catalysts were investigated. Towards this direction, TiO_2 nanoparticles were synthesized by a sol-gel method and Pt-Ru/C-TiO_2 anode hybrid catalysts containing 5, 15, and 25 wt.% of in-house synthesized TiO_2 with respect to the amount of commercial Pt-Ru/C anode hybrid catalyst were prepared. Then, Pt-Ru/C-TiO_2 anode hybrid catalysts with the same weight ratios were also prepared using commercial TiO_2 materials. The DMFCs based on these anode hybrid catalysts were manufactured and a series of experiments were conducted to evaluate the performances of the DMFCs under various operating temperatures (45°C, 60°C, and

80°C) and methanol concentrations (0.50 M, 0.75 M, 1.00 M, and 1.50 M). In addition, 4 h short-term stability tests were carried out for all the DMFCs to assess their short-term stability characteristics.

3.3.1 Materials

The commercially available Nafion® 115 membrane was obtained from DuPont Corp. (Delaware, USA). The cathode electrocatalyst (Platinum, nominally 60% on high surface area advanced carbon support, HiSPEC® 9100) and the anode electrocatalyst (Platinum, nominally 50%, Ruthenium nominally 25% on high surface area advanced carbon support, HiSPEC® 12100) were purchased from Alfa Aesar® (Karlsruhe, Germany). The PTFE treated carbon cloth (ELAT LT1400W) was used as the anode backing layer and obtained from Nuvant Systems Inc. (Crown Point, IN, USA) and used as received. Hydrogen peroxide (Emsure®, chemical purity 30 wt.%) and sulphuric acid (Emsure®, chemical purity 95-97 wt.%) were purchased from Merck (Darmstadt, Germany) and used without further purification. 15 wt.% Nafion solution (equivalent weight = 1100 g mol^{-1} SO_3H) was obtained from Ion Power Inc. (Delaware, USA). All chemicals including isopropyl alcohol (Aldrich) and methanol (Aldrich) were reagent grade and used without further purification. The commercially available TiO_2 (P25) nanoparticles were obtained from Degussa-Huls (Frankfurt-Main, Germany). For the sol-gel synthesis, TiO_2, tetrabutyl-orthotitanate (TBOT) (99% purity, from Aldrich Inc.), nitric acid (65% purity, from Aldrich Inc.), and ethanol (99% purity, from Aldrich Inc.) were used without further purification.

3.3.2 Preparation of In-house TiO_2 Nanoparticles

In this study, a sol-gel method given in (Campbell et al., 1992) was modified to synthesize TiO_2 material having small crystallite sizes. The molar ratio of $[HNO_3]/[Ti] = 0.087$, $[H_2O]/[Ti] = 4$, and $[Ethanol]/[Ti] = 27$ were used in the preparation. First, the required amount of TBOT and ethanol were mixed at room temperature and then water mixed with HNO_3 was added to this ethanol-TBOT mixture. After adding the water-acid mixture, hard transparent TiO_2 gel was obtained in 5 min. The gel was heated from room temperature to 400°C at 10°C/min and calcined at 400°C for 6 h. Finally, calcined TiO_2 gel was ground and sieved to less than 200 µm to use in the preparation of anode hybrid catalyst composites.

3.3.3 Membrane Activation and MEA Manufacturing Process

In order to clean and activate the membranes, the Nafion® 115 membranes (10 cm x 10 cm) were boiled for 1 h at 90°C in each of the following solutions consecutively; 3 wt.% hydrogen peroxide (H_2O_2), deionized (DI) water, 5 wt.% sulphuric acid (H_2SO_4), and deionized (DI) water. After the membranes were cleaned and activated, the following steps were carried out in the MEA manufacturing process. These steps are given in more detail in Section 3.2.2.

As the first step, the electrocatalyst inks were prepared for both the anode and cathode sides. The electrocatalyst loadings at the anode and cathode sides were taken as 4 mg_{PtRu}/cm^2 and 2 mg_{Pt}/cm^2, respectively. Appropriate amounts of deionized water, Nafion® solution, and isopropyl alcohol were added to the electrocatalyst powder to form the ink. Then, the ink was first mixed by magnetic stirrer for 45 min and then ultrasonic bath for 2 h to make the ink more homogeneous. These steps were applied in the preparation of both the cathode and anode electrocatalysts. After the electrocatalyst ink preparation process, electrocatalyst coating process was applied as the second step in the MEA manufacturing process. In this study, the prepared electrocatalyst inks were put into the container of the air spray and then the backing layers with an area of 25 cm^2 were coated by air-spraying technique. During the electrocatalyst coating process, backing layers (carbon cloth for the anode side and the carbon paper for the cathode side) were placed to the vacuum table at 55°C. As the last step, the hot-press process was carried out. In this process, the membrane was placed between the coated cathode and anode backing layers and pressed at 120°C and 6.89 MPa for 4 min (Zhao et al., 2005; Chen et al., 2006).

3.3.4 Performance Testing

The performance tests of the fabricated DMFCs were conducted using the methodology discussed in this section. Firstly, two gaskets with the thickness of 0.1 mm were placed on the cathode and anode flow field plates. The MEA was placed between these gaskets and the assembled cell was tightened. The torque applied for tightening the cell was increased gradually until the compression ratio of the MEA reaches to the range of 20±5% (User instructions for DMFC electrodes & MEAs prior to installation, n.d.). Keeping the compression ratio in this range is crucial for preventing the possible leakage during the operation of the cell and getting higher performance values. This ratio was found by dividing the difference between the non-compressed and compressed MEA thicknesses to the non-compressed thickness of a given MEA as discussed in Section 3.2.3.

After the single cell was assembled as discussed above, the pretreatment procedure was carried out to make the MEA fully-hydrated. In this regard, deionized water and humidified oxygen with very high volumetric flow rates (5 ml/min for the flow rate of deionized water and 1000 ml/min for the flow rate of oxygen) were passed through the anode and cathode flow channels of the single cell, respectively. The operation conditions, such as cell temperature and cathode inlet pressure were chosen as 80°C and 1.35 bar absolute, respectively. This pretreatment period took almost 28 h for each MEA.

After the pretreatment procedure was completed, a performance testing procedure was followed to generate the polarization curve. In-house tests were performed using a custom-built computer aided DMFC test station. During the tests, oxygen gas was passed through a mass flow controller and a humidifier just before entering the cathode side of the fuel cell. At this stage, the line that humidified oxygen passes is heated to keep the temperature of the cell more uniform. On the other hand, methanol solution passes through a magnetic drive gear pump before entering the anode side of the cell. The line that methanol solution passes is also heated. More detailed information about this test station and its components can be found in Section 3.2.4. During the experiments, the flow rates of the methanol solution and oxygen were set to 1.94 ml/min and 400 ml/min, respectively. The outlet pressure of the oxygen tank and the cathode inlet pressure were set to 1.50 and 1.35 bar absolute, respectively. The methanol concentration was varied from 0.50 M to 1.50 M. The operating temperature of the cell was altered from 45°C to 80°C. The voltage was changed between open circuit voltage (OCV) and 0.2 V and the corresponding current values at the steady state conditions were recorded. This procedure was repeated until the difference between the two consecutive polarization curves became negligible.

3.4 Nafion/ZrP Composite Membrane and Pt/C-ZrP Cathode Catalyst Based DMFCs

The literature survey discussed above demonstrates that Nafion/ZrP composite membranes may have a great potential for being used as state-of-the-art material for DMFCs, notably at elevated operating temperatures (>80°C). Although there has been some studies conducted for PEMFCs based on these materials in the literature, there is no significant study comparing the performance of DMFCs having Nafion/ZrP composite membranes (made of different ZrP weight ratios) with DMFCs having Nafion® membranes. In addition, to the best of our knowledge, there is also no work related to the comparison of DMFCs having both Pt/C-ZrP cathode catalyst and Nafion/ZrP composite membrane with DMFC made of conventional materials. Hence, in this study, the effect of Nafion/ZrP composite membranes on the performance of DMFCs was compared with that of DMFC having commercial Nafion® 115 membrane. The performance comparison studies of these DMFCs were conducted at different temperatures (40°C, 60°C, 80°C, and 100°C) and methanol concentrations (0.75 M, 1.00 M, and 1.50 M). In addition, the performance of the DMFC based on Pt/C-ZrP cathode catalyst and Nafion/ZrP membrane was compared with that of the DMFC based on the same membrane but the conventional Pt/C cathode catalyst at the same temperatures and methanol concentrations. In addition, 4 h short-term stability tests were conducted for all the manufactured MEAs to assess their stability characteristics.

3.4.1 Materials

Two different commercially available cathode catalyst powders were purchased: 1) Platinum, nominally 60% on high surface area advanced carbon support, HiSPEC® 9100 from Alfa Aesar® (Karlsruhe, Germany) and 2) HP 60 wt.% Pt on Vulcan XC-72. The commercially available anode catalyst powder (HP 60 wt.% Pt-Ru on Vulcan XC-72) was used as anode catalyst. The commercially available Teflon treated carbon cloth (ELAT LT1400W) used as anode backing layer was obtained from Nuvant Systems Inc. (Crown Point, IN, USA) and used as received. Nafion® 115 membrane was purchased from DuPont Corp. (Delaware, USA). 15 wt.% Nafion solution (equivalent weight = 1100 g mol^{-1} SO_3H) was obtained from Ion Power Inc. (Delaware, USA). Hydrogen peroxide (Emsure®, chemical purity 30 wt.%) and sulphuric acid (Emsure®, chemical purity 95-97 wt.%) were obtained from Merck (Darmstadt, Germany) and used without further purification. N-N Dimethylacetamide (DMAc), was purchased from Merck (Germany). Zirconium hydrogen phosphate (ZrP) was obtained from ChemCruz® Biochemicals (USA). All solvents used were high grade materials without further need for purification. All chemicals, including isopropyl alcohol (Aldrich) and methanol (Aldrich), were of reagent grade and used without further purification.

3.4.2 Membrane Preparation and Characterization

Nafion/ZrP nanocomposite membranes were prepared using the recasting method. A total of 15 wt.% Nafion solution was evaporated at 70ºC until a dry residue was obtained. Nafion resin was redissolved in DMAc to form a solution containing 5 wt.% Nafion. Appropriate amount of ZrP powder was added to achieve better dispersion of ZrP particles and then the mixture was sonicated for an hour. Resulting mixture was cast onto petri dishes and the solvent evaporated at 80ºC. The membrane was removed from the petri dish by wetting with de-ionized water.

Thermal stability of the membranes was determined by TGA method, with Perkin Elmer Pyris 1 TGA Equipment. Temperature range was 25°C-800°C with heating rate of 10°C/min under nitrogen atmosphere.

The crystal structures of the membranes were determined by X-Ray Diffraction (XRD) analysis, using Bruker D8 Advance equipment, over the range $5° \leq 2\Theta \leq 80°$.

The membrane and cathode and anode catalyst layer morphologies were observed by Scanning Electron Microscope (SEM), QUANTA 400F Field Emission SEM system equipped with an energy dispersive X-ray (EDX) spectrometer. Before measurements, the samples were coated with a layer of gold to enhance electrical conduction. Membrane samples were prepared by freezing the membranes in liquid nitrogen and then fracturing them for cross-section SEM images.

Water uptake is considered as one of the most important characteristic properties for proton exchange membranes, which confirms the successful incorporation of hydrophilic groups inside the membrane. For water uptake measurements, membranes were dried in a vacuum oven at 100 °C for 6 h and weighed. Then, the samples were immersed in distilled water for 24 h. Excess water was gently wiped off with a tissue and membrane samples were weighed immediately. The water uptake was calculated using Eq. (3.1).

Proton conductivities of the membranes were determined by electrochemical impedance spectroscopy (EIS), four probe method, using ZIVESP2 Electrochemical Workstation. Four probe method consists of four equally spaced (1 cm for each space) Pt probes. The membranes were cut to fit in the measurement cell so that it interacts with all four probes. AC impedance was measured between 30 MHz and 65 mHz for all the membranes. The measurements were conducted under five different temperatures, 25ºC, 50ºC, 60ºC, 70ºC, and 80ºC. All the measurements were performed in longitudinal direction; in air/water vapour atmosphere with 100% relative humidity. Equation used for calculation of conductivity is given in Eq. (3.2).

Using the conductivity data, activation energies were calculated by Arrhenius equation. Ion transport activation energies were calculated from Arrhenius equation shown in Eq. (3.4) (Park & Yamazaki, 2004):

$$\sigma = \sigma_0 \, exp\left(\frac{-E_a}{RT}\right) \tag{3.4}$$

Where σ ($S\ cm^{-1}$), σ_0 ($S\ cm^{-1}$), E_a ($J\ mol^{-1}$), R ($J\ mol^{-1}\ K^{-1}$), and T (K) denote the ionic conductivity, frequency factor, activation energy for conduction, universal gas constant, and temperature, respectively.

3.4.3 MEA Manufacturing Process

The first step in the MEA manufacturing process is the catalyst ink preparation process. In this process, two different catalyst inks were prepared for the anode and cathode sides to be used in air spraying technique. For this purpose, appropriate amounts of catalyst powder, deionized water, Nafion® solution, and isopropyl alcohol were consecutively mixed by a magnetic stirrer and ultrasonic bath for 30 min and 3 h, respectively. However, to prepare the Pt/C-ZrP cathode catalyst ink, 10 wt.% of ZrP with respect to the amount of cathode catalyst (Pt/C) was added directly to the prepared mixture just before mixing process. Then, the backing layers (carbon cloth for anode and carbon paper for cathode) were placed on a heated-vacuum table (at 50°C) and the prepared inks were sprayed through an air spray gun. The spraying continued until the catalyst loadings of the anode and cathode sides reached to a desired value (4 mg_{PtRu}/cm^2 for the anode and 4 mg_{Pt}/cm^2 for the cathode). The active areas of the backing layers were taken as 25 cm^2. After the coating, the coated backing layers were dried at the room temperature. As the last step in the MEA manufacturing process, the hot-press process was applied. In this process, the membrane dictated by the test of interest (Nafion® 115 or Nafion/ZrP composite membrane) was located between the coated anode and cathode backing layers and pressed at 120°C and 6.89 MPa for 4 min (Lim & Wang, 2003; Chen et al., 2006). The composition of all the MEAs prepared for testing is summarized in Table 3.2.

Table 3.2 Specifications of the MEAs

MEA	**Membrane Type**	**wt.% ZrP in Membrane**	**Catalyst Type**	**Anode Loading (mg_{PtRu}/cm^2)**	**Cathode Loading (mg_{Pt}/cm^2)**	**wt.% ZrP in the cathode catalyst**
MEA-1	Nafion® 115	0	HP	4	4	0
MEA-2	NZ-2.5	2.5	HP	4	4	0
MEA-3	NZ-5	5	HP	4	4	0
MEA-4	NZ-2.5	2.5	HiSPEC® 9100	4	4	0
MEA-5	NZ-2.5	2.5	HiSPEC® 9100	4	4	10

3.4.4 Performance Testing

The performances of the MEAs manufactured using the procedure discussed in Section 3.3.4 were tested through in-house experimental studies. Before the experiments, the channels of the flow-field plates were cleaned using a soft brush to remove the undesired inorganic particles. Then, two gaskets with the thicknesses of 0.1 mm were placed to the anode and cathode sides to prevent the cell from leakage problem. The MEA located between the gaskets was compressed applying a compression torque, which was increased gradually until a desired value of relative MEA compression ratio (Eq. (3.5)) was achieved. For this study, this ratio was considered as 20 ± 5% (User instructions for DMFC electrodes & MEAs prior to installation, n.d.). In this equation, uncompressed MEA thickness was calculated taking the average values of 9 different points within the active area of the MEA.

$$\text{Relative MEA Compression (\%)} = \frac{(\text{Uncompressed MEA thickness}) - (\text{Compressed MEA thickness})}{(\text{Uncompressed MEA thickness})} \tag{3.5}$$

After the MEA was placed to the single cell, a series of in-house experiments were carried out using a computer-aided DMFC test station. The schematic of the test station is shown in Figure 3.6 in Section 3.2.4. The operating principle of the test station can be summarized as follows. Methanol flows through the magnetic gear pump before it enters the cell, whereas oxygen first flows through the micro-flow controller and then enters the humidifier. Humidified oxygen enters the cell in order to keep the cathode side of the membrane hydrated. In addition, to keep the temperature inside the cell at a desired value and uniform, several heaters are placed before the anode and cathode inlets and also on the top and bottom of the cell. At the cathode outlet, the products are passed through a seperator to seperate the liquid and gas streams before they enter the back pressure regulator.

At the beginning of the experiments, the pretreatment procedure was carried out to make the membrane well-hydrated and the MEA ready for performance testing procedure. Towards this direction, deionized water with the flow rate of 5 ml/min and humidified oxygen with the flow rate of 1000 ml/min were passed through the anode and cathode flow channels, respectively, for 3 h. The pressure at the cathode inlet of the cell was kept at 1.35 bar using a pressure regulator. Once the pretreatment procedure was completed, the flow rates of the humidified oxygen and methanol solution were set to 200 ml/min and 1.94 ml/min, respectively. After the open circuit voltage (OCV) was achieved, several voltage steps (between OCV and 0.2 V) interrupted by OCV steps were applied. Several polarization curves were generated recording the current density at each voltage step. This process continued until the difference between two consecutive curves became negligible. The values at the last iteration were used for plotting the polarization curve of that specific experiment. Once all the relevant data were obtained, the flow rates of the humidified oxygen and methanol solution were set to zero, and nitrogen gas was sent through the flow channels to dry the fully soaked membrane and the flow channels.

CHAPTER FOUR
RESULTS AND DISCUSSIONS

4.1 Introduction

In chapter four, experimental results of chapter three are discussed separately. Firstly, characterization results of Nafion/TiO_2 and Nafion/SiO_2 composite membranes and performance results of DMFCs based on these membranes are given and discussed in this chapter. Secondly, physical characterizations of PtRu/C and PtRu/C-TiO_2 hybrid catalyst, and performance testing results of PtRu/C-TiO_2 anode catalyst based DMFCs are given and discussed. In the last part of this chapter, characterization results for Nafion/ZrP based composite membranes and Pt/C-ZrP based cathode catalyst and experimental results for DMFCs based on these materials are given and discussed.

4.2 Nafion/TiO_2 and Nafion/SiO_2 Composite Membrane Based DMFCs

4.2.1 Membrane Characterization

Table 4.1 shows the proton conductivity of the Nafion and composite membranes. The addition of nanoparticles enhances the proton conductivity of the Nafion-based composites. The proton conductivities of the Nafion/TiO_2 and Nafion/SiO_2 composite membranes are higher than Nafion membrane with increasing temperature. At all temperatures the Nafion/TiO_2 membranes showed higher conductivity than both the bare Nafion and the composite membranes with SiO_2. The maximum proton conductivity at 75°C is ordered amongst the samples as follows: Nafion/TiO_2>Nafion/SiO_2>Nafion. The highest proton conductivity of the Nafion/TiO_2 nanocomposite membrane was 0.255 Scm^{-1}, 25 % higher than that of the Nafion membrane at 75°C. The increase degree of the proton conductivities by inserted nanoparticles in the composite membranes is acceptable and reasonable in this experiment. The improved proton conductivity could be explained by the hydrophilic nature of TiO_2 and SiO_2 nanoparticles. The increase trend of the proton conductivities agrees with the results reported by Devrim (2014). Water uptake values were determined by measuring the weight of water swollen and dry membranes. As proton conductivity is thermally activated, it is obvious to expect a rise in the proton conductivity with temperature. At high temperature Nafion membrane has lower proton conductivity than composite membranes. The lower values in the conductivity observed at high temperatures for Nafion membrane suggests dehydration of the membrane. Table 4.1 also shows the water uptake of Nafion and composite membranes. The water uptake values follow the order Nafion>Nafion/TiO_2>Nafion/SiO_2. This result is due to the hygroscopic affinity of the inorganic filler and their high water-absorption capacity (Sahu et al., 2009).

Table 4.1. Water uptake and proton conductivity of Nafion and Nafion composite membranes (Ercelik et al., 2017)

Membrane	**Water uptake (%)**	**Proton conductivity (S/cm)**		
		30°C	**55°C**	**85°C**
Nafion	37	0.135	0.187	0.205
Nafion/TiO_2	39	0.130	0.190	0.280
Nafion/SiO_2	47	0.115	0.189	0.240

The morphological properties of the composite membranes depend on dispersibility between the inorganic components and polymer. The morphological properties of the Nafion, Nafion composite membranes were characterized by SEM analysis. The surface of bare Nafion membranes was generally smooth (Figure 4.1). The EDX spectrum of Nafion membrane shows the presence of carbon, oxygen, flour and sulphur. Figure 4.1b shows SEM image of Nafion/TiO_2 membrane. TiO_2 particles were dispersed in the matrix homogeneously and no sedimentation was observed for this membrane. The EDX spectrum confirms the presence of C, O, F, S and Ti indicating TiO_2 particles reside in the Nafion/TiO_2 composite membrane.

SEM image and EDX spectrum of the Nafion/SiO_2 composite membrane are shown in Figure 4.1c. The EDX spectrum confirms the presence of C, O, F, S and Si indicating SiO_2 particles in the Nafion/SiO_2 composite membrane. As seen from SEM images, TiO_2 and SiO_2 additives were incorporated into composite membranes homogeneously and they were uniformly distributed.

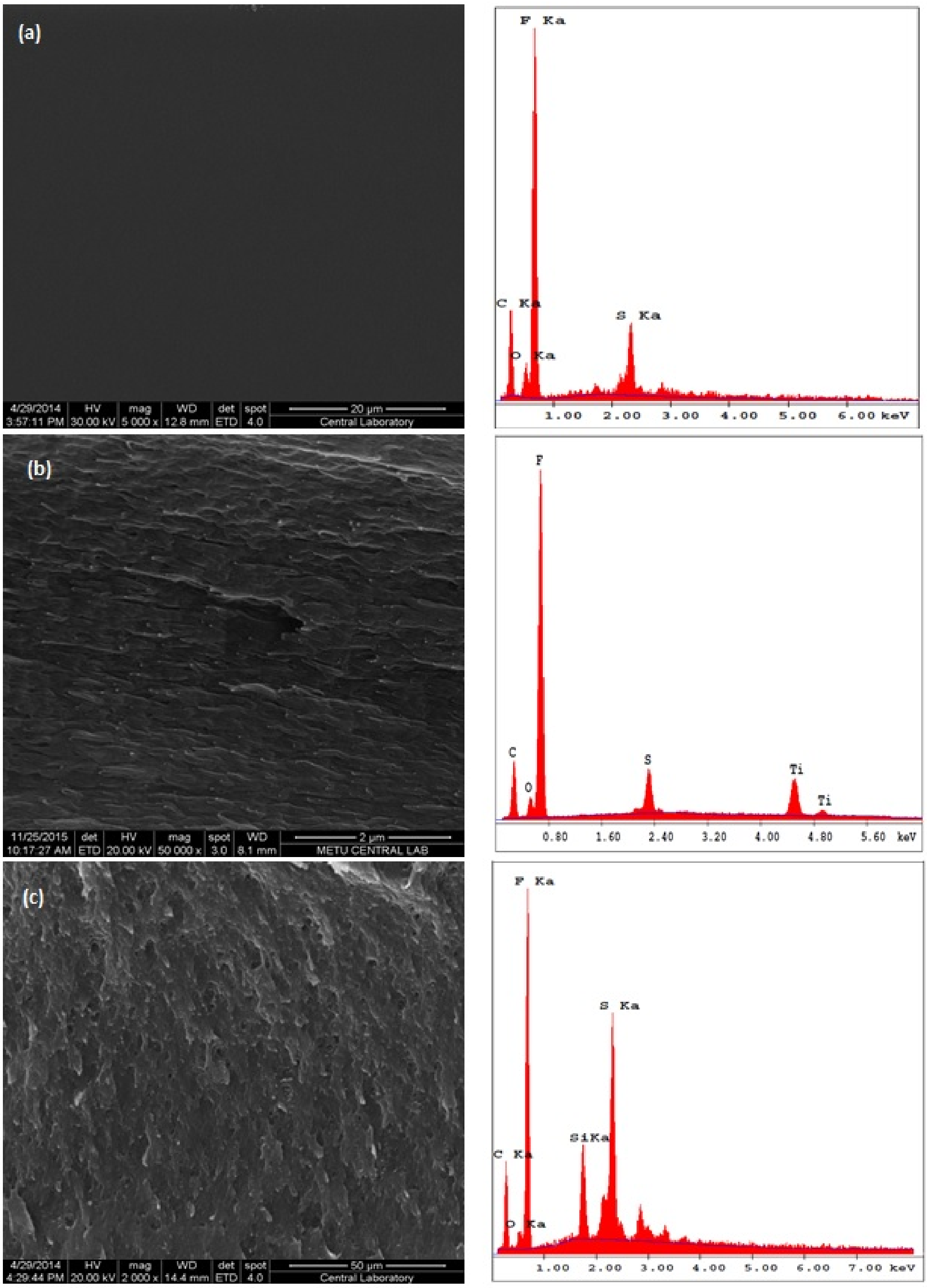

Figure 4.1 SEM images and EDX spectrum of a) Nafion, b) Nafion/TiO_2 and c) Nafion/SiO_2 membranes (Ercelik et al., 2017)

EDX spectrum of Nafion/SiO_2 membrane confirms the presence of Si, C, O, F and S. Presence of Si, indicates SiO_2 inorganic particles reside in the composite membrane.

4.2.2 Performance Study

4.2.2.1 Effect of Methanol Concentration

The effect of different methanol concentrations (0.75 M, 1.00 M, and 1.50 M) on the performance of commercial Nafion® 115 membrane was first investigated. Then, the highest performance of Nafion® 115 found was compared with the performances of Nafion/SiO_2 and Nafion/TiO_2 composite membranes at different operating temperatures (60°C, 80°C, and 95°C). For these purposes, the MEAs were manufactured using ultrasonic coating technique as mentioned in Section 3.2.3. With the help of the ultrasonic coating technique, the anode and cathode catalyst inks were coated homogeneously and efficiently. As can be seen from Table 3.1, the thickness of the coated membrane is almost constant through the active area (25 cm^2).

Methanol concentration is one of the key parameters affecting the performance of the DMFCs. In the literature, there is a conflict between the conducted studies on the effect of methanol concentration on the DMFC performance. That is, the maximum power density is achieved at different values of methanol concentrations (Yang et al., 2001; Chien et al. 2013; Liang et al., 2016; Gago et al., 2015; Surampudi et al., 1994; Changhwan et al., 2009). As the performance of a DMFC depends on the MEA architecture and the fuel cell station, it was essential to carry out experiments to find the value of the methanol concentration that gives the highest performance of the MEA having Nafion® 115. The results of the experiments conducted for studying the effect of the methanol concentration on the MEA having Nafion® 115 membrane are shown in Figure 4.2. The results show that the maximum power density achieved was found as 612.96 W/m^2 when the concentration of methanol was taken as 1.00 M; and thus the optimum methanol concentration for this study could be considered as 1.00 M. When the concentration of methanol was taken as 0.75 M and 1.50 M, the power densities were found as 603.84 W/m^2 and 427.28 W/m^2, respectively. As discussed in the literature (e.g. Surampudi et al., 1994), the reason of the performance drop after 1.00 M methanol concentration could be related to the increase in the negative effects of methanol crossover and carbon monoxide (CO) poisoning of anode electrocatalyst.

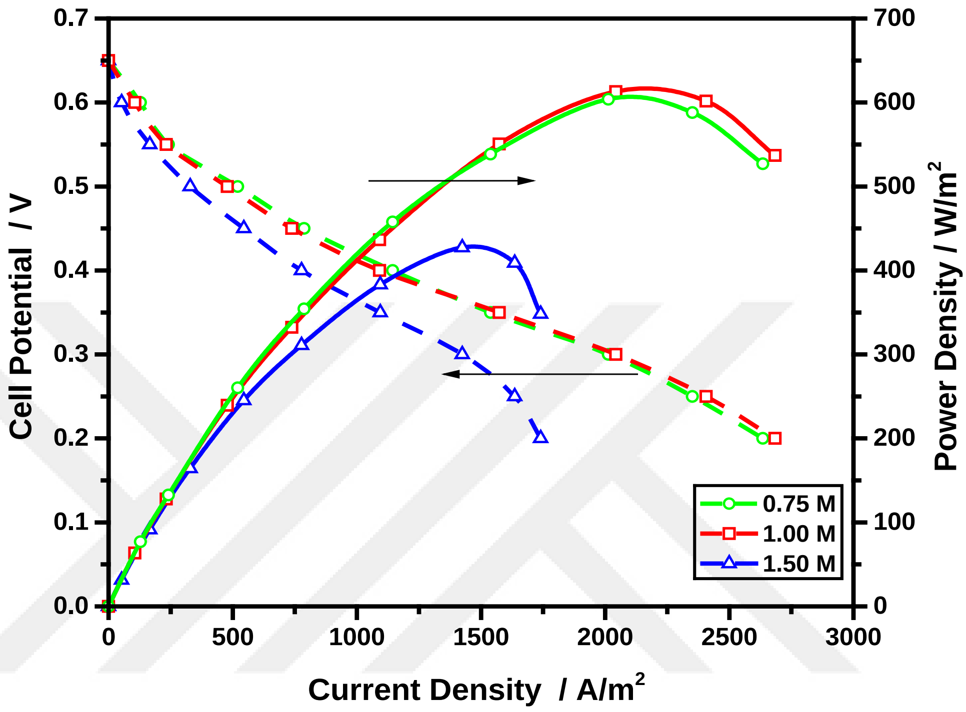

Figure 4.2 Power and polarization curves of the 0.75 M, 1.00 M and, 1.5 M methanol concentration

4.2.2.2 Effect of Operating Temperature

After finding the highest performance of the MEA having Nafion® 115 membrane (maximum power density of 612.96 W/m^2), the experiments were carried out to compare this membrane with the Nafion based composite membranes. In these experiments, the molar concentration of methanol was taken as constant at 1.00 M. The polarization curves generated as a result of these experiments are given in Figure 4.3, 4.4, and 4.5 for temperatures of 60°C, 80°C, and 95°C, respectively.

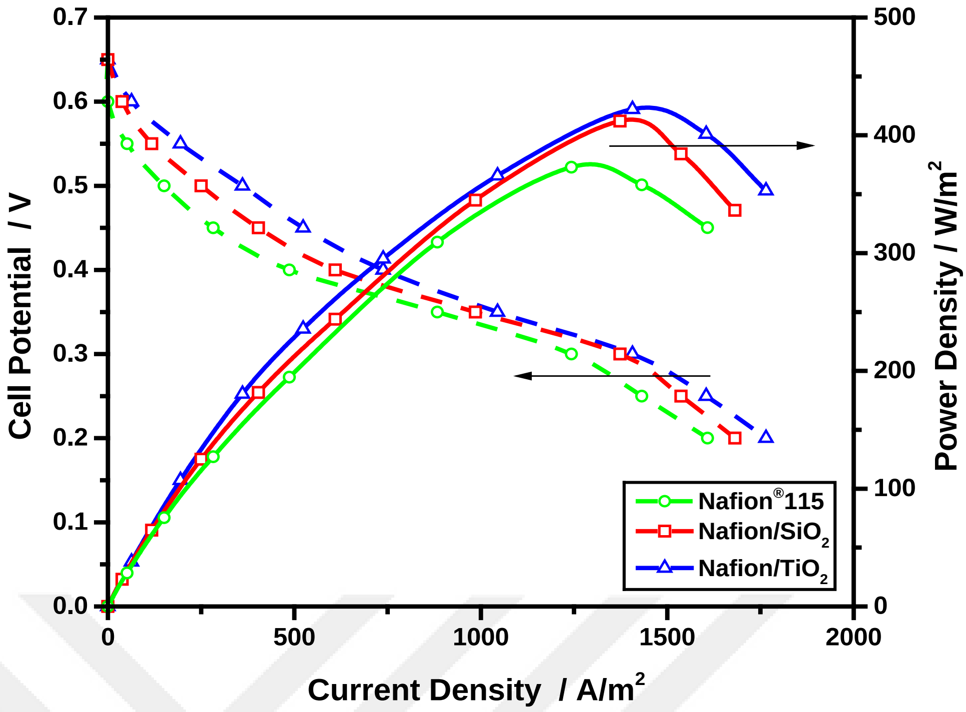

Figure 4.3 Power and polarization curves at 60°C

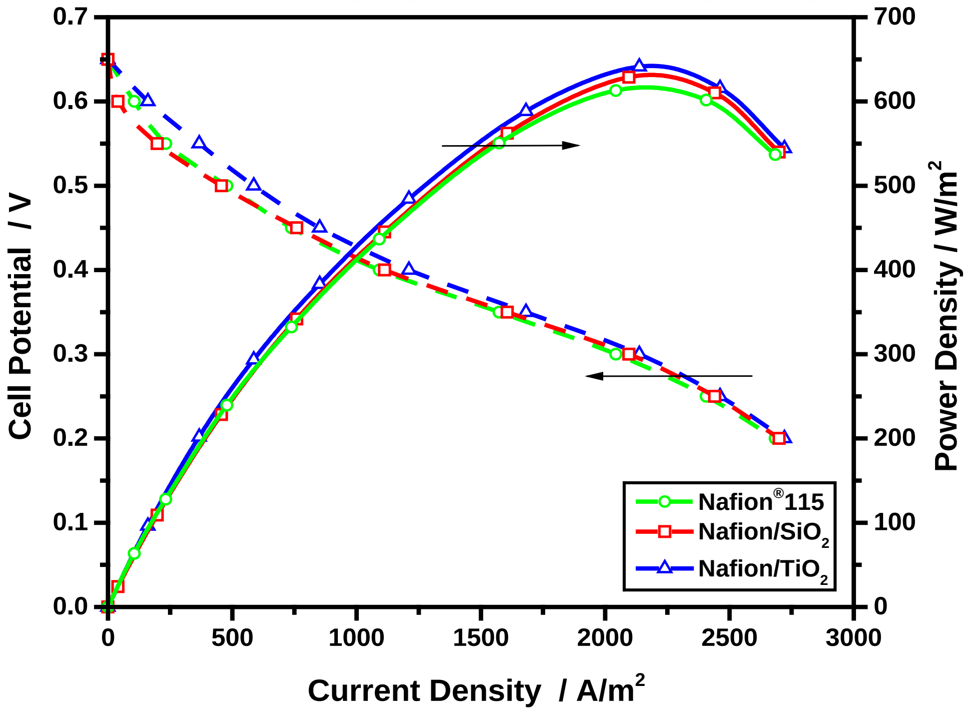

Figure 4.4 Power and polarization curves at 80°C

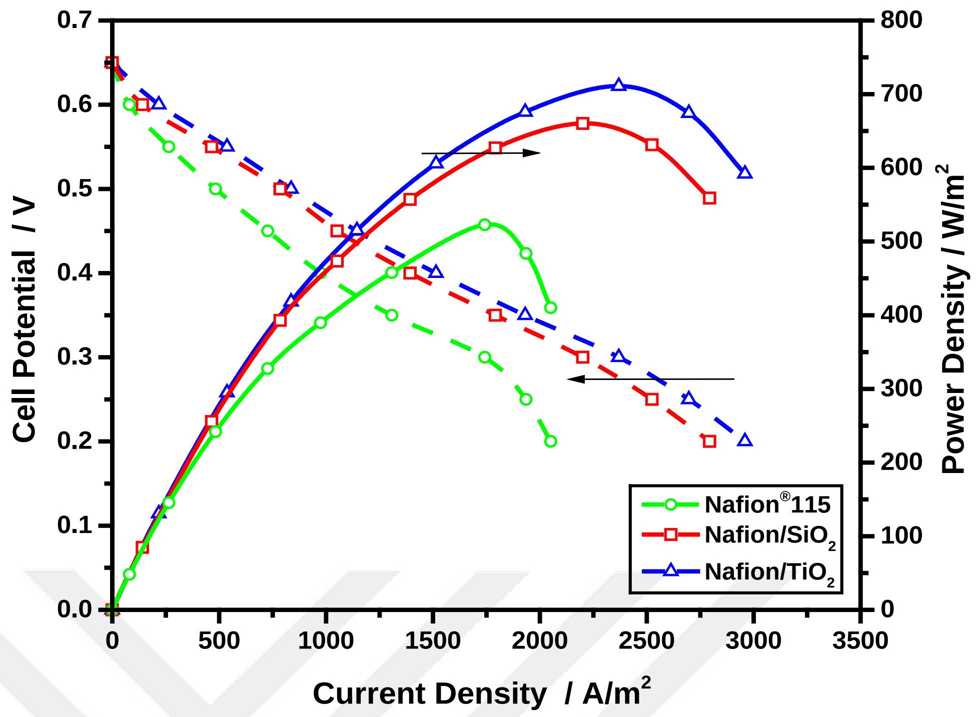

Figure 4.5 Power and polarization curves at 95°C

As it can be seen from Figure 4.3, 4.4. and 4.5, for all the MEAs, as the temperature increases from 60°C to 80°C, the performance improves as expected. More specifically, for this increase of temperature, the maximum power density increases from 372.96 W/m^2 to 612.96 W/m^2, 412.08 W/m^2 to 628.68 W/m^2, 422.04 W/m^2 to 641.16 W/m^2 for the MEAs having Nafion® 115, Nafion/SiO_2, and Nafion/TiO_2, respectively. As the temperature gets higher than 80°C, the reaction kinetics increase and the risk of CO poisoning decreases, meanwhile, the Nafion® membranes lose their ability to conduct protons because of drying (Yang et al., 2001; Tang et al., 2006). The problem of drying is eliminated incorporating some inorganic materials including SiO_2 and TiO_2 particles into membrane to generate bonds between the water molecules and ions. With the help of these bonds, the composite membranes maintain its ability to conduct protons and thus they yield better performance at elevated temperatures. When the temperature increases from 80°C to 95°C, the performances of the MEAs having Nafion/SiO_2 (from 628.68 W/m^2 to 660.24 W/m^2), and Nafion/TiO_2 (from 641.16 W/m^2 to 710.88 W/m^2) composite membranes increase; whereas the MEA having Nafion® 115 membrane decreases (from 612.96 W/m^2 to 552.72 W/m^2).

When the operating temperature was set to 60°C, the maximum power density (422.04 W/m^2) of the Nafion/TiO_2 composite membrane based MEA was found to be higher than that of the MEAs with Nafion® 115 (372.96 W/m^2) and Nafion/SiO_2 (412.08 W/m^2) membranes. For the comparison of the membranes at 80°C, it was seen that the difference in the polarization curves between the commercial Nafion® 115 and Nafion based composite membranes got lower. The maximum power densities are measured as 641.16 W/m^2, 628.68 W/m^2, and 612.96 W/m^2 for the MEAs having Nafion/TiO_2, Nafion/SiO_2, and Nafion® 115, respectively. As the temperature gets 80°C, the MEA having Nafion® 115 membrane yields its best performance. However, at elevated temperatures, membrane resistance and charge-transfer resistance increase considerably. On the other hand, it is also known that, when the fuel cell temperature increases, a methanol crossover enhancement is evident, and there is an increase in membrane diffusivity to methanol (Casalegno et al., 2007). Similar behavior can also be observed in the results of the experiments conducted by Tang. et al. (2006) and Casalegno et al. (2007). The superiority of the Nafion based composite membranes on the performance of the DMFC becomes more visible at 95°C. For this temperature, the Nafion/TiO_2 composite membrane based MEA provided much higher power density (with the value of 710.88 W/m^2) as compared to other MEAs with Nafion/SiO_2 and Nafion® 115 membranes. The maximum power density of the MEA having Nafion/SiO_2 (660.24 W/m^2) showed better performance than that of the MEA having Nafion® 115 membrane (522.72 W/m^2). The composite membranes provide much better performance due to their improved proton conductivity especially at elevated temperatures. Nafion® 115 membranes, however, demonstrates worse performance because of membrane hydration as the temperature reaches to high temperature values.

4.3 Pt-Ru/C-TiO_2 Anode Catalyst Based DMFCs

4.3.1 Physical Characterization of Electrocatalysts

Wide-angle X-Ray Diffraction (XRD) (Philips X'pert Pro XRD, operated at 40 kV and 45 mA) was used to determine the crystalline phases present in the anode composite, sol-gel made TiO_2 and commercial TiO_2 (P25) and also average crystallite sizes were calculated from the peak broadening of the highest intensity diffraction peaks using Scherrer equation. As seen from Figure 4.6 (a) and (b), the diffraction peaks observed at ~25.3° of 2Θ corresponds to carbon (002) crystalline plane and also to (101) crystalline plane of anatase TiO_2. Unfortunately, it is difficult to distinguish TiO_2 from carbon since the amount of carbon is much larger than TiO_2; thus, not being possible to observe the other diffraction peaks of TiO_2 at higher 2Θ. However, as seen in Figure 4.6(c) and (d), XRD patterns of sol-gel made TiO_2 and commercial TiO_2 (P25) show that the sol-gel made TiO_2 consists of solely anatase crystalline phase of TiO_2, whereas commercial TiO_2 (P25) is a mixture of anatase and rutile crystalline phases. The locations of the diffraction peaks are found using Powder Diffraction File of International Centre for Diffraction Data (Joint Committee on Powder Diffraction Standards (JCPDS)-International Centre for Diffraction Data (ICDD), 2014). The average crystallite size for the anatase phase in sol-gel made TiO_2 calculated using Scherrer equation is 11.98 nm (±1 nm), while the average crystallite sizes for anatase and rutile phases in the commercial TiO_2 are 19.51 nm (±1 nm) and 33.89 nm (±1 nm), respectively. Sol-gel made TiO_2 has smaller crystallite size than commercial TiO_2. Besides, the 2Θ peaks observed at ~40, 47 and 68° 2Θ as seen in Figure 4.6 (a) and (b) are due to the presence of metallic Pt, whereas no diffraction peaks corresponding to metallic Ru is observed; thus, the crystallite size of Ru is less than 5 nm. In fact, it is known that the crystallite sizes less than 3-5 nm cannot be observed with wide-angle X-Ray Diffraction (XRD) (Cullity, 1978). In this thesis, XRD results for PtRu/C are in parallel with the literature (Khotseng et al., 2016; Wang et al., 2008). Moreover, it was found that the addition of TiO_2 made with modified sol-gel method did not change the crystalline phases of PtRu/C anode hybrid catalyst.

The element mapping obtained using Energy Dispersive X-Ray (EDX) seen in Figure 4.7 (a) and (b) shows that Ti, Ru, Pt, and O elements are fairly well dispersed on the anode which are in parallel with the XRD results seen in Figure 4.6 (a), (b), (c), and (d).

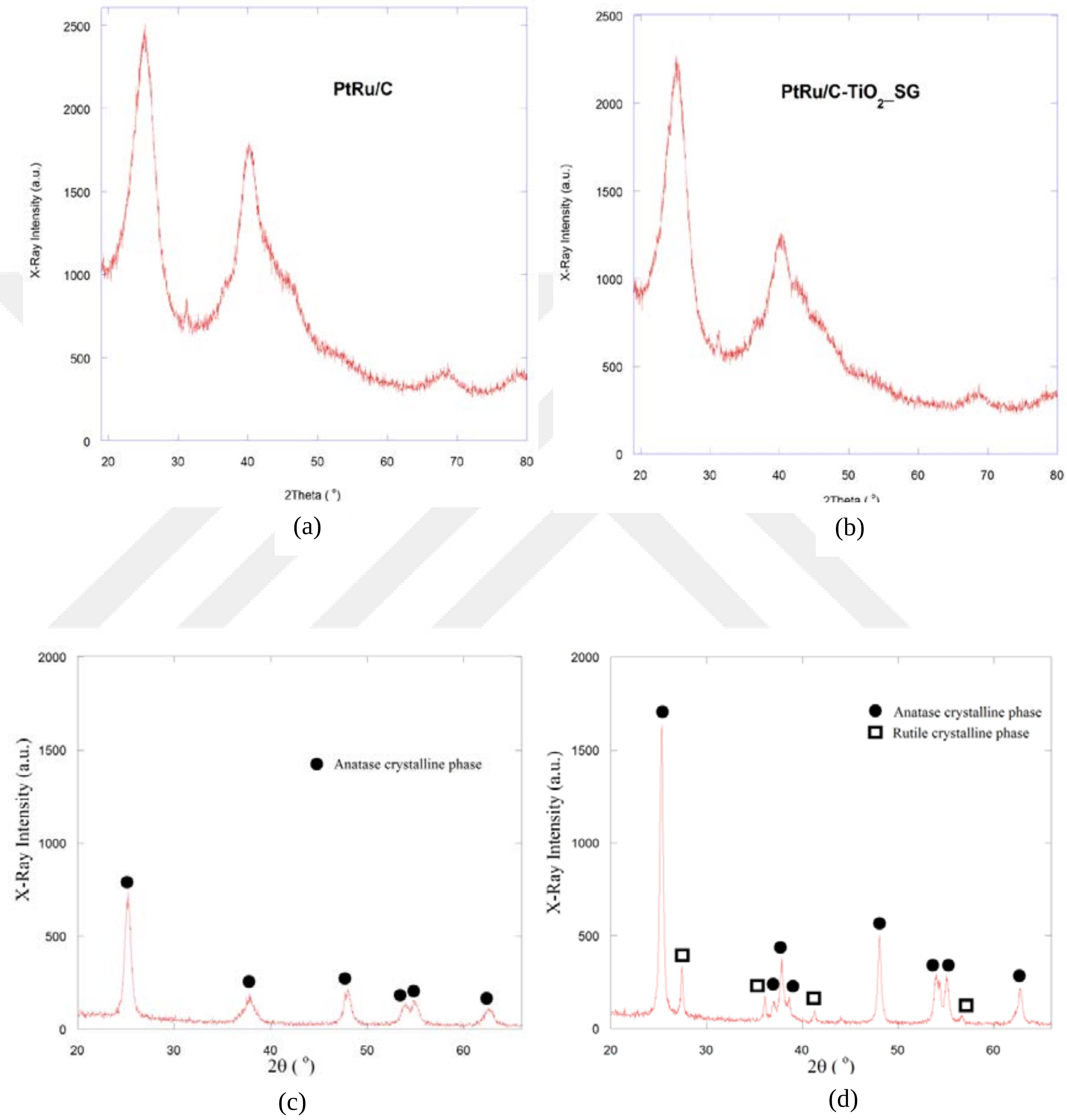

Figure 4.6 XRD diffraction patterns for a) PtRu/C anode, b) PtRu/C sol-gel made TiO_2 anode composite, c) sol-gel made TiO_2, and d) Commercial TiO_2 (P25) (Ercelik et al., 2016)

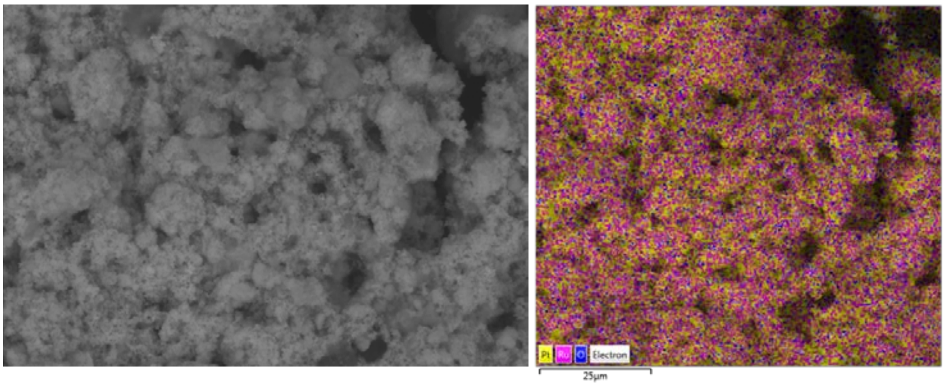

(a)

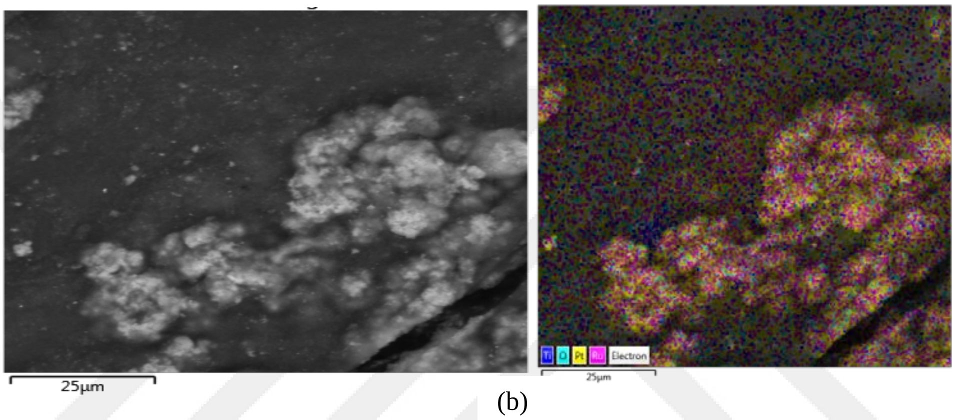

(b)

Figure 4.7 EDX element analyses for a) PtRu/C anode and b) PtRu/C sol-gel made TiO_2 anode composite (Ercelik et al., 2016)

4.3.2 Performance Testing of the DMFCs

As discussed in Section 3.2.4, the MEAs with 25 cm^2 active areas were manufactured using air-spraying technique to investigate the effect of introduction of TiO_2 nanoparticles directly to commercial Pt-Ru/C anode hybrid catalyst and to compare the performances of DMFCs based on Pt-Ru/C-TiO_2 and Pt-Ru/C anode electrocatalysts. In this section, the effects of operating temperature, methanol concentration, the weight ratio of TiO_2 on the performance of the manufactured DMFCs are discussed. In addition, the results of the short-term stability tests of these DMFCs are presented.

4.3.2.1 *Effect of Operating Temperature*

Operating temperature is one of the main parameters that has an influence on both the electrode activation (Chu & Jiang, 2006; Kumar et al., 2007) and methanol crossover (Jiang & Chu, 2004). Basically, increasing operating temperature leads to following effects: an improvement in the reaction rate of electro-oxidation of methanol at the anode, an increase in the rate of undesired methanol crossover from the anode to cathode mainly due to swelling of the membrane, a deterioration in the dimensional stability of the membrane, and finally an improvement in the rate of oxygen reduction reaction (ORR) at the cathode (Tang et al., 2006; Casciola et al., 2006). The simultaneous effects of the above-mentioned phenomena generally bring an increase in the overall performance of the DMFCs made of conventional materials up to 80°C. Taking the operating temperature higher than 80°C is known to cause membrane dehydration (Devrim et al., 2012), a higher rate of methanol crossover (Zhao & Xu, 2009), and catalyst degradation (Yang et al., 2001). As the introduction of TiO_2 to the anode hybrid catalyst may cause a different combined effect, a series of experiments were carried out at the operating temperatures of 45°C, 60°C, and 80°C, the constant methanol concentration of 1.00 M, the methanol flow rate of 1.94 ml/min, and the oxygen flow rate of 400 ml/min.

The power and polarization curves obtained from the experiments conducted with the DMFCs based on Pt-Ru/C-TiO_2 (in-house synthesized and commercial) and Pt-Ru/C anode electrocatalysts are presented in Figure 4.8. Figure 4.8 (a), (b), and (c) exhibit the effect of operating temperature on the performance of the DMFCs based on Pt-Ru/C-TiO_2 anode hybrid catalysts containing 5, 15, and 25 wt.% of TiO_2, whereas Figure 4.8 (d) exhibits the performance of the DMFC based on Pt-Ru/C anode electrocatalyst.

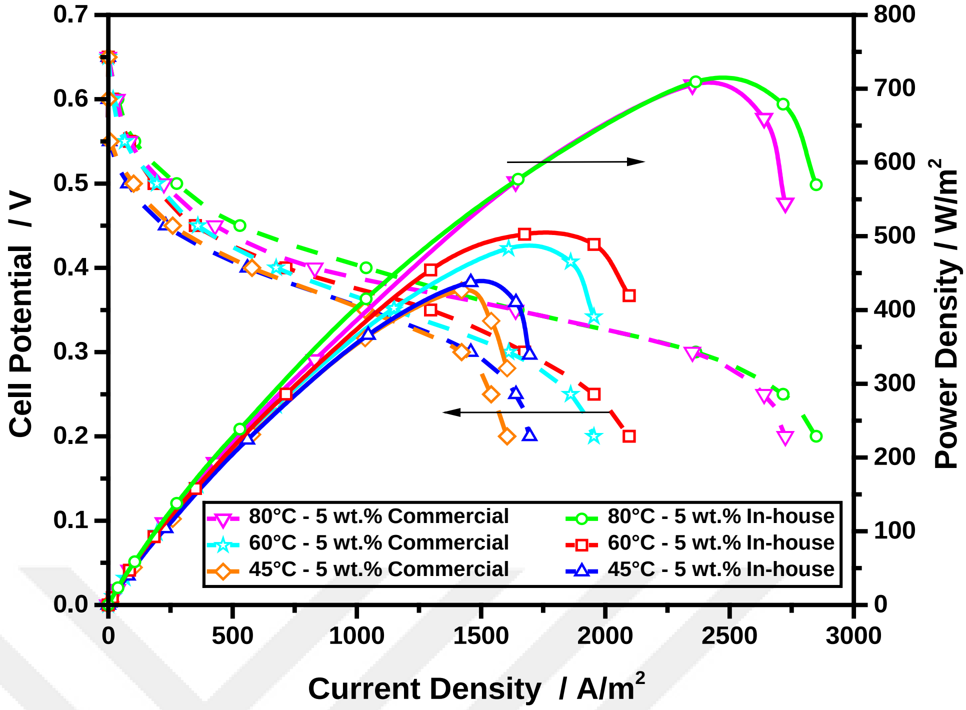

(a)

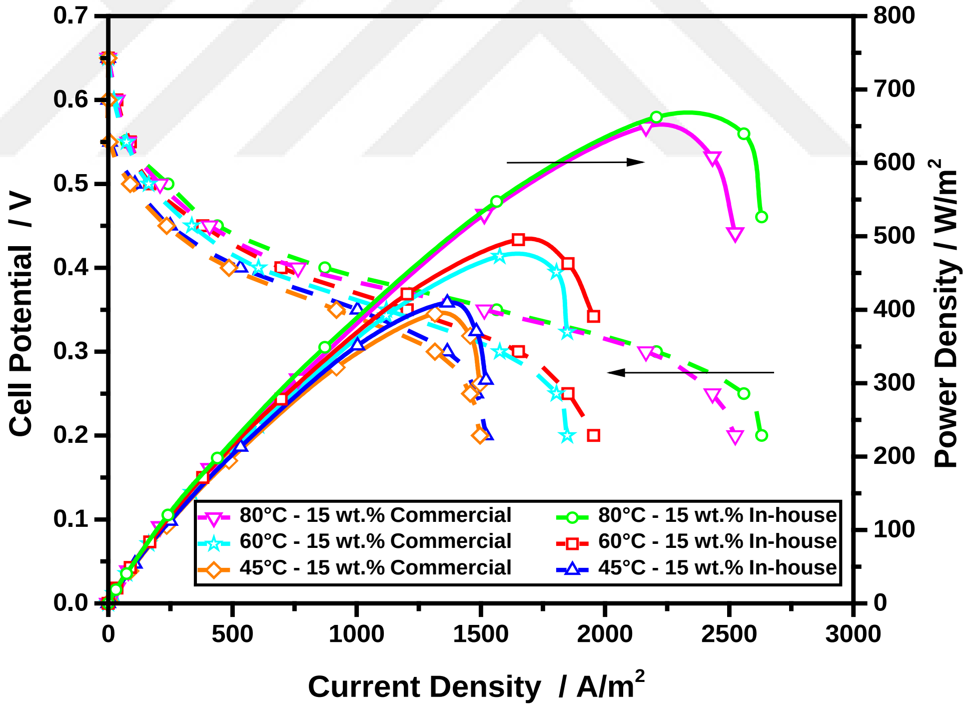

(b)

Figure 4.8 Power and polarization curves at 45°C, 60°C, and 80°C and 1.00 M methanol concentration for the DMFCs based on Pt-Ru/C-TiO_2 anode hybrid catalyst a) with 5 wt.% of commercial and in-house TiO_2, b) with 15 wt.% of commercial and in-house TiO_2, c) with 25 wt.% of commercial and in-house TiO_2, and d) without TiO_2

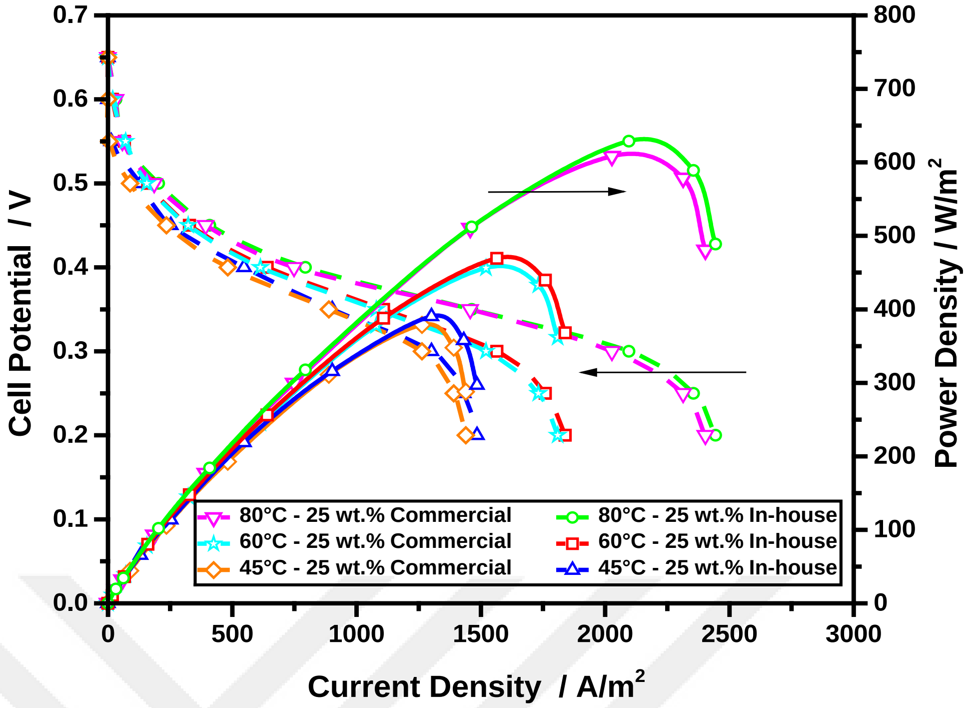

(c)

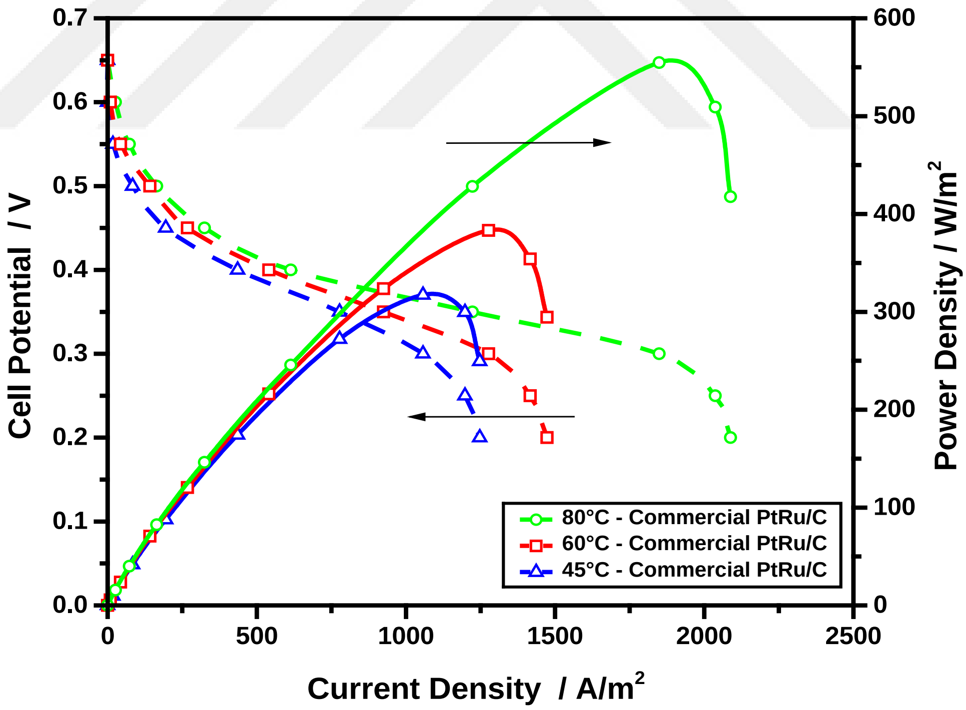

(d)

Figure 4.8 Power and polarization curves at 45°C, 60°C, and 80°C and 1.00 M methanol concentration for the DMFCs based on Pt-Ru/C-TiO_2 anode hybrid catalyst a) with 5 wt.% of commercial and in-house TiO_2, b) with 15 wt.% of commercial and in-house TiO_2, c) with 25 wt.% of commercial and in-house TiO_2, and d) without TiO_2 (continue)

These figures elucidate that with an increase in the operating temperature in the range of 45°C and 80°C, the performance of the DMFCs containing Pt-Ru/C-TiO_2 anode hybrid catalysts improves in a similar manner with the DMFC containing conventional Pt-Ru/C anode electrocatalyst. It was also seen that the DMFCs based on Pt-Ru/C-TiO_2 anode hybrid catalysts containing 15 and 25 wt.% of both in-house and commercial TiO_2 yield better performance in comparison to the TiO_2-free DMFC at any given temperature. As the temperature increases from 45°C to 80°C, the peak power densities for the DMFC without TiO_2 and with 5, 15, and 25 wt.% of in-house TiO_2, increase from 317.16 W/m^2 to 554.64 W/m^2, 437.52 W/m^2 to 709.32 W/m^2, 409.44 W/m^2 to 662.16 W/m^2, 390.48 W/m^2 to 628.68 W/m^2, respectively. At 80°C, it was found that the maximum power densities of the DMFCs based on Pt-Ru/C-TiO_2 anode hybrid catalyst containing 5 wt.% of commercial and in-house TiO_2 are 27.1% and 27.9% higher than that of the DMFC based on commercial Pt-Ru/C anode electrocatalyst. The better performance gained by the addition of TiO_2 to the anode electrocatalyst could be explained as follows (Baglio et al., 2013). The robust electronic interactions between the introduced TiO_2 nanoparticles and Pt-Ru/C may deteriorate adsorption ability of the intermediates and thus facilitates the conversion of the intermediates into CO. In addition, TiO_2 nanoparticles play a significant role in the enhancement of the electrocatalytic properties of the Pt-Ru/C anode hybrid catalyst by increasing the interface and utilizing Pt. TiO_2 nanoparticles could also be beneficial in increasing the rate of water displacement process, which is basically intermediary process in the MOR. Ordinarily, this intermediary process is conducted by Ru in conventional DMFCs based on commercial Pt-Ru/C anode electrocatalyst. Therefore, the main contribution of TiO_2 nanoparticles to the DMFC performance could also be related to this acceleration in the water discharging.

4.3.2.2 Effect of Methanol Concentration

The methanol concentration is another key parameter that possesses a significant effect on the performances of the DMFCs (Barbera et al., 2016). Thus, in order to investigate the effect of methanol concentration on the performance of the DMFC containing Pt-Ru/C-TiO_2 anode hybrid catalyst, the experiments were carried out at the methanol concentrations of 0.50 M, 0.75 M, 1.00 M, and 1.50 M, the operating temperature of 80°C, the methanol flow rate of 1.94 ml/min, and the oxygen flow rate of 400 ml/min. The results of the performed experiments demonstrated that as the methanol concentration was increased from 0.50 M to 1.00 M, the peak power densities also increased, whereas the peak power densities decreased at the methanol concentrations more than 1.00 M for all the DMFCs based on both Pt-Ru/C-TiO_2 hybrid catalyst and commercial Pt-Ru/C anode electrocatalysts (Figure 4.9). When the DMFCs were fed with 1.00 M methanol solution, the maximum power densities were achieved as 705.12 W/m^2, 649.44 W/m^2, 608.16 W/m^2, 709.32 W/m^2, 662.16 W/m^2, and 628.68 W/m^2 for the DMFCs based on Pt-Ru/C-TiO_2 anode hybrid catalysts with 5, 15, and 25 wt.% of commercial and in-house TiO_2, respectively. For the DMFC based on commercial Pt-Ru/C anode electrocatalyst, the value of the maximum power density was found as 554.64 W/m^2 when the DMFC was operated at 1.00 M solution. For all studied methanol concentrations (0.50 M, 0.75 M, 1.00 M, and 1.50 M), the maximum power densities were provided by the DMFC based on Pt-Ru/C-TiO_2 anode hybrid catalyst with 5 wt.% of in-house TiO_2, whereas the lowest power densities were achieved for the DMFC based on Pt-Ru/C anode electrocatalyst.

The results of the above-mentioned experiments can be explained by the fact that the concentration of the methanol supplied to the DMFC has a remarkable impact on both the mass transport rate of the methanol from flow channels to the electrocatalyst coated surface of the backing layer and the rate of methanol crossover from the anode to cathode. When methanol is supplied at low concentrations such as 0.50 M, the limiting current density becomes low and thus results in a poor DMFC performance (Zhao & Xu, 2009). As the methanol concentration increases, the negative effects of methanol crossover phenomenon become more prominent. As can be seen from Figure 4.9, as the methanol concentration was increased, the voltage at especially low current densities started to decrease due to adverse effects of the previously-mentioned methanol crossover phenomenon. In addition, the permeated methanol initiates an exothermic reaction with oxygen (Liu et. al., 2005), resulting in an increase in the consumption rate of oxygen within the Pt/C cathode electrocatalyst. The escalating rate of the generated water also increases the mass transfer resistance within the cathode electrocatalyst. As a result, the ratio of the usable oxygen at the cathode decreases, leading to a significant increase in the cathode activation and concentration polarizations. Therefore, there should be an optimal methanol concentration that yields the best performance, which corresponds to ~1.00 M at 80°C for each DMFC manufactured in this study.

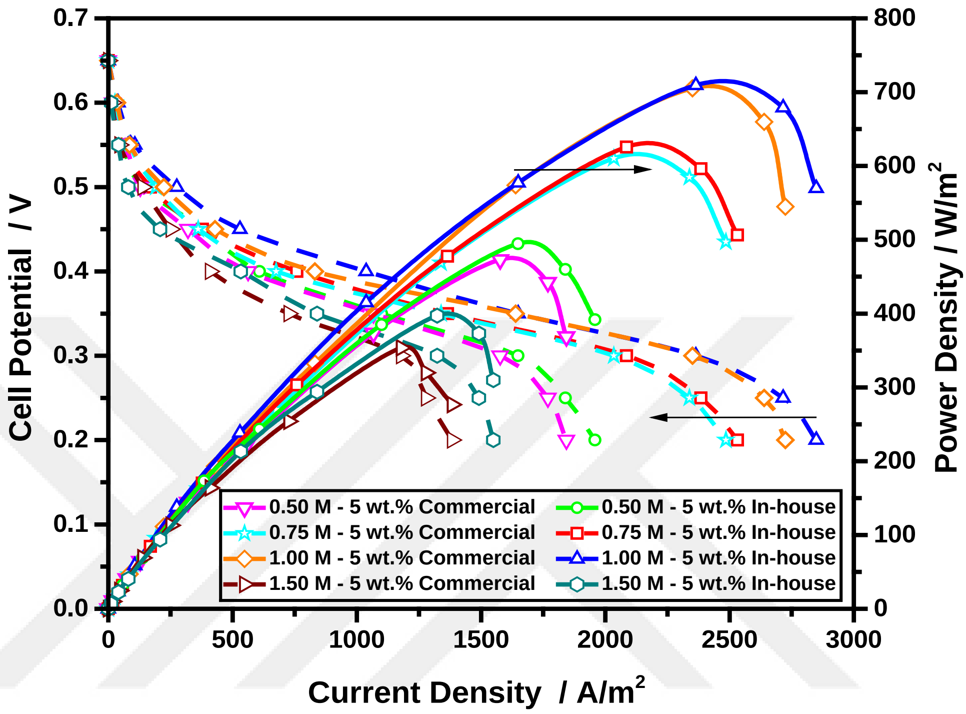

(a)

Figure 4.9 Power and polarization curves at 0.50 M, 0.75 M, 1.00 M, and 1.50 M and 80°C for the DMFCs based on Pt-Ru/C-TiO_2 anode hybrid catalyst a) with 5 wt.% of commercial and in-house TiO_2, b) with 15 wt.% of commercial and in-house TiO_2, c) with 25 wt.% of commercial and in-house TiO_2, and d) without TiO_2

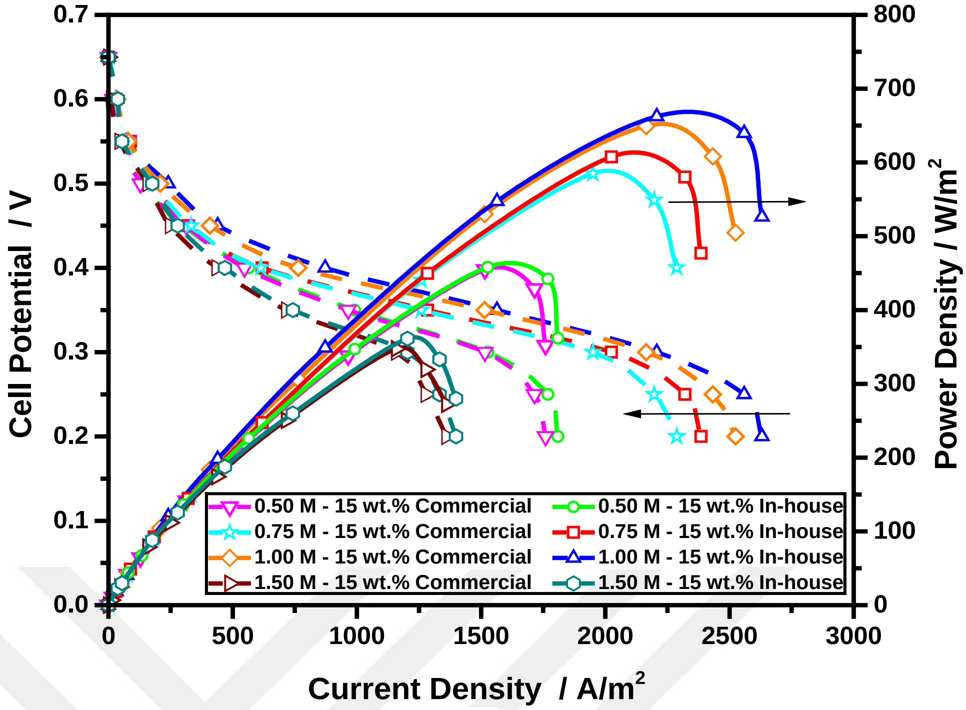

(b)

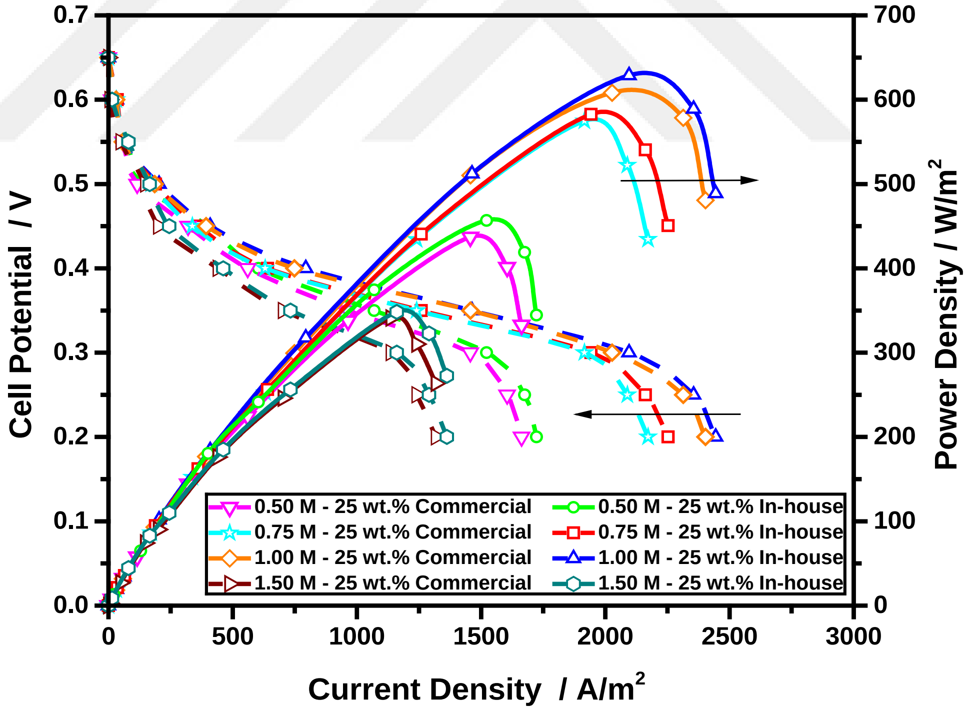

(c)

Figure 4.9 Power and polarization curves at 0.50 M, 0.75 M, 1.00 M, and 1.50 M and 80°C for the DMFCs based on Pt-Ru/C-TiO_2 anode hybrid catalyst a) with 5 wt.% of commercial and in-house TiO_2, b) with 15 wt.% of commercial and in-house TiO_2, c) with 25 wt.% of commercial and in-house TiO_2, and d) without TiO_2 (continue)

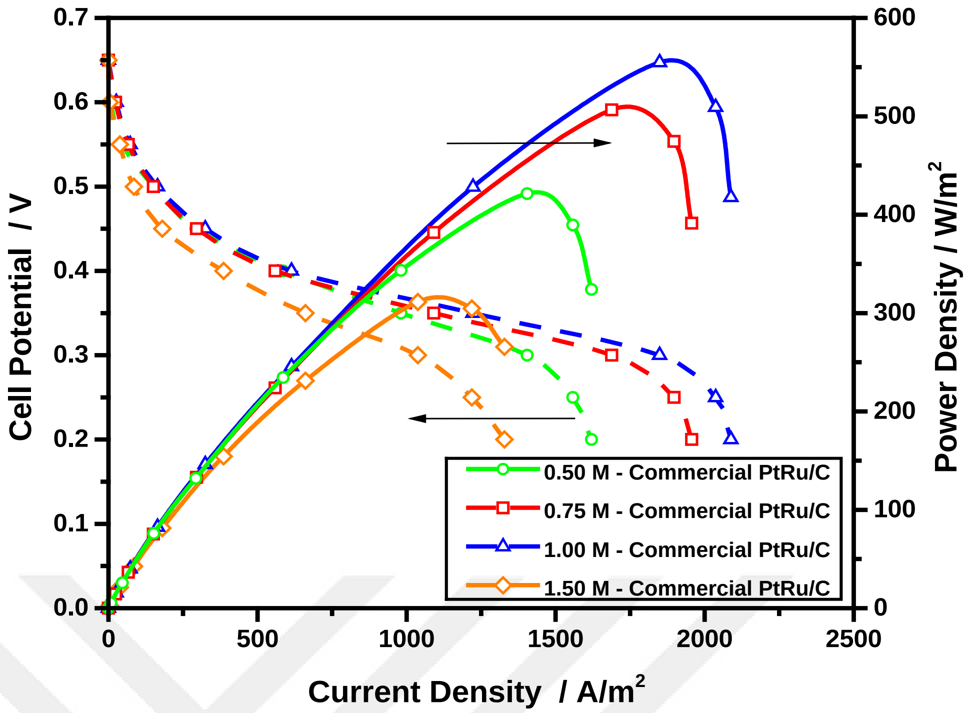

(d)

Figure 4.9 Power and polarization curves at 0.50 M, 0.75 M, 1.00 M, and 1.50 M and 80°C for the DMFCs based on Pt-Ru/C-TiO_2 anode hybrid catalyst a) with 5 wt.% of commercial and in-house TiO_2, b) with 15 wt.% of commercial and in-house TiO_2, c) with 25 wt.% of commercial and in-house TiO_2, and d) without TiO_2 (continue)

4.3.2.3 Effect of Weight Ratio of TiO_2

The results of the conducted experiments for investigating the effect of the operating temperature indicated that the highest power density was achieved as 709.32 W/m^2 at 80°C and 1 M methanol concentration and provided by the DMFC based on Pt-Ru/C-TiO_2 anode hybrid catalyst containing of 5 wt.% of in-house TiO_2. This performance is about 27.9% higher than that of the DMFC based on commercial Pt-Ru/C anode electrocatalyst. This could be explained by the fact that the introduction of TiO_2 nanoparticles into Pt-Ru/C anode electrocatalyst enhances the MOR activity by facilitating the conversion of CO into CO_2. Introduced TiO_2 nanoparticles provide additional OH species and these OH species facilitate the conversion of CO derivative intermediates into CO_2 (Liu et al., 2005).

On the other hand, it should be emphasized that the performances of the DMFCs based on Pt-Ru/C-TiO_2 anode hybrid catalysts containing commercial or in-house

TiO_2 deteriorate as the weight ratio of TiO_2 is increased from 5 wt.% to 25 wt.%. More specifically, as the TiO_2 weight ratio was increased from 5 wt.% to 15 wt.%, the peak power densities at 80°C and 1 M as presented in Figure 4.10 (a) and Figure 4.10 (b) decreased from 705.12 W/m^2 to 649.44 W/m^2, 709.32 W/m^2 to 662.16 W/m^2 for the DMFCs based on on Pt-Ru/C-TiO_2 anode hybrid catalysts containing of commercial and in-house TiO_2, respectively. Furthermore, as the TiO_2 weight ratio was increased from 15 wt.% to 25 wt.%, the performance deterioration trend continued. The decrease in the performances could be associated with the fact that excessive amount of TiO_2 may prevent the transportation of the electrons to the Pt-Ru anode electrocatalyst by creating an additional barrier between the electrons and Pt-Ru. As previously mentioned, the additional OH species, which are originated from the presence of TiO_2, may also obstruct the adsorption of CH_3OH by occupying the active areas (Wang et al., 2013).

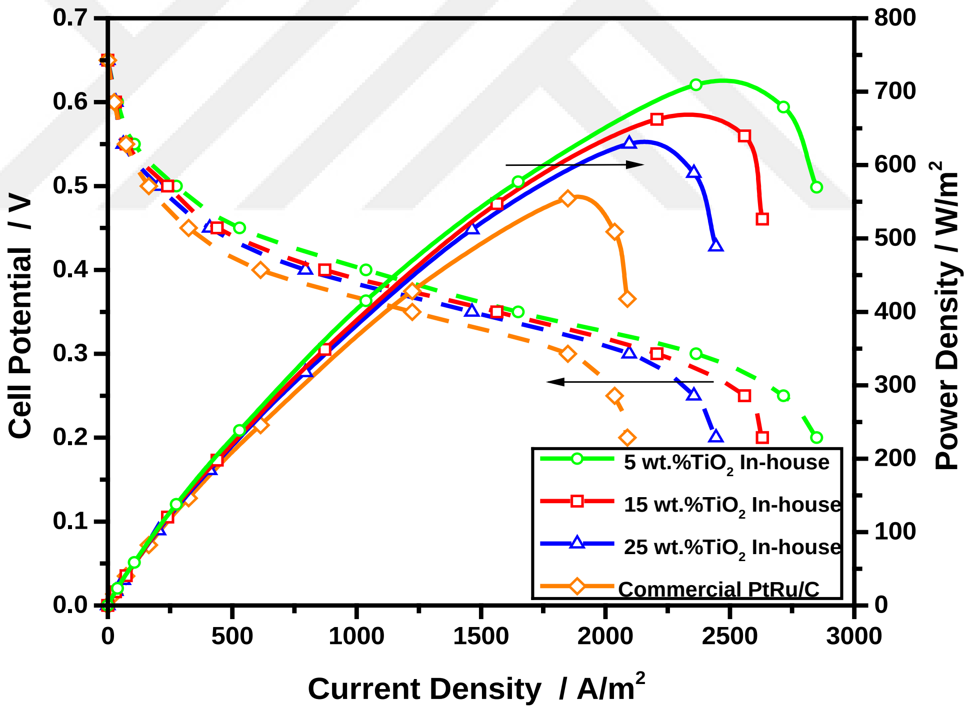

(a)

Figure 4.10 Power and polarization curves for the DMFCs based on Pt-Ru/C-TiO_2 anode hybrid catalyst (a) with 0, 5, 15, and 25 wt.% of in-house synthesized TiO_2 and (b) with 0, 5, 15, and 25 wt.% of commercial TiO_2 at 80°C and 1 M

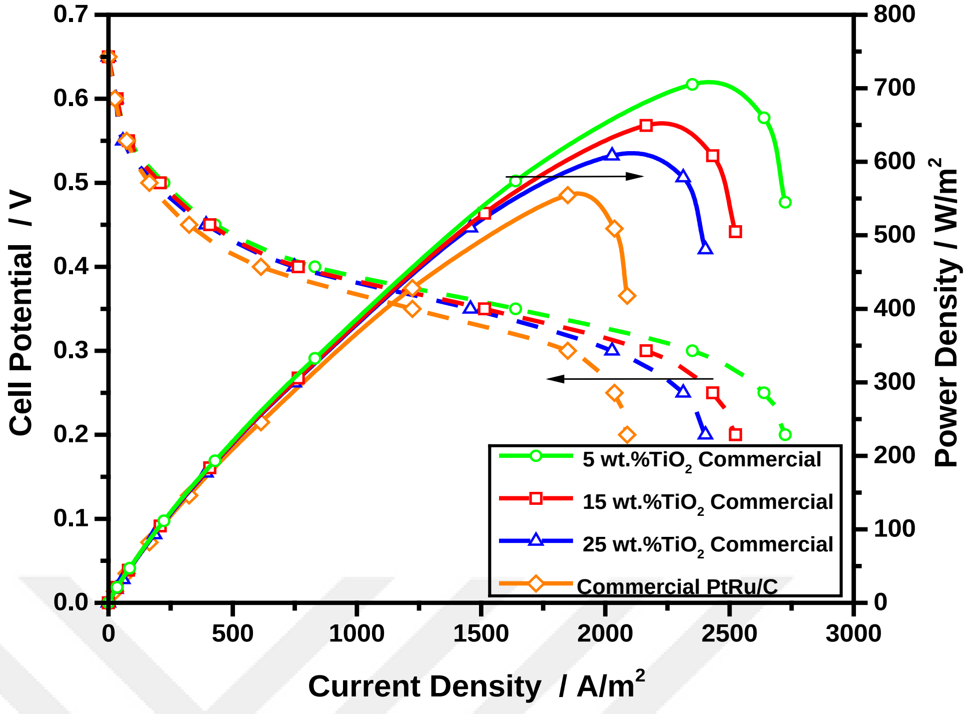

(b)

Figure 4.10 Power and polarization curves for the DMFCs based on Pt-Ru/C-TiO_2 anode hybrid catalyst (a) with 0, 5, 15, and 25 wt.% of in-house synthesized TiO_2 and (b) with 0, 5, 15, and 25 wt.% of commercial TiO_2 at 80°C and 1 M (continue)

4.3.2.4 Stability Tests

The stability characteristic demonstrates a DMFC's ability to provide constant power or current density at a fixed voltage during continuing operation (Wu et al., 2008); therefore, it possesses a considerable importance as a criterion in the performance evaluation of DMFCs. It is desired that a DMFC provides a constant power density value at a given voltage for a certain period of time during its operation. Therefore, the short-term stability tests were conducted to evaluate the stability performances of all the DMFCs manufactured.

In this section, the operating temperature and cathode inlet pressure were kept at 80°C and 1.35 bar absolute, respectively. The flow rates of the 1.00 M methanol solution and oxygen were set to 1.94 ml/min and 400 ml/min, respectively. In order to record the power density values, the voltage was set to 0.3 V and kept at this value for 4 h. As can be seen from Figure 4.11, the stability characteristics of all the

DMFCs were determined using the recorded power density values. Apparently, the majority of the power density loss occurred in the first 20 minutes of the stability tests. This drop in the power density could be both related to instabilities, such as insufficient diffusion of methanol to the anode reaction area and oxygen to the cathode reaction area (Chen & Tsao, 2006). Therefore, the power density values after the first 20 minutes were considered in the determination of stability characteristics of the DMFCs.

On the one hand, as seen from Figure 4.11 a slow decline in the power density during the short-term stability tests, and this decrease in the power density could be related to decrease in the rate of MOR due mainly to the platinum electrocatalyst poisoning, increasing rate of methanol crossover because of the swelling of the membrane, decrease in the ORR because of the crossed-over methanol at the cathode, and increasing amount of water at the cathode. In addition, during the tests sudden power density drops and increases were observed. These fluctuations in the power densities could be related to heterogeneity of the methanol concentration and unforeseen events during the short-term stability tests. Here it is also worthwhile to note that similar to proton exchange membrane fuel cells (PEMFCs), DMFCs suffer from the negative effect of so-called water flooding phenomenon that occurs at the cathode. Hence, the time-dependent power density fluctuations could also be attributed to the water flooding phenomenon. That is, possible adequacies in the water removal process could block the oxygen flow paths temporarily, leading to an instantaneous drop in the power density. However, as can be seen from Figure 4.11, the fluctuations especially in the power density value of the DMFC based on Pt-Ru/C-TiO_2 anode hybrid catalyst containing 5 wt.% of commercial TiO_2 were much lesser than those of other DMFCs. This can be an indicator for the improved stability of the DMFC based on Pt-Ru/C-TiO_2 anode hybrid catalyst with the 5 wt.% of commercial TiO_2. The improved stability characteristic of this DMFC is explained by the enhanced electrocatalytic properties of Pt-Ru/C-TiO_2 anode hybrid catalyst and utilizing of Pt.

Furthermore, after 3 h operation at previously-mentioned operating conditions, the recorded power densities started to decrease; however, the decline in the power density of the DMFC based on Pt-Ru/C-TiO_2 hybrid catalyst containing 5 wt.% of commercial TiO_2 was almost negligible. This can be associated with the improved electrocatalytic properties of Pt-Ru/C-TiO_2 anode hybrid catalyst containing 5 wt.% of commercial TiO_2 hence TiO_2 nanoparticles facilitates the conversion of CO into CO_2. As previously mentioned in Section 4.3.2.3, this facilitation in the conversion of CO into CO_2 mitigates the electrocatalyst poisoning phenomenon and improves the stability of the anode electrocatalyst towards the MOR (Wang et al., 2013). The stability characteristics of the DMFCs based on Pt-Ru/C-TiO_2 anode hybrid catalysts with relatively higher TiO_2 weight ratios (15 and 25 wt.%) are consistent with their performances. These relatively worse stability characteristics of the DMFCs based on Pt-Ru/C-TiO_2 with 15 and 25 wt.% of TiO_2 may be related to occupied active sites because of the excessive amount of TiO_2. Namely, excessive amount of TiO_2 might also obstruct the adsorption of CH_3OH, leading to a significant drop in the power density.

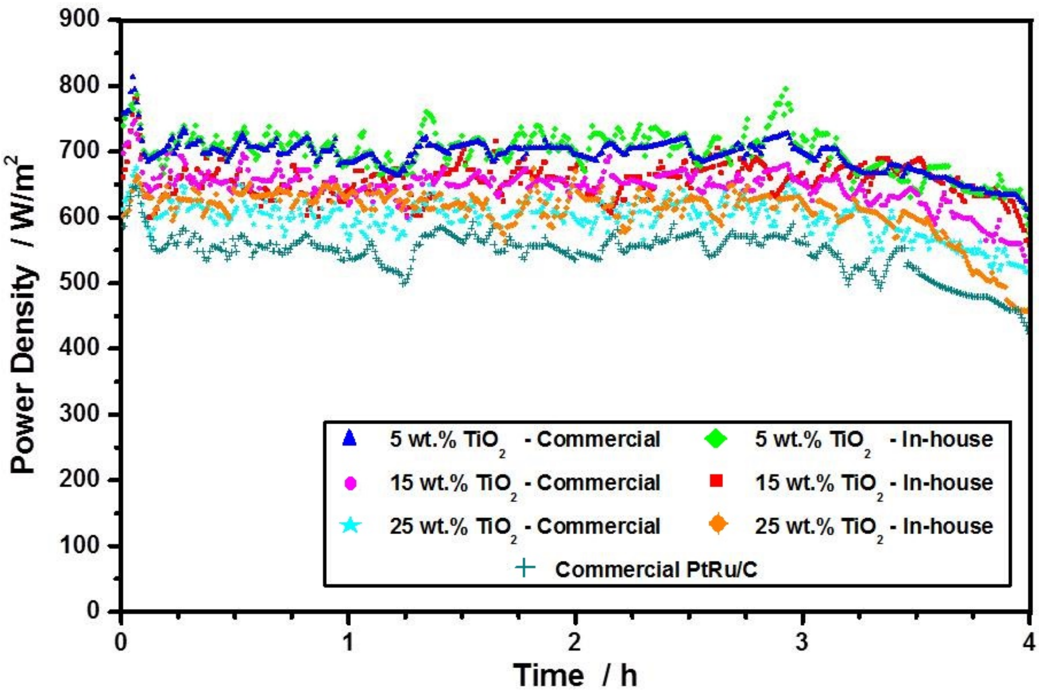

Figure 4.11 Short-term stability tests of the DMFCs based on Pt-Ru/C-TiO_2 anode hybrid catalyst with 0, 5, 15, 25 wt.% of commercial and in-house TiO_2 at the cell voltage of 0.3 V, the operating temperature of 80°C, and the methanol concentration of 1.00 M

4.3.3 Repeatability Tests

In the experimental studies, it is not always possible to achieve the same results or values when the experiments are repeated in the same conditions due to the error in measurement and precision in the manufacturing and instrumentation. In order to assess the repeatability of the experimental studies, six DMFCs with 2 mg_{PtRu}/cm^2 anode and 1 mg_{Pt}/cm^2 cathode electrocatalyst loadings were fabricated applying the same manufacturing process discussed in Section 3.3.3. The performances of these DMFCs were investigated at the operating temperature of 80°C, the methanol concentration of 1.00 M, the methanol flow rate of 1.94 ml/min, and the oxygen flow rate of 400 ml/min. The results of these conducted experiments for six different DMFCs are presented in Figure 4.12. In order to calculate the deviation from the average peak power density value, firstly, the average peak power densities of these DMFCs were calculated. Then, the differences between the lowest peak power density and average peak power density and the highest peak power density and average peak power density were calculated. All these calculations revealed that the error in the value of the peak power density for the conducted experiments is estimated to be +10.94% and -12.34%.

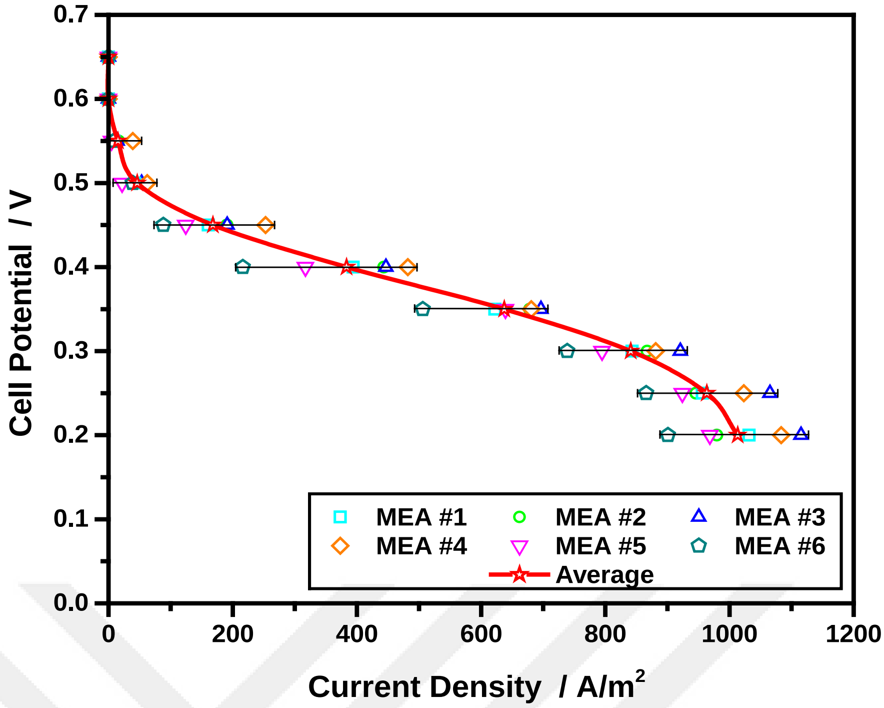

(a)

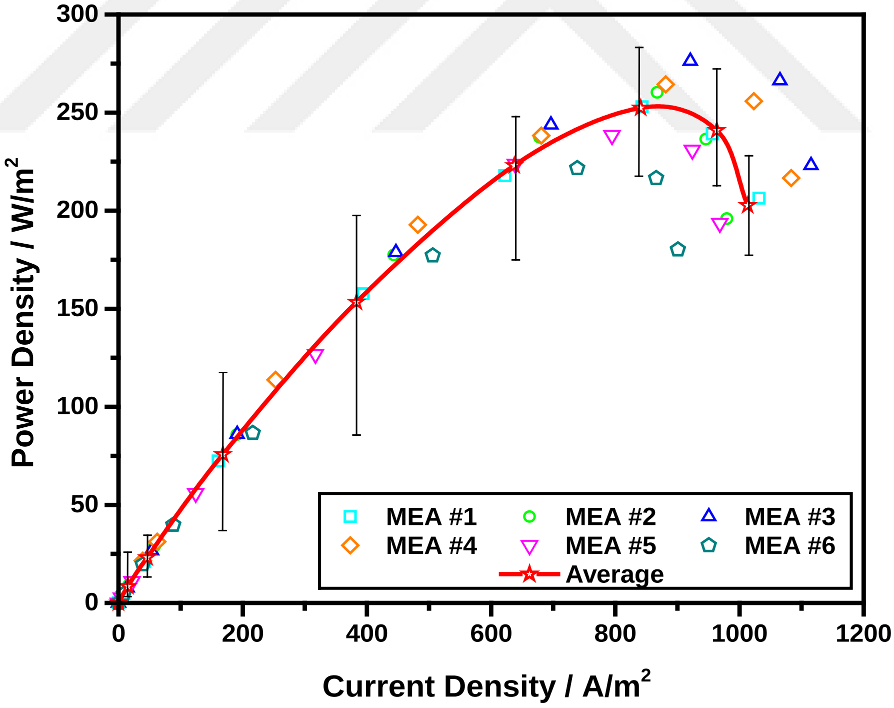

(b)

Figure 4.12 (a) Polarization curves generated from six different DMFCs based on commercial Pt-Ru/C anode electrocatalyst at 80°C and methanol concentrations of 1.00 M and (b) Power curves obtained from six different DMFCs based on commercial Pt-Ru/C anode electrocatalyst at 80°C and 1.00 M

4.4 Nafion/ZrP Composite Membrane and Pt/C-ZrP Cathode Catalyst Based DMFCs

4.4.1 Characterization of The Nafion®115 and Nafion/ZrP Nanocomposite Membranes

4.4.1.1 Thermal Stability (TGA)

The results of the thermal stability measurements for the Nafion and Nafion/ZrP composite membranes are presented in Figure 4.13. It was observed that all the membranes retain more than 90% of its weight up to a temperature of about 300ºC. The results of the thermal degradation of Nafion membranes agree well with the results from literature (Barbora et al., 2009). The first weight loss, between 50ºC and 200ºC, corresponds to moisture removal from the membranes. Second weight loss region between 200ºC-400ºC indicates the degradation of -SO_3H groups (Figure 4.13). The last weight loss region was observed between 400ºC and 550ºC and this was related to the decomposition of Nafion (Figure 4.13, inset) (Devrim, 2014). Thermal decomposition behaviour of Nafion/ZrP composite membranes was similar to that of pristine Nafion membrane. However, the decomposition temperature of the polymer main chain was shifted to a slightly higher temperature with the addition of 5 wt.% ZrP. Major polymer main chain decomposition temperature for pristine Nafion was spotted at about 425ºC, while NZ-5 membrane showed decomposition at approximately 430 ºC (Figure 4.13, inset). This shows that zirconium phosphate with a layered structure may lead to an increase in thermal degradation temperature (Kuan et al., 2006). NZ-2.5 membrane and pristine Nafion membrane showed very close thermal degradation temperatures. Addition of zirconium phosphate had no effect in this case. This is probably due to the low amount of zirconium phosphate.

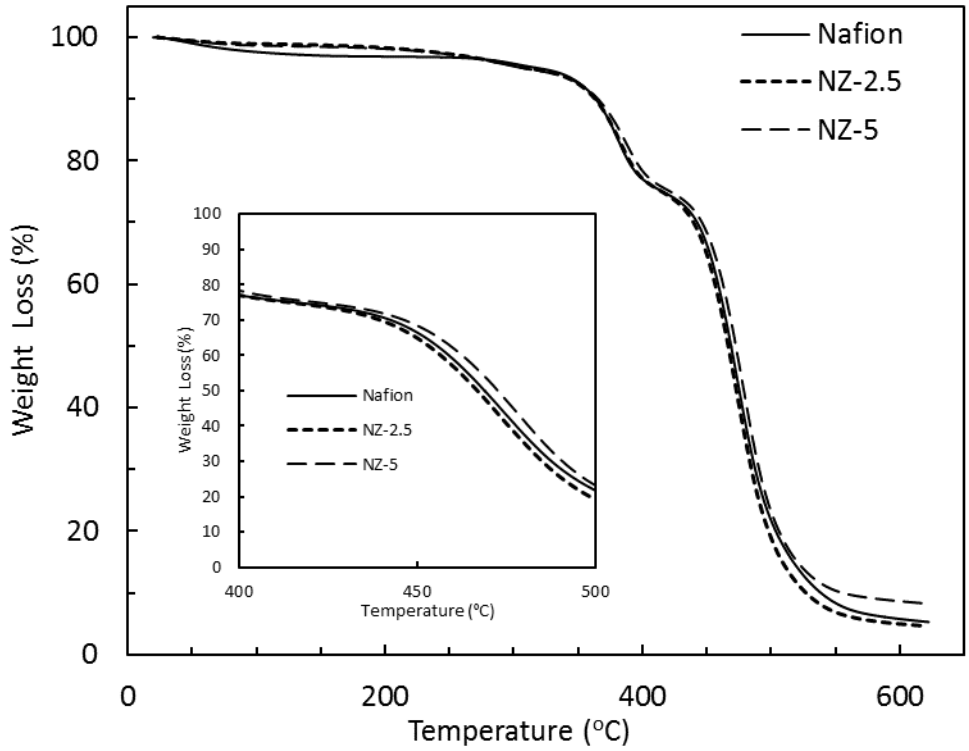

Figure 4.13 TGA curves of the Nafion and Nafion/ZrP composite membranes (Ozden et al., 2017)

4.4.1.2 XRD Study

XRD patterns of Nafion, Nafion/ZrP composite membranes, and ZrP particles are illustrated in Figure 4.14. The bare Nafion membrane shows two main peaks at 17.5º (2θ) and 38.3º (2θ) (Figure 4.14), which are consistent with those reported in literature (Kuan et al., 2006). The broad peak at 17.5º (2θ) was related to the crystalline scattering of the polyfluorocarbon chains in membranes, which overlapped the X-ray scattering from the amorphous region of the membrane at lower Bragg angles.

The XRD pattern of ZrP particles shows very weak diffraction peaks at 21.11º (2θ) and 26.73º (2θ) (Figure 4.14, inset), thus ZrP particles can be defined as amorphous NZ-2.5 showed no discrete, sharp reflexes which indicates that there were no structural changes in polymer matrix. NZ-5 membrane also showed no sharp peaks indicating structural changes in XRD results. These were the expected results since the particles used were also amorphous.

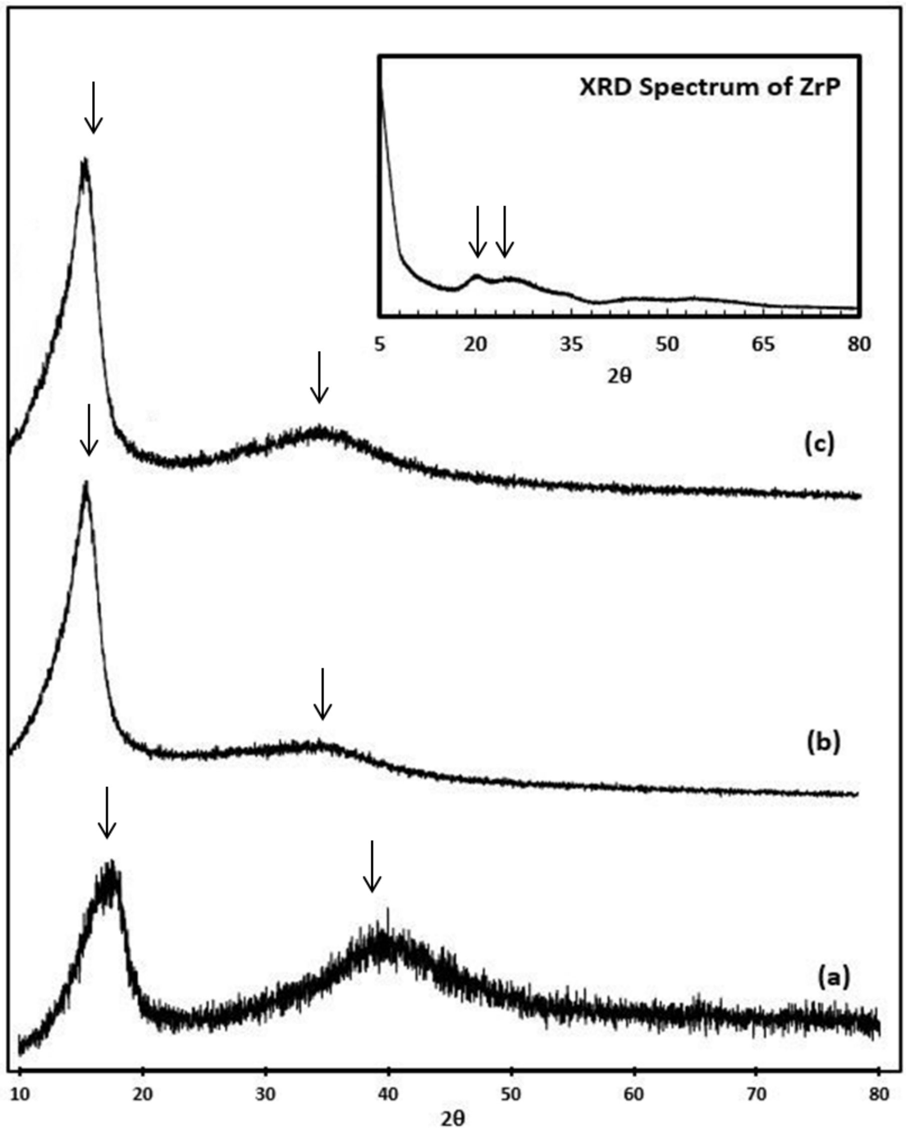

Figure 4.14 XRD spectrums of (a) Nafion membrane, (b) NZ-2.5, and (c) NZ-5 and ZrP nano particles (Ozden et al., 2017)

4.4.1.3 Scanning Electron Microscopy (SEM) analysis

Scanning electron microscopy (SEM) was used to investigate the microstructure of the bare Nafion membrane as well as those of the composite membranes with different contents of ZrP. The morphological properties of the composite based membranes depend on the degree of compatibility and dispersibility between the polymer and filler. Figure 4.15 shows the SEM images of the bare Nafion and Nafion/ZrP nanocomposite membranes. Figure 4.15 (a) shows the surface of the pristine Nafion membrane. The surface of the Nafion membrane presents a smooth surface without any cracks or pinholes. As seen from Figure 4.15 (b) and Figure 4.15 (c), slight agglomerations were observed in the NZ-5 membrane matrix. This result can be attributed to the incompatibility of ZrP with Nafion at high ZrP loadings. Figure 4.15 (d) and Figure 4.15 (e) display the cross-section image of the Nafion/ZrP membrane with 2.5 wt.% ZrP loading. As seen from Figure 4.15 (d) and Figure 4.15 (e), ZrP particles are uniformly distributed within the composite membrane as a result of the interaction between the Nafion polymer and ZrP. It is worthwhile to note that no big agglomerates are visible, which means ZrP particles can be dispersed homogeneously in the polymeric matrix for NZ-2.5 composite membrane. This indicates the effectiveness of compatibility for ZrP embedded into the polymer matrix (Mokhtaruddin et al., 2011). The thicknesses of the composite membranes were around 64±5 µm (Figure 4.15 (c) and Figure 4.15 (e), insets).

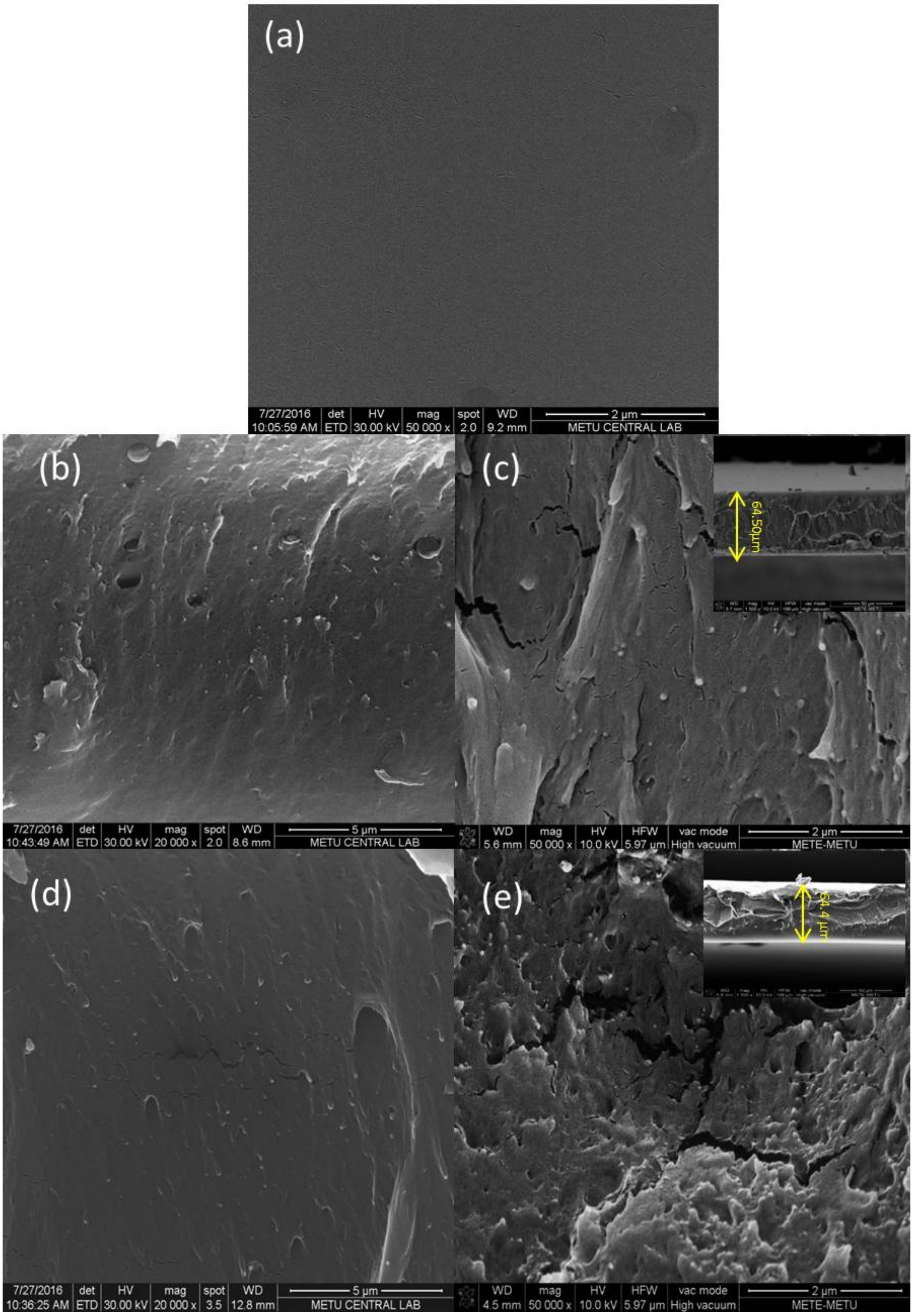

Figure 4.15 SEM images of (a) Nafion membrane (x50000), (b) NZ-5 (x20000), (c) NZ-5 (x50000), (d) NZ-2.5 (x20000), and (e) NZ-2.5 (x50000) membranes (Ozden et al., 2017)

EDX spectrum of Nafion and Nafion composite membranes are shown in Figure 4.16. EDX spectrum of pure Nafion membrane is shown in Figure 4.16 (a). The spectrum shows the presence of carbon (C), oxygen (O), sulphur (S), and Fluorine (F). Figure 4.16 (b) and Figure 4.16 (c) show the EDX spectrums of the composite membranes. EDX spectrums of Nafion/ZrP nanocomposite membranes confirm the presence of ZrP particles reside in the composite membranes. The peaks are the reflection of the presence of Zr, C, O, S, and F components in the composite membranes, which is the evidence of that ZrP particles added to the polymer solution were fixed in the polymer network.

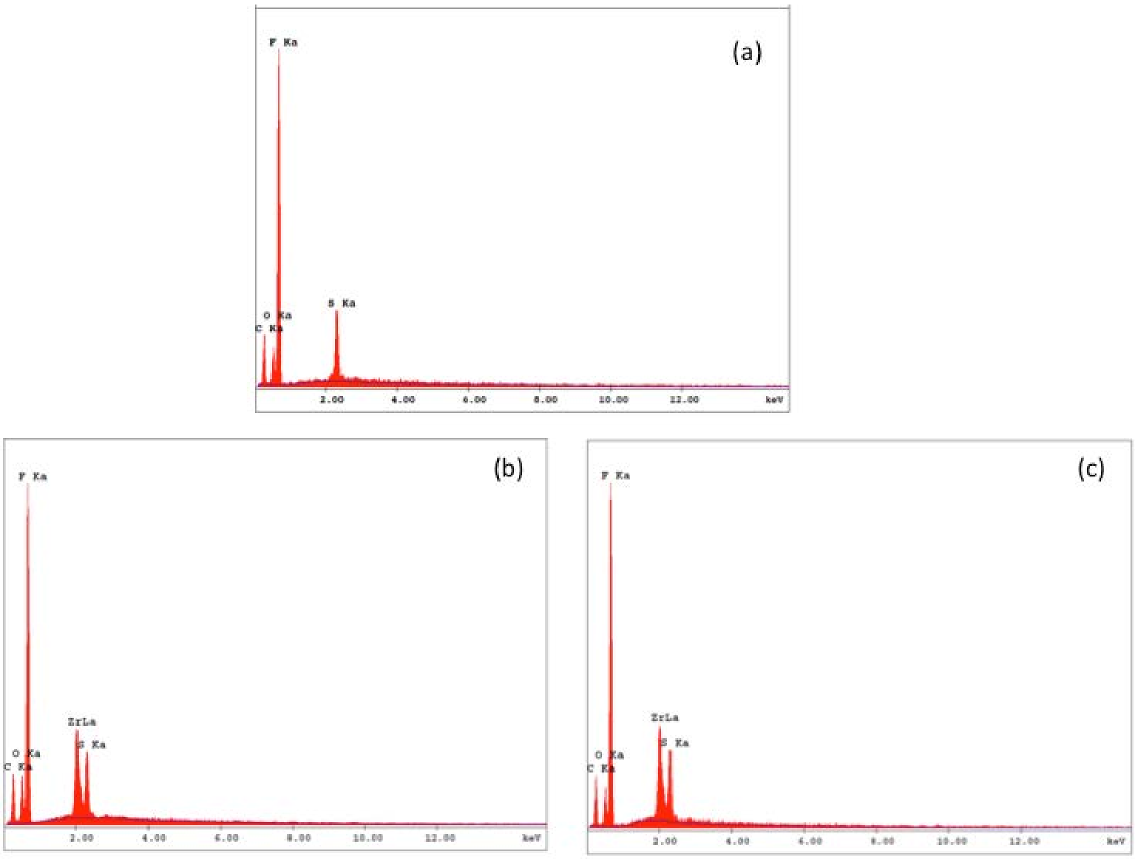

Figure 4.16 EDX spectra of (a) Nafion, (b) NZ-2.5, and (c) NZ-5 membranes (Ozden et al., 2017)

4.4.1.4 Water Uptake

Water uptake plays a significant role in proton exchange membrane characterization. The hydration of the membrane is closely related to the proton conductivity. To investigate the effect of ZrP nano particles on the water retention capability of the Nafion/ZrP composite membranes, water uptake tests were conducted. Water uptake values for Nafion® 115, NZ-2.5, and NZ-5 membranes are represented in Table 4.2. Nafion® 115 showed the lowest water uptake value amongst the membranes. As the ZrP loading increased from 2.5 wt.% to 5 wt.%, water uptake percent increased from 11 to 13.3. These results indicate that addition of ZrP particles contributes to the water retention capability of membranes. ZrP increases the water content of the membranes due to its disruption of the cohesive forces of Nafion. Additionally, ZrP particles interact with Nafion polymer probably through hydrogen bonding between -SO_3H groups, which are combined with the increase of the water uptake and the water mobility. These findings are compatible with literature (Bauer & Willert-Porada, 2004; Rodgers et al., 2009).

4.4.1.5 Proton Conductivity

Electrochemical Impedance Spectroscopy (EIS) was conducted to determine the proton conductivities of the membranes. The proton conductivities of the Nafion® 115 and Nafion/ZrP composite membranes at five different temperatures were measured. Since temperature plays a vital role in proton conduction kinetics and the mobility of polymer chains, all the membranes exhibited an increase in the proton conductivity as the temperature increased. High temperature promotes the dissociation of hydrogen which results in higher conductivity values. The results showed that introducing ZrP to polymer matrix enhanced proton conductivity values of Nafion membrane. At temperatures 25°C, 50°C, 60°C, and 70°C, NZ-2.5 membrane exhibited the highest proton conductivities amongst the samples. At 80°C, however, NZ-5 had higher proton conductivity with the value of 0.223 S/cm (Table 4.2). The improved proton conductivity of nano composite membranes can be explained by the layered structure of ZrP. Each zirconium atom is coordinated with six oxygen atoms belonging to six different OH-PO_3 groups. This is a group of inorganic proton conductors that show high proton conductivity (He et al., 2003). The proton conductivity increase can also be explained by hydrophilicity of ZrP particles. ZrP particles supply additional proton conducting moieties in the membrane. Water uptake plays an important role in proton conductivity. As the water uptake values become higher, the number of interconnecting channels between ionic groups also increases for the protons to use to cross the membrane. All the membranes exhibited an increase in conductivity with temperature. At temperatures lower than 80 ºC, NZ-5 membrane had lower proton conductivity values compared to NZ-2.5 membrane. This can be attributed to slight agglomerations of ZrP particles in NZ-5 membrane which were observed in SEM pictures (Figure 4.15). It can also be seen that ZrP particle distribution was not uniform over the polymer matrix for NZ-5 membrane. At 80 ºC, NZ-5 membrane shows slightly higher proton conductivity value that NZ-2.5. This is due to the higher water retention capacity of NZ-5 membrane.

Table 4.2 Conductivity, activation energy and water uptake data for Nafion® 115 and Nafion/ZrP composite membranes

Membrane type	**Activation Energy (kJ/mol)**	**Water Uptake (%)**	**Proton Conductivity(S/cm)**				
			25°C	**50°C**	**60°C**	**70°C**	**80°C**
Nafion® 115	10.7	10.1	0.081	0.107	0.119	0.129	0.132
NZ-2.5	15.4	11.0	0.101	0.175	0.206	0.213	0.218
NZ-5	19.5	13.3	0.078	0.140	0.172	0.198	0.223

Activation energies and conductivity values obtained are shown in Table 4.2. In the Nafion-based membranes, the proton conduction is dominated by the Grothuss mechanism. In this mechanism, the proton which forms as H_3O^+ ion jumps to the neighboring lone pair of electrons of a water molecule. For such a mechanism, the activation energy for proton conduction should be around 14-40 kJ mol^{-1}. The results are compatible with these values; therefore, it can be concluded that the proton conduction mechanism is dominated by Grotthus mechanism. E_a values for composites with ZrP particles are higher than that for pristine Nafion membrane. This may be explained by the addition of inorganic fillers to the polymer matrix (Shao et al., 2004). Nano fillers act as a carrier-bridge; thereby, this process requires more energy. Although the activation energies for nanocomposite membranes were found to be higher than that for Nafion® 115 membrane, proton conductivity of the nanocomposite membranes is higher than that of Nafion® 115. This is due to the increased hydrogen bonding by introduction of ZrP particles to the polymer matrix. Hydrogen bondings act as a proton conduction channel and improve proton conduction of the membranes. Additionally, since incorporation of ZrP increases water uptake, proton conductivity becomes higher in nanocomposite membranes (Singha & Jana, 2014).

4.4.2 SEM Analysis of Cathode and Anode Catalyst Layers

The cell performance of MEA is strongly dependent on the pore structure of the electrodes. Figure 4.17 shows SEM surface images and EDX spectras of the anode and cathode electrode structures. As shown in SEM images, no agglomerates are visible for all electrodes. This means that ZrP and Pt/C particles are homogeneously dispersed in the electrodes. Electrodes also showed no cracks or mud-like morphologies. As seen from EDX spectra in Figure 4.17 (b), C, O, S, F, Pt, and Zr peaks were detected for cathode catalyst layer. This can be attributed to the presence of ZrP in the cathode electrodes. Figure 4.17 (d) and Figure 4.17 (f) show the C, O, S, F, and Pt peaks for the cathode and anode electrode without ZrP filler, respectively.

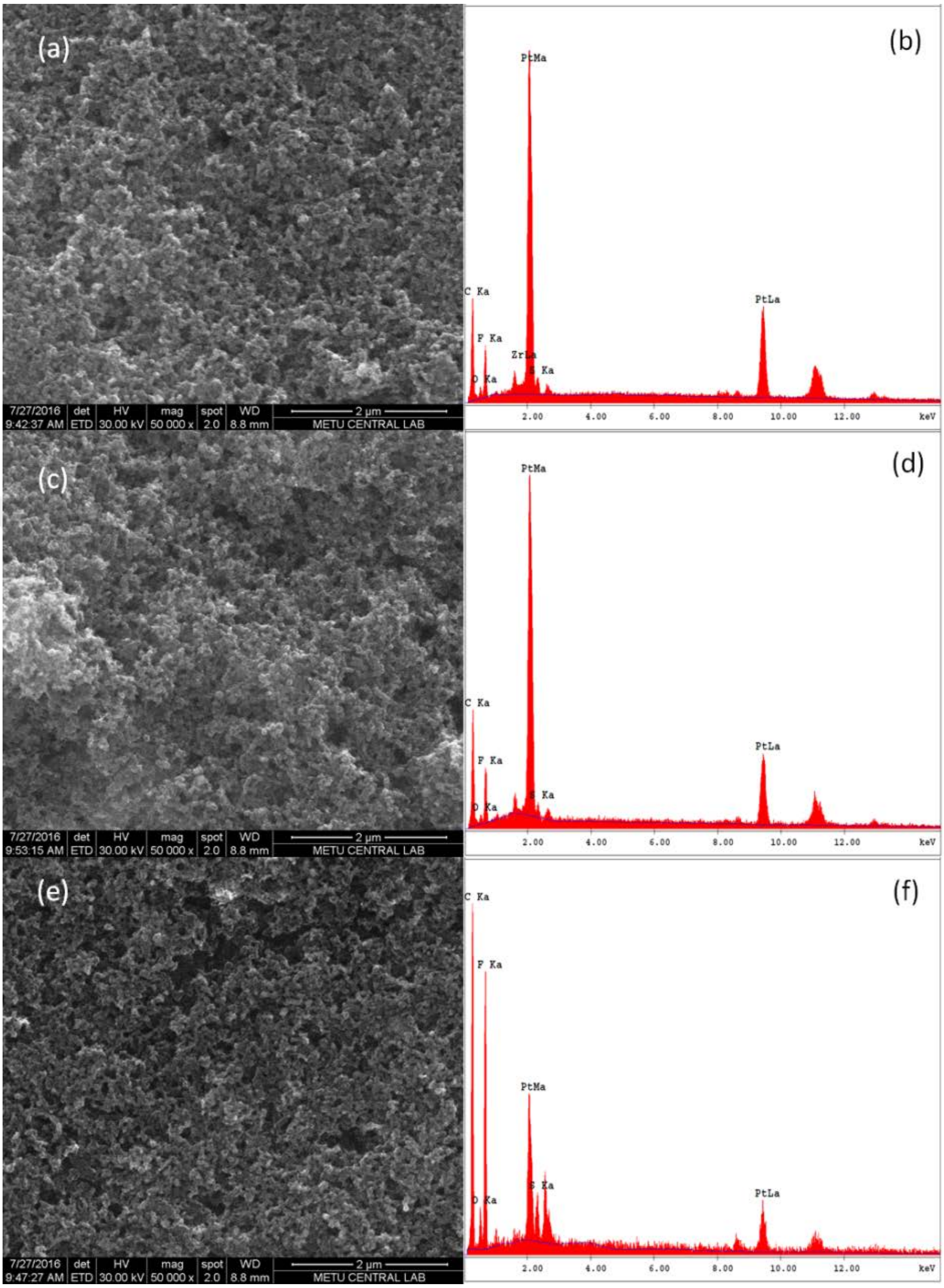

Figure 4.17 SEM surface images of (a) Cathode catalyst layer with ZrP, (c) Cathode catalyst layer without ZrP, (e) Anode catalyst layer, and EDX spectrums of (b) Cathode catalyst layer with ZrP, (d) Cathode catalyst layer without ZrP, (f) Anode catalyst layer (Ozden et al., 2017)

4.4.3 Performance testing of the MEAs

Three different MEAs with 25 cm^2 active areas were fabricated using air-spraying technique as mentioned in Section 3.4.3. The differences in these MEAs mainly originate from using different membranes: commercial Nafion® 115 membrane, NZ-2.5, and NZ-5. In this section, the effects of operating temperature, supplied methanol concentration, and type of cathode catalyst on the performance of the DMFCs are discussed. In addition, the stability characteristics of these DMFCs are both presented and interpreted.

4.4.3.1 Effect of operating temperature

Operating temperature is one of the main parameters that affects the performance of these MEAs (Park & Yamazaki, 2004). Fundamentally, the increase in the operating temperature of DMFCs results in several adverse effects: an increase in the reaction kinetics at both the anode and cathode, an improvement in the ionic conductivity of Nafion membranes, a deterioration in the water retention capability of the membrane, and a triggering of the undesired methanol crossover from the anode to cathode (Bauer & Willert-Porada, 2006; Ravikumar & Shukla, 1996). Therefore, in spite of the fact that the increase in the operating temperature causes some opposite effects as mentioned above, the overall performance of DMFCs generally improves with increasing operating temperature until a certain temperature value. After a certain operating temperature value, the previously mentioned negative effects (e.g., methanol crossover and dehydration of membrane) become more dominant, leading to a deterioration in DMFC performance significantly. As the usage of Nafion/ZrP composite membranes and introduction of ZrP to the cathode catalyst could potentially change the compound effect, the experimental studies were conducted at different operating temperatures (40°C, 60°C, 80°C, and 100°C) and the methanol concentration of 1.00 M. The results of the experiments conducted for investigating the effect of the operating temperature on the performance of MEA-1 are shown in Figure 4.18 (a). As seen from Figure 4.18 (a), the maximum power density was found as 537.48 W/m^2 at 80°C and 1.00 M methanol concentration. In addition, the peak power densities at 40°C, 60°C, and 100°C (for 1.00 M methanol concentration) were found as 239.52 W/m^2, 362.64 W/m^2, and 441.36 W/m^2, respectively.

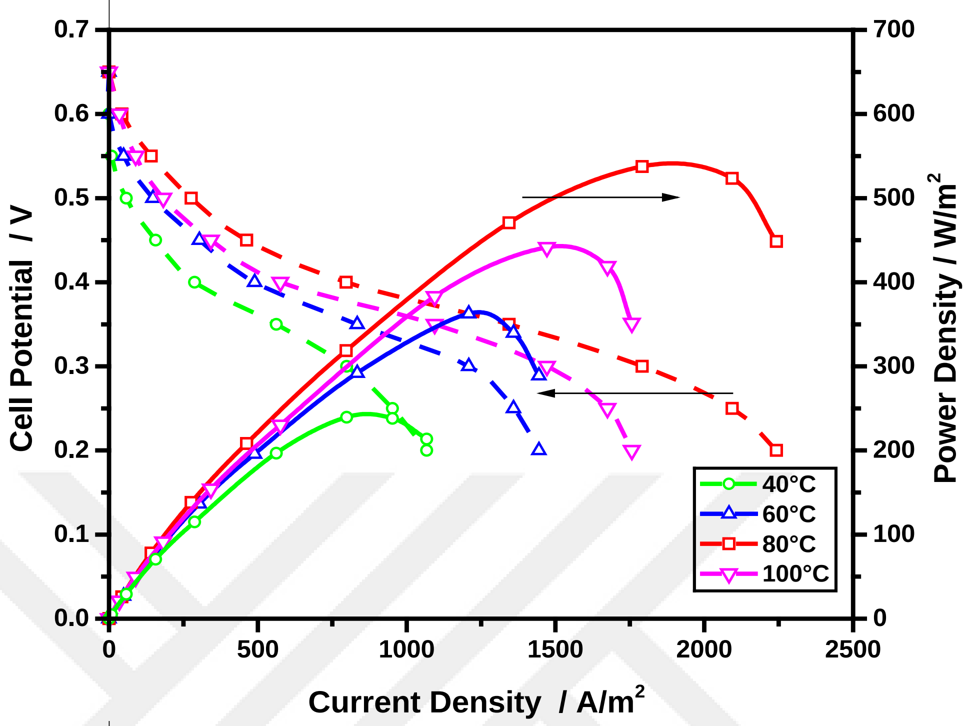

(a)

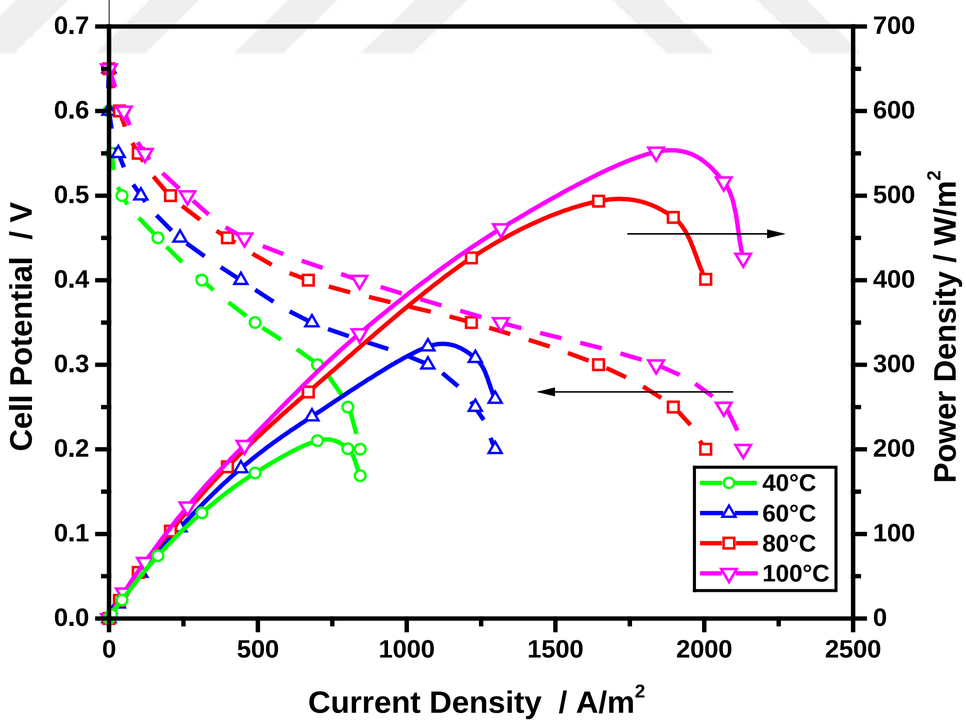

(b)

Figure 4.18 Power density and polarization curves at 40°C, 60°C, 80°C, 100°C and 1.00 M methanol concentration for (a) MEA-1, (b) MEA-2, and (c) MEA-3

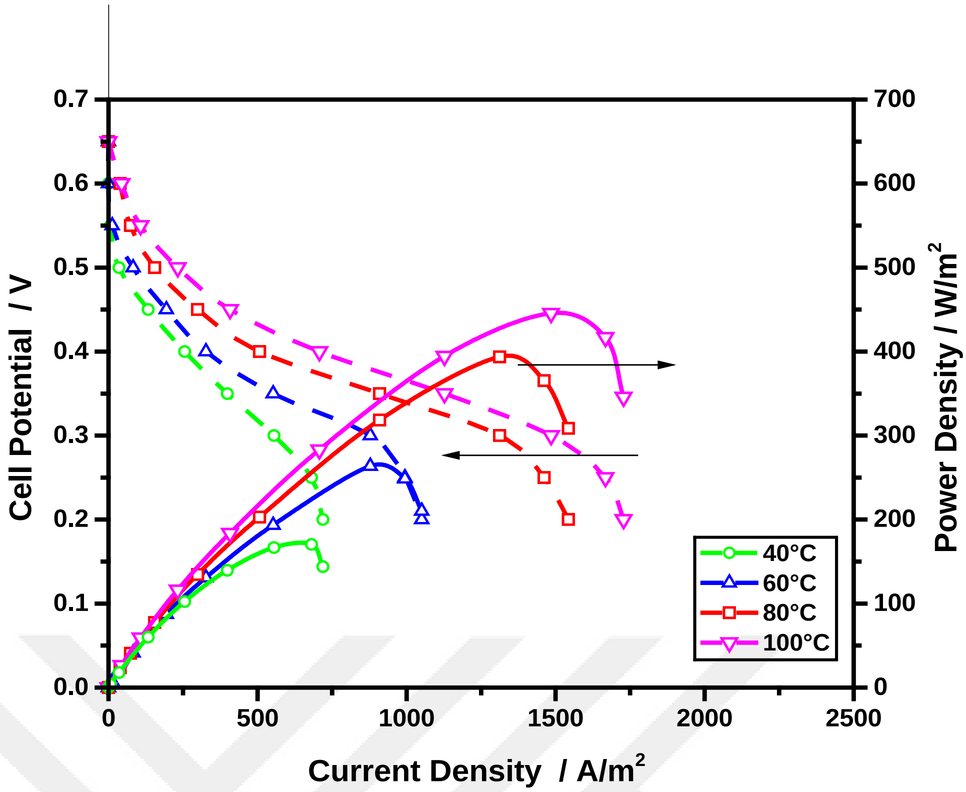

(c)

Figure 4.18 Power density and polarization curves at 40°C, 60°C, 80°C, 100°C and 1.00 M methanol concentration for (a) MEA-1, (b) MEA-2, and (c) MEA-3 (continue)

As can be seen in Figure 4.18 (a), the best performance of MEA-1 was achieved at 80°C as expected. The experiments conducted for MEA-1 were repeated for MEA-2 and MEA-3 to compare the performances of these two MEAs with that of MEA-1. Figure 4.18 (b) and Figure 4.18 (c) present the power density and polarization curves of MEA-2 and MEA-3 at these temperatures, respectively. As can be seen from Figure 4.18 (b), the maximum power density of MEA-2 was achieved as 551.52 W/m^2 at 100°C and 1.00 M. In addition, the peak power densities at 40°C, 60°C, and 80°C and 1.00 M were found as 210.24 W/m^2, 321.36 W/m^2, and 493.44 W/m^2, respectively. As seen from Figure 4.18 (c), the best performance of MEA-3 was achieved as 445.44 W/m^2 at 100°C, whereas the peak power densities at 40°C, 60°C, and 80°C (for 1.00 M methanol concentration) were found as 166.68 W/m^2, 263.52 W/m^2, and 393.72 W/m^2, respectively.

As seen from Figure 4.18 (a)-(c), when the operating temperature increases from 40°C to 80°C, the performances improve as expected. More specifically, for this increase of temperature, the peak power densities increase from 239.52 W/m^2 to 537.48 W/m^2, 210.24 W/m^2 to 493.44 W/m^2, 166.68 W/m^2 to 393.72 W/m^2 for MEA-1, MEA-2, and MEA-3, respectively. The reason of the performance improvement as the operating temperature increases from 40°C to 80°C could be related to the increase in the electrochemical reaction kinetics at both the anode and cathode as well as to the significant enhancement in the proton conductivity of both the bare Nafion® membrane and Nafion/ZrP composite membranes. However, as the operating temperature increases from 80°C to 100°C, the maximum power density value of MEA-1 decreases from 537.48 W/m^2 to 441.36 W/m^2. The reason of the performance deterioration as the operating temperature becomes higher may be related to the dehydration problem of commercial Nafion® 115 membrane, which leads to a significant deterioration in the proton conductivity of the membrane. The increase in the operating temperature also triggers the undesired methanol permeation from the anode to cathode by increasing the diffusion of methanol through the membrane which in turn decreases the performance of the cell (Devrim et al., 2012). In addition, as the operating temperature reaches to 100°C, the chemical stability of the bare Nafion® membrane deteriorates. In contrast, the peak power density values of MEA-2 and MEA-3 increase from 493.44 W/m^2 to 551.52 W/m^2, 393.72 W/m^2 to 445.44 W/m^2, respectively, for the same temperature increment. This performance improvement is consistent with those reported in literature (Costamagna et al., 2002; Xie et al., 2006) and can be explained by the fact that the chemical stability and water retention ability of Nafion/ZrP composite membranes enhance as the temperature reaches to 100°C (Rodgers et al., 2009). In addition, the methanol impermeability characteristic of Nafion/ZrP composite membranes is much more advanced in comparison to Nafion® 115 membrane (Ozden, Ercelik, Ouellette, et al., 2017), thus reduces the amount of crossed-over methanol at the cathode and eventually improves the performance as the temperature increases. Given these facts, Nafion/ZrP composite membranes seem more promising as compared to Nafion® 115 membrane, specifically regarding chemical and physical stability, methanol impermeability, and water retention ability during the high-temperature operation.

There is also a more subtle point that must be considered is that high temperature operation (e.g., 100°C) provides a significant advantage with regard to improvement in the carbon monoxide tolerance of the catalyst, thus promotes the performance noticeably.

4.4.3.2 Effect of Methanol Concentration

Methanol concentration is another crucial parameter which has a significant importance on the performance of DMFCs (Ravikumar et al., 1996; Ozden, Ercelik, Ouellette, et al, 2017). The experiments therefore were repeated at the operating temperatures that yield highest performance (80°C for MEA-1 and 100°C for MEA-2 and MEA-3) with the methanol concentrations of 0.75 M and 1.50 M to investigate the effect of the methanol concentration on the performances of the MEAs. The power density and polarization curves obtained from these experiments are shown in Figure 4.19. As seen from Figure 4.19 (a), the peak power densities at 0.75 M and 1.50 M for MEA-1 were found as 518.52 W/m^2 and 418.68 W/m^2, respectively. In addition, the maximum power density (537.48 W/m^2) of this MEA was achieved at 80°C and 1.00 M methanol concentration. As previously mentioned, however, the most appropriate operating temperature that gives the highest performance for MEA-2 and MEA-3 was found as 100°C. Therefore, the experiments were carried out at this temperature varying the methanol concentration from 0.75 M to 1.50 M. As seen from Figure 4.19 (b) and Figure 4.19 (c), the peak power densities of MEA-2 and MEA-3 at the methanol concentrations of 0.75 M were found as 485.40 W/m^2 and 419.04 W/m^2, respectively. As the methanol concentration increases from 0.75 M to 1.50 M, the power densities of MEA-2 and MEA-3 decrease from 485.40 W/m^2 to 441.72 W/m^2 and 419.04 W/m^2 to 312.12 W/m^2, respectively. In addition, the maximum power densities of MEA-2 and MEA-3 were found as 551.52 W/m^2 and 445.44 W/m^2, respectively, when the methanol was supplied with the concentration of 1.00 M.

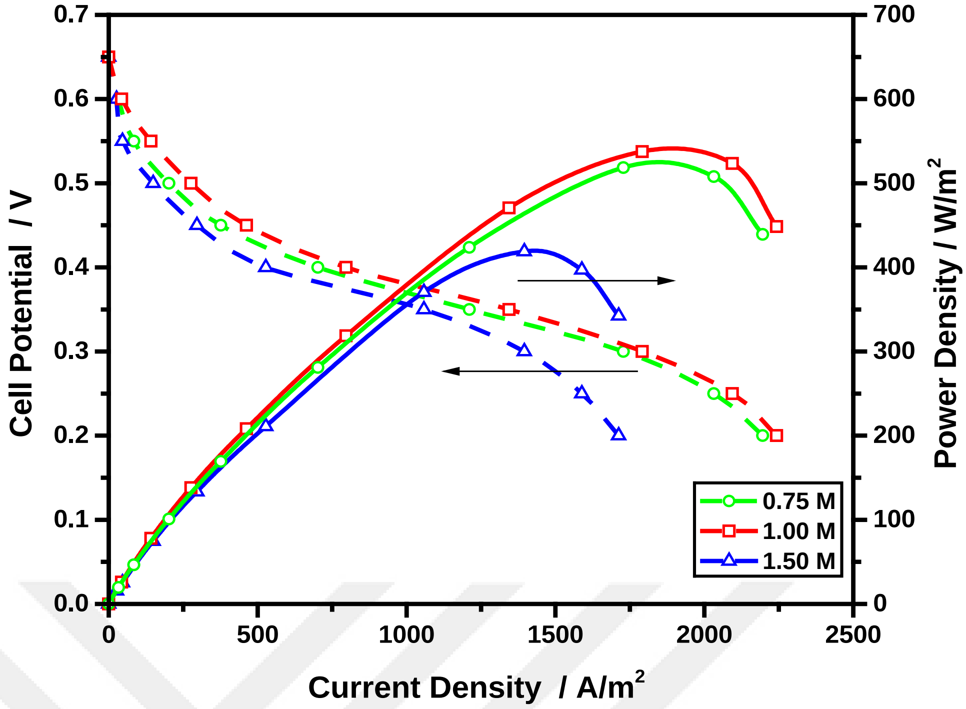

(a)

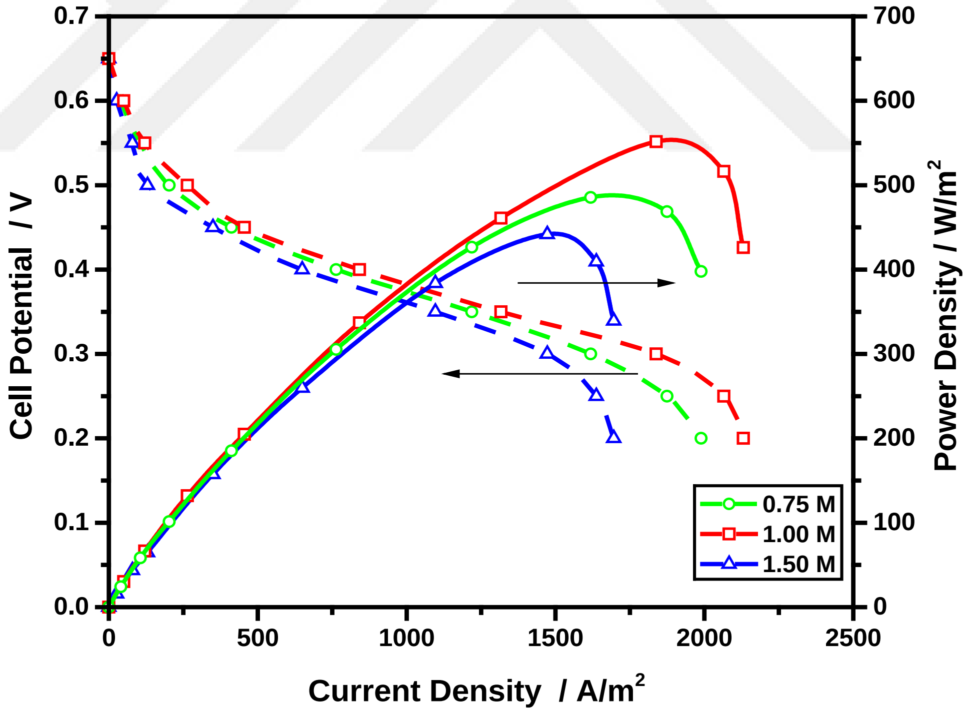

(b)

Figure 4.19 Power density and polarization curves at the methanol concentrations of 0.75 M, 1.00 M, and 1.50 M for (a) MEA-1 at 80°C, (b) MEA-2 at 100°C, and (c) MEA-3 at 100°C

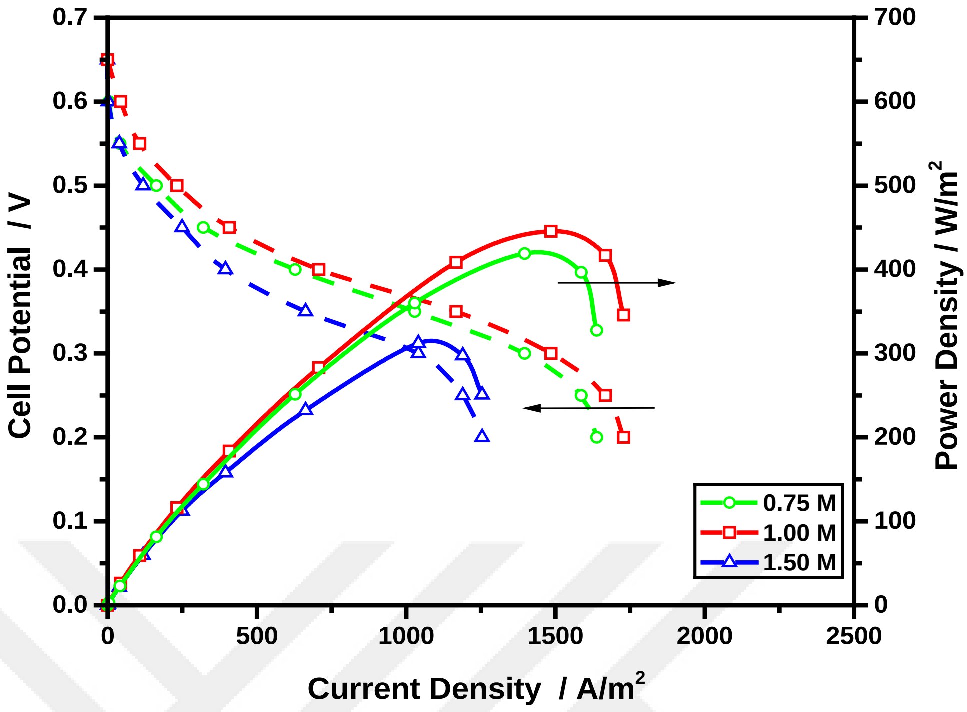

(c)

Figure 4.19 Power density and polarization curves at the methanol concentrations of 0.75 M, 1.00 M, and 1.50 M for (a) MEA-1 at 80°C, (b) MEA-2 at 100°C, and (c) MEA-3 at 100°C (continue)

As presented in Figure 4.19 (a)-Figure 4.19 (c), methanol concentration affects the performance of each DMFC considerably. This is because the concentration of methanol supplied to DMFC has a significant effect on the mass transport rate of methanol to the backing layers and the rate of methanol crossover from the anode to cathode. If the methanol with the optimum concentration is supplied to DMFC, it could be possible to achieve an improved DMFC performance. When the cell is fed with relatively low methanol concentrations, the OCV value becomes higher, whereas the limiting current density becomes lower because of the mass transport limitations. As the methanol concentration is increased from 1.00 M to 1.50 M, the cell voltage at low current densities becomes very low due to the significant increase in the rate of methanol crossover. The crossed-over methanol at the cathode is generally oxidized by the cathode catalyst, and thus leads to a mixed potential and undeniable voltage drop. Because of this methanol crossover problem, both the oxygen consumption and water generation rates within the cathode catalyst increase. The accumulated water causes a considerable increase in the mass transfer resistance within the cathode backing and catalyst layers. This would further decrease the available oxygen at the catalyst layer. These effects would, in the end, increase the cathodic activation and concentration polarizations. Due to the previously discussed negative effects of the methanol crossover problem, the achieved power densities become less after a certain methanol concentration value, which corresponds to ~1.00 M. As can be seen from Figure 4.19 (a)-Figure 4.19 (c), with a further increase in the methanol concentration, the drop in the performance of MEA-1 becomes much more significant as compared to those of MEA-2 and MEA-3. This could be explained by the fact that with an increase in the methanol concentration, Nafion® 115 membrane loses its ability to remain physically stable, and the methanol crossover phenomenon becomes much more drastic. This results in a remarkable performance deterioration due to crossed-over methanol at the cathode. However, Nafion/ZrP composite membranes could remain physically stable and limit the methanol crossover in comparison to Nafion® 115 with the increase in the methanol concentration.

4.4.3.3 Effect of Incorparation of ZrP into Pt/C Cathode Catalyst

ZrP is a solid proton conductor and provides solid state ion conductivity and high chemical and thermal stability (Jiang et al., 2006). Therefore, addition of ZrP directly to the commercial Pt/C cathode catalyst may improve the proton conductivity, reinforce the chemical and thermal stability, and allow operating at higher temperatures for DMFCs. In order to investigate the effect of Pt/C-ZrP cathode catalyst on the performance of the DMFCs, two different MEAs having the same NZ-2.5 but different cathode catalysts were manufactured. Then, to investigate the effect of operating temperature on the performances of these MEAs and make performance comparison, the experiments were conducted at different operating temperatures (40°C, 60°C, 80°C, and 100°C) and the methanol concentration of 1.00 M. Figure 4.20 presents the results of the experiments conducted for investigating the effect of operating temperature. As seen from Figure 4.20 (a), the peak power densities at 40°C, 60°C, 80°C (for 1.00 M methanol concentration) were achieved as 243.72 W/m^2, 361.44 W/m^2, and 517.44 W/m^2 for MEA-4, respectively. In addition, the maximum power density was found as 591.02 W/m^2 at 100°C and 1.00 M. The same experiments were also conducted at the same operating temperatures and the methanol concentration of 1.00 M for MEA-5. As seen from Figure 4.20 (b), the peak power densities at 40°C, 60°C, 80°C and 1.00 M were found as 280.20 W/m^2, 388.92 W/m^2, 561.84 W/m^2, respectively. The maximum power density was achieved as 620.88 W/m^2 at 100°C and 1.00 M. The potential reason of performance improvement with increasing operating temperature could be explained by the same mechanisms as discussed in Section 4.4.3.1. It is also found that MEA-5 yielded 5.06% more peak power density as compared to MEA-4. This performance improvement could be explained by the positive effects of incorporation of ZrP into commercial Pt/C cathode catalyst: higher and stable solid-state ion conductivity and better thermal and chemical stability.

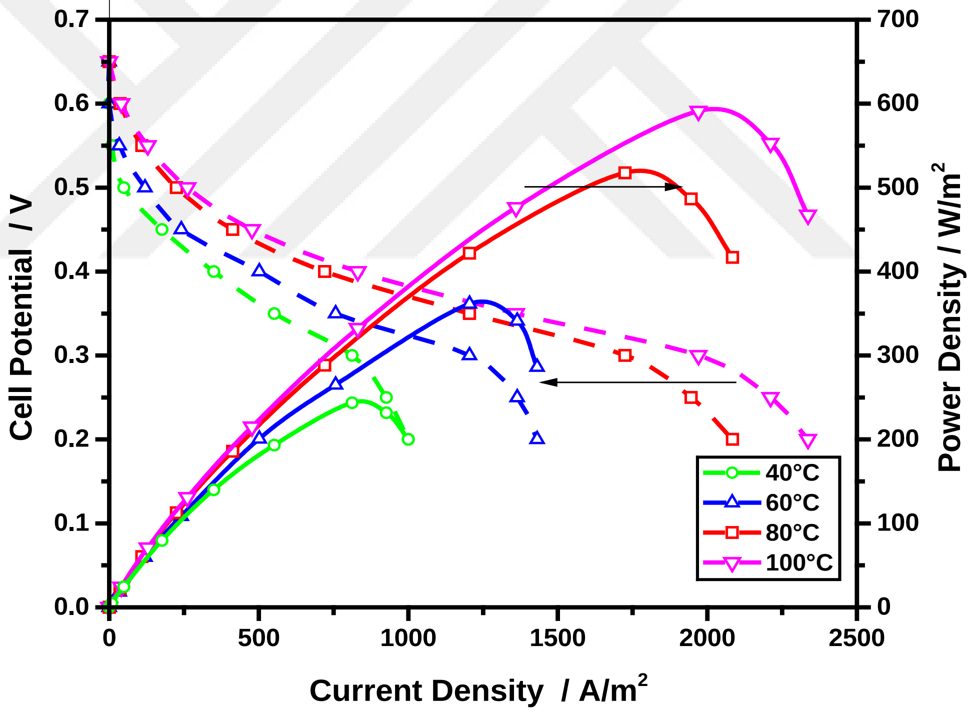

(a)

Figure 4.20 Power density and polarization curves at 40°C, 60°C, 80°C, 100°C and 1.00 M methanol concentration for (a) MEA-4, (b) MEA-5

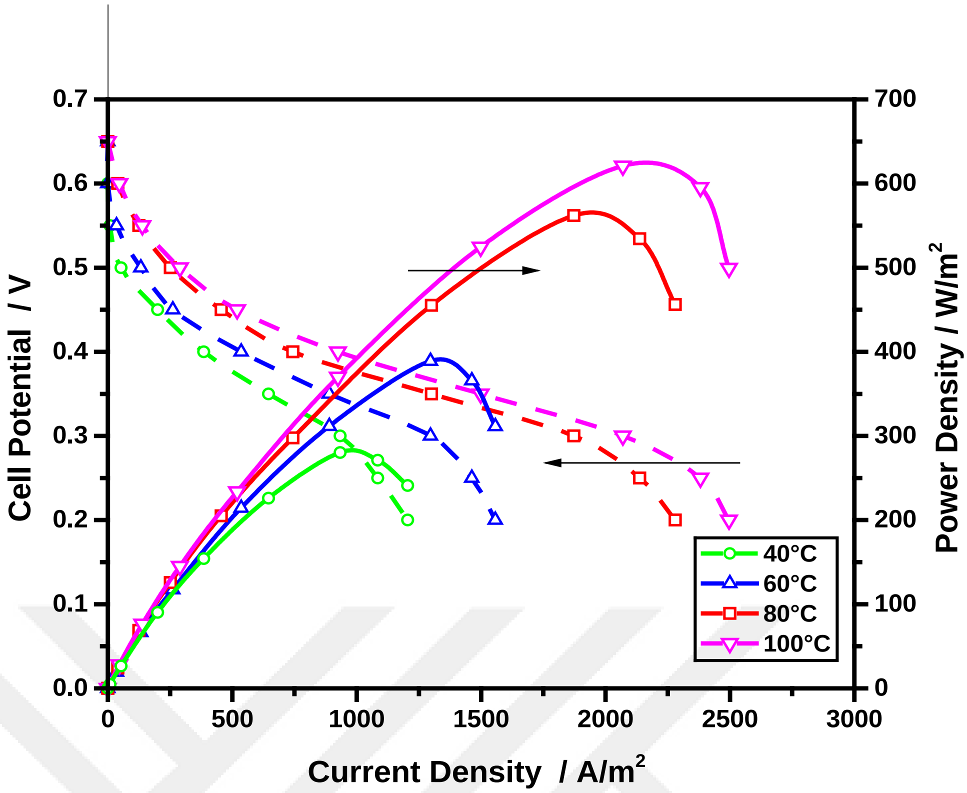

(b)

Figure 4.20 Power density and polarization curves at 40°C, 60°C, 80°C, 100°C and 1.00 M methanol concentration for (a) MEA-4, (b) MEA-5 (continue)

As reported above, the maximum performances of the MEAs were achieved at 100°C. Then, the experiments were carried out at different methanol concentrations (0.75 M and 1.50 M) and this operating temperature to investigate the effect of methanol concentration on the DMFC performance. As presented in Figure 4.21 (a), the maximum power density was found as 591.02 W/m^2 for MEA-4 at 1.00 M and 100°C. As seen from Figure 4.21 (b), the similar trend was also performed by MEA-5 with the maximum power density value of 620.88 W/m^2 at 1.00 M and 100°C. These trends in the performance variation with different methanol concentration were similar to those discussed in Section 4.4.3.2. Therefore, the performance variation with the change in methanol concentration could be explained by the same mechanisms as discussed in Section 4.4.3.2. On the other hand, as the concentration of the methanol was increased from 1.00 M to 1.50 M, the achieved peak power densities demonstrated a noticeable decrease (18.8% and 16.5%) for MEA-4 and MEA-5, respectively. The observed performance deterioration for MEA-5 was relatively low and this could be associated with the improved chemical stability and proton conductivity of this MEA due to the incorporation of ZrP.

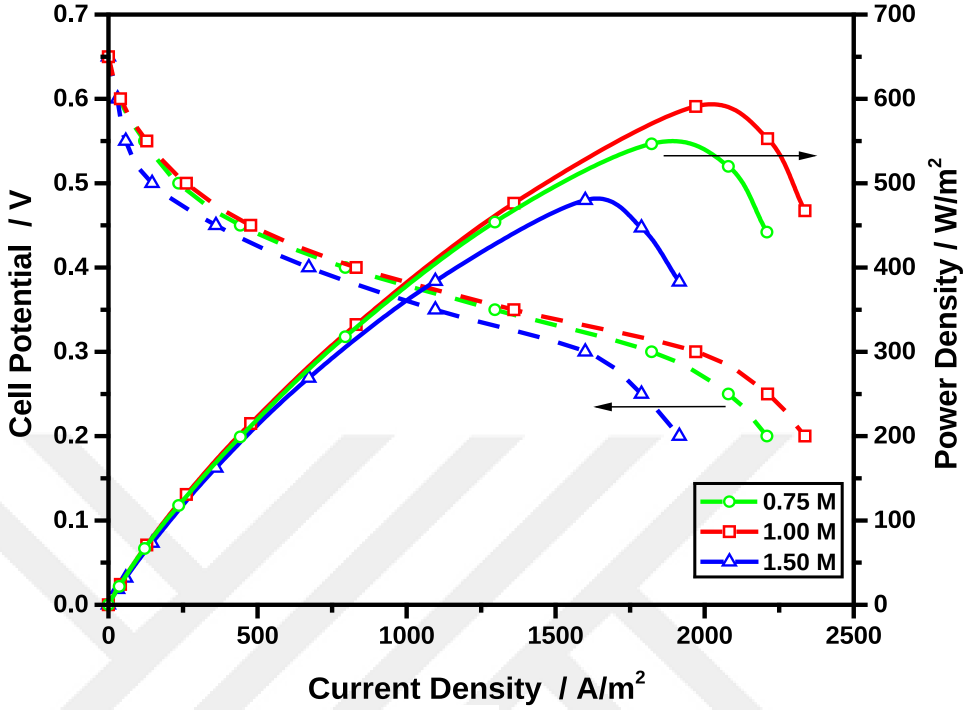

(a)

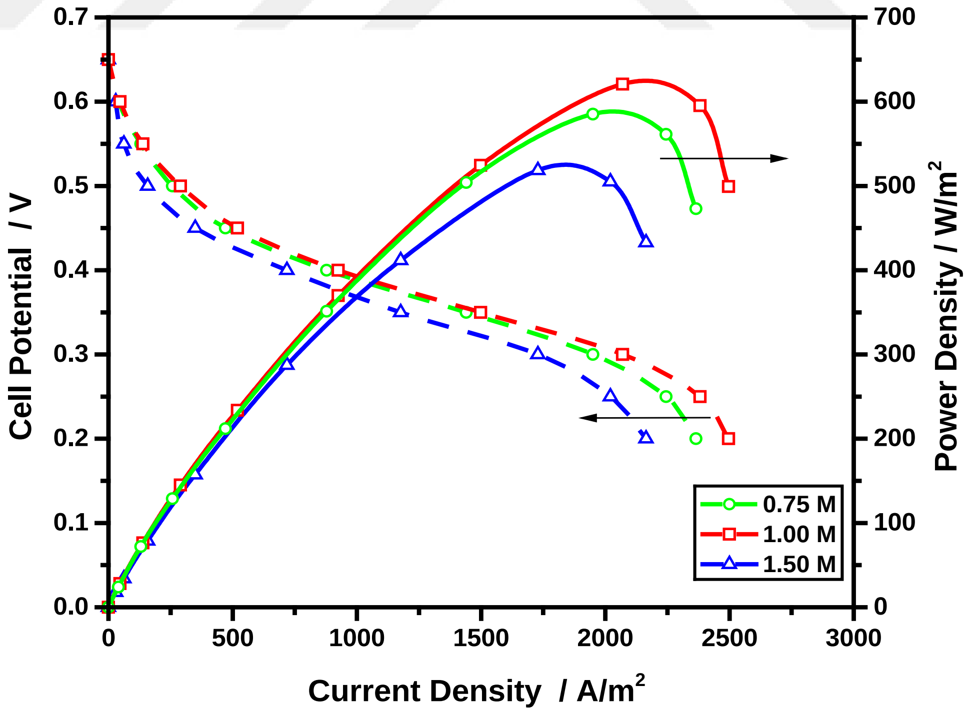

(b)

Figure 4.21 Power density and polarization curves at 0.75 M, 1.00 M, and 1.50 M and 100°C for (a) MEA-4, (b) MEA-5

4.4.3.4 Stability tests

In addition to the polarization curve, the stability of MEA is an important factor for evaluating its suitability. In this regard, it is desired for a fuel cell that the power density drop with time is minimum (Ercelik et al., 2016). Therefore, the short-term stability tests were carried out for all the MEAs to investigate their stability characteristics. During the stability tests, the flow rates of the 1.00 M methanol solution and oxygen gas were kept at 1.94 ml/min and 200 ml/min, respectively. The cell temperature and the voltage were set to 80°C and 0.3 V, respectively. The power density values were recorded for 4 h as seen in Figure 4.22. This figure shows that the majority of power density loss occured in the first 15 minutes due to the instability of testing. In addition, a slow drop in the power densities of the MEAs associated with increasing amount of methanol at the cathode due to undesired methanol crossover was observed. Therefore, the presented stability characteristics in Figure 4.22 could also give a hint of each MEA's ability to mitigate this performance-limiting phenomenon. On the other hand, sudden drops and increases in the power densities were also observed due mainly to some occasional situations during the short-term stability tests. As seen from Figure 4.22, after 3 h operation at above-mentioned conditions, MEA-1, MEA-2, and MEA-3 started to provide less power densities at 0.3 V; however, the drops in the power densities of MEA-2 and MEA-3 much more than that of MEA-1 (Figure 4.22). These differences could be an indicator of the superiority of Nafion® 115 membrane over both NZ-2.5 and NZ-5 as regards stability. However, as seen from Figure 4.22, the drop in the power density of MEA-3 at 0.3 V is much more observable that of MEA-2; therefore, the stability characteristic of NZ-2.5 is considered to be more promising in comparison to NZ-5. Figure 4.22 also clearly indicates that MEA-4 exhibits better stability characteristics as compared to MEA-2. This behavior could be attributed to the superiority of the HiSPEC® 9100 over commercial HP cathode catalyst (60 wt.% Pt on Vulcan XC-72) in terms of stability. Finally, as seen from Figure 4.22, incorporation of ZrP into commercial (HiSPEC® 9100) cathode catalyst could be the main reason for the MEA-5 demonstrating much better stability as compared to MEA-4.

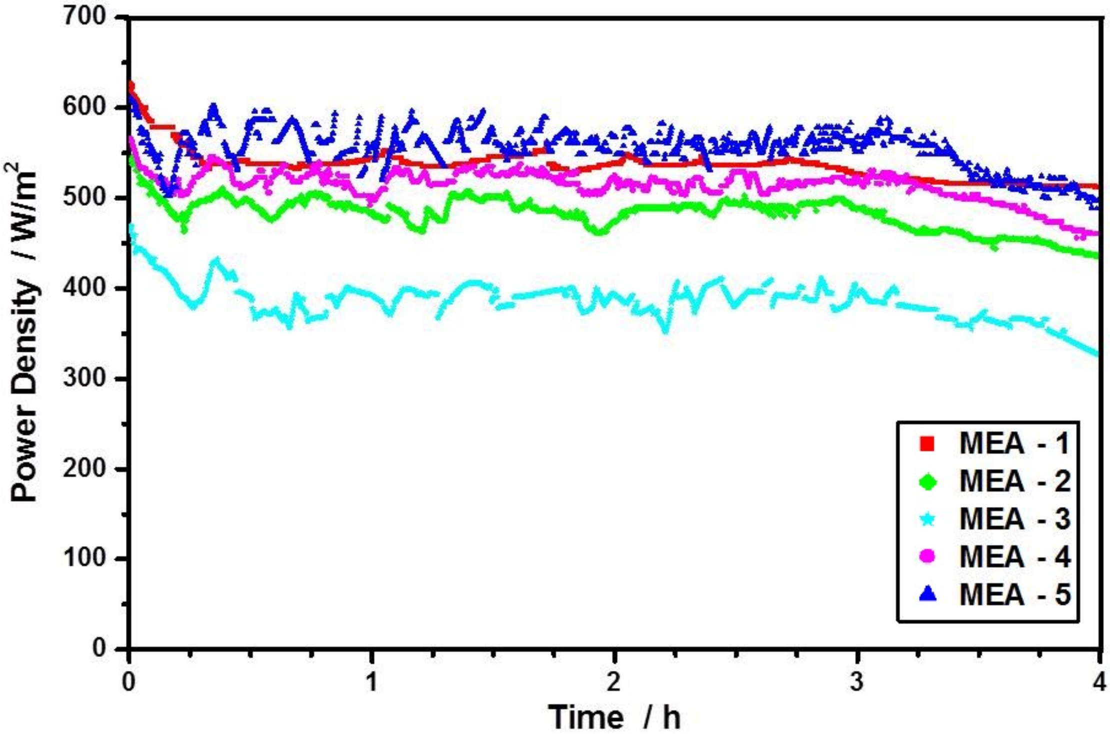

Figure 4.22 Short-term stability characteristics of the MEAs

CHAPTER FIVE
CONCLUSIONS

In this thesis, firstly, the effect of using Nafion based composite membranes (Nafion/TiO_2 and Nafion/SiO_2) on the performance of DMFCs was investigated experimentally. The performances of the MEAs having these membranes were compared with that of the MEA having a commercial Nafion® 115 membrane. In addition, the experiments were conducted at different operating temperatures (60°C, 80°C, and 95°C) to assess how the temperature changes the performance of the DMFCs having these membranes. The main conclusions derived from the experiments are listed as follows.

- The maximum power density of the MEA having Nafion® 115 membrane was found as 612.96 W/m^2 when the temperature and methanol concentration were taken as 80°C and 1 M, respectively.
- As the temperature increases from 60°C to 95°C, the performance of the MEA having Nafion based composite membranes increases; whereas that of the MEA having Nafion® 115 membrane increases up to 80°C and then decreases after this temperature.
- For all the different values of operating temperatures studied, the maximum power density of the DMFC was achieved as 710.88 W/m^2 at 95°C when Nafion/TiO_2 composite membrane was used.
- The maximum power density of the Nafion/TiO_2 and Nafion/SiO_2 composite membrane based MEAs yielded 26% and 36% more power density, respectively, than that of the Nafion® 115 membrane based MEA at 95°C.

The results of this study demonstrated that the Nafion/TiO_2 and Nafion/SiO_2 composite membrane based MEAs provide distinguishably better performance as compared to the MEA with commercial Nafion® 115 at relatively high temperature such as 95°C. Therefore, it can be concluded that the MEAs having Nafion based composite membranes are very promising for DMFC applications for high temperature levels.

Secondly, the performances of the DMFCs based on Pt-Ru/C-TiO_2 anode hybrid catalysts containing of 5, 15, and 25 wt.% of either in-house synthesized or commercial TiO_2 were investigated experimentally. The performances of these DMFCs were also compared to that of the DMFC based on commercial Pt-Ru/C anode electrocatalyst. In this regard, the performance tests were conducted at different temperatures (45°C, 60°C, and 80°C) and 1.00 M methanol concentration to assess how the temperature affects the performance of these DMFCs. Then, the effect of different methanol concentrations (0.50 M, 0.75 M, 1.00 M, and 1.50 M) on the performances of these DMFCs were investigated keeping the operating temperature constant at 80°C. The main conclusions derived from the experiments are listed as follows.

- As the operating temperature is increased from 45°C to 80°C, the performances of all the DMFCs based on both Pt-Ru/C-TiO_2 and commercial Pt-Ru/C anode electrocatalysts improve significantly.
- For all the studied methanol concentrations (0.50 M, 0.75 M, 1.00 M, and 1.50 M), all the DMFCs based on Pt-Ru/C-TiO_2 and commercial Pt-Ru/C anode electrocatalysts provide their maximum power densities at 1.00 M methanol concentration.
- The DMFC based on Pt-Ru/C-TiO_2 anode electrocatalyst containing of 5 wt.% of commercial TiO_2 provided the best performance with the power density value of 705.12 W/m^2 at 80°C and 1.00 M methanol concentration among all the DMFCs based on Pt-Ru/C-TiO_2 anode hybrid catalysts containing of commercial TiO_2.
- Of all the DMFCs based on Pt-Ru/C-TiO_2 anode hybrid catalysts containing in-house synthesized TiO_2, the maximum power density was found as 709.32 W/m^2 at 80°C and 1.00 M methanol concentration and provided by the DMFC based on Pt-Ru/C-TiO_2 anode hybrid catalyst containing of 5 wt.% of in-house synthesized TiO_2.
- The DMFCs based on Pt-Ru/C-TiO_2 anode hybrid catalysts containing 5 wt.% of commercial TiO_2 and in-house synthesized TiO_2 yielded 27.1% and 27.9% more power density in comparison to the DMFC based on commercial Pt-Ru/C anode electrocatalyst.

- The DMFC based on Pt-Ru/C-TiO_2 anode hybrid catalyst containing of 5 wt.% of commercial TiO_2 has more promising characteristic with regard to stability as compared to all other DMFCs tested in this study.

The results of this study indicated that the DMFCs based on Pt-Ru/C-TiO_2 anode hybrid catalysts containing 5 wt.% of in-house synthesized TiO_2 or commercial TiO_2 provide distinguishably better performance as compared to the DMFC based on commercial Pt-Ru/C anode electrocatalyst. Pt-Ru/C-TiO_2 anode hybrid catalysts seem to be very promising in terms of achieving an improved performance and better stability for DMFC applications. As a future study, it is intended to make a long-term stability tests for DMFCs based on Pt-Ru/C-TiO_2 anode hybrid catalysts.

Thirdly, the performances of the MEAs having commercial Nafion® 115 membrane and NZ-2.5 and NZ-5 were investigated experimentally. The experiments were first performed at different temperatures (40°C, 60°C, 80°C, and 100°C) with the methanol concentration of 1.00 M to determine the temperatures, which each MEA yields its highest power density value. These temperature values were found as 80°C and 100°C for the MEAs having commercial Nafion® 115 membrane and Nafion/ZrP composite membranes, respectively. Then, a set of experiments were conducted at these temperatures with three different methanol concentrations (0.75 M, 1.00 M, and 1.50 M) to assess how the performances of the MEAs change depending on the methanol concentration. In addition, the performance of the MEA based on Pt/C-ZrP cathode catalyst and Nafion/ZrP composite membrane was compared with that of the MEA based on the same membrane but the conventional Pt/C cathode catalyst. In addition, short-term stability tests were carried out for all the MEAs. The main conclusions derived from the conducted study are listed as follows.

- The maximum power density of the MEA with commercial Nafion® 115 membrane was achieved at 80°C and 1.00 M methanol concentration with the power density value of 537.48 W/m^2.

- The MEA having NZ-2.5 provided its maximum power density (551.52 W/m^2) at the temperature of 100°C and 1.00 M methanol concentration.
- The maximum power density provided by the MEA having NZ-5 was found as 445.44 W/m^2 at 100°C and 1.00 M methanol concentration.
- As the temperature increases 80°C to 100°C, the performance of the MEA having Nafion® 115 membrane deteriorates, whereas those of the MEAs having Nafion/ZrP composite membranes improve.
- For all the studied operating temperatures (40°C, 60°C, 80°C, and 100°C), the maximum power density (551.52 W/m^2) was provided by the MEA having NZ-2.5 at 100°C.
- For all the studied methanol concentrations (0.75 M, 1.00 M, and 1.50 M), all the MEAs manufactured in this study provided their maximum power density values at 1.00 M methanol concentration.
- The MEA having commercial Nafion® 115 membrane shows more promising behavior regarding stability as compared to the MEAs having NZ-2.5 and NZ-5.
- Introduction of ZrP to commercial (HiSPEC® 9100) cathode catalyst improves both the performance and the stability characteristic of the MEA.
- The MEA with NZ-2.5 and commercial (HiSPEC® 9100) cathode catalyst seems more promising in terms of both performance and stability as compared to the MEA having the same membrane but commercial (HP 60 wt.% Pt on Vulcan XC-72) cathode catalyst.

The results of this study have revealed that the MEA having NZ-2.5 provides distinguishably better performance in comparison to the MEA with commercial Nafion® 115 membrane at elevated operating temperatures. The results of this study are expected to be useful towards the development and commercialization of high temperature DMFCs that could be used in a wide range of portable applications. As a future study, long-term stability tests will be carried out to assess the suitability of these membranes for DMFC applications.

REFERENCES

Abdelkareem, M. A., Ito, Y., Tsujiguchi, T., & Nakagawa, N. (2013). Carbon-TiO_2 composite nanofibers as a promising support for PtRu anode catalyst of DMFC. *ECS Transactions*, *50*(2), 1959-1967.

Adjemian, K. T., Lee, S. J., Srinivasan, S., Benziger, J., & Bocarsly, A. B. (2002). Silicon oxide nafion composite membranes for proton-exchange membrane fuel cell operation at 80-140 C. *Journal of the Electrochemical Society*, *149*(3), A256-A261.

Alberti, G., Casciola, M., Costantino, U., Levi, G., & Ricciardi, G. (1978). On the mechanism of diffusion and ionic transport in crystalline insoluble acid salts of tetravalent metals—I Electrical conductance of zirconium bis (monohydrogen ortho-phosphate) monohydrate with a layered structure. Journal *of Inorganic and Nuclear Chemistry*, *40*(3), 533-537.

Antolini, E., Salgado, J. R., & Gonzalez, E. R. (2006). The stability of Pt–M (M= first row transition metal) alloy catalysts and its effect on the activity in low temperature fuel cells: a literature review and tests on a Pt–Co catalyst. *Journal of Power Sources*, *160*(2), 957-968.

Arico, A. S., Srinivasan, S., & Antonucci, V. (2001). DMFCs: from fundamental aspects to technology development. *Fuel cells*, *1*(2), 133-161.

Baglio, V., Zignani, S. C., Siracusano, S., Stassi, A., D'Urso, C., & Aricò, A. S. (2013). Composite anode electrocatalyst for direct methanol fuel cells. *Electrocatalysis*, *4*(4), 235-240.

Barbera, O., Stassi, A., Sebastian, D., Bonde, J. L., Giacoppo, G., D'Urso, C., et al. (2016). Simple and functional direct methanol fuel cell stack designs for application in portable and auxiliary power units. *International Journal of Hydrogen Energy*, *41(*28), 12320-12329.

Barbir, F. (2012). *PEM fuel cells: theory and practice*. USA, Elsevier Academic Press.

Barbora, L., Acharya, S., & Verma, A. (2009). Synthesis and ex-situ characterization of Nafion/TiO_2 composite membranes for direct ethanol fuel cell. *Macromolecular Symposia,277*, 177-189. Germany, WILEY-VCH.

Barron, O., Su, H., Linkov, V., Pollet, B. G., & Pasupathi, S. (2015). Enhanced performance and stability of high temperature proton exchange membrane fuel cell by incorporating zirconium hydrogen phosphate in catalyst layer. *Journal of Power Sources, 278*, 718-724.

Basri, S., Kamarudin, S. K., Daud, W. R. W., & Yaakub, Z. (2010). Nanocatalyst for direct methanol fuel cell (DMFC). *International Journal of Hydrogen Energy, 35*(15), 7957-7970.

Bauer, F., & Willert-Porada, M. (2004). Microstructural characterization of Zr-phosphate–Nafion® membranes for direct methanol fuel cell (DMFC) applications. *Journal of Membrane Science, 233*(1), 141-149.

Bauer, F., & Willert-Porada, M. (2006). Comparison between Nafion® and a Nafion® Zirconium Phosphate Nano-Composite in Fuel Cell Applications. *Fuel Cells, 6*(3-4), 261-269.

Bébin, P., Caravanier, M., & Galiano, H. (2006). Nafion®/clay-SO_3H membrane for proton exchange membrane fuel cell application. *Journal of Membrane Science, 278*(1), 35-42.

Beydaghi, H., Javanbakht, M., Bagheri, A., Salarizadeh, P., Ghafarian-Zahmatkesh, H., Kashefi, S., & Kowsari, E. (2015). Novel nanocomposite membranes based on blended sulfonated poly (ether ether ketone)/poly (vinyl alcohol) containing sulfonated graphene oxide/Fe_3O_4 nanosheets for DMFC applications. *RSC Advances*, *5*(90), 74054-74064.

Campbell, L. K., Na, B. K., & Ko, E. I. (1992). Synthesis and characterization of titania aerogels. *Chemistry of Materials, 4*(6), 1329-1333.

Casalegno, A., Grassini, P., & Marchesi, R. (2007). Experimental analysis of methanol cross-over in a direct methanol fuel cell. *Applied Thermal Engineering, 27*(4), 748-754.

Casciola, M., Alberti, G., Sganappa, M., & Narducci, R. (2006). On the decay of Nafion proton conductivity at high temperature and relative humidity. *Journal of Power Sources*, *162*(1), 141-145.

Chalkova, E., Fedkin, M. V., Wesolowski, D. J., & Lvov, S. N. (2005). Effect of TiO_2 surface properties on performance of Nafion-based composite membranes in high temperature and low relative humidity PEM fuel cells. *Journal of The Electrochemical Society, 152*(9), A1742-A1747.

Changhwan, C. H. O., Yongchan, K. I. M., & Chang, Y. S. (2009). Performance analysis of direct methanol fuel cell for optimal operation. *Journal of Thermal Science and Technology*, *4*(3), 414-423.

Chen, C. Y., Yang, P., Lee, Y. S., & Lin, K. F. (2005). Fabrication of electrocatalyst layers for direct methanol fuel cells. *Journal of Power Sources, 141*(1), 24-29.

Chen, C. Y., & Tsao, C. S. (2006). Characterization of electrode structures and the related performance of direct methanol fuel cells. *International Journal of Hydrogen Energy*, *31*(3), 391-398.

Chen, L. C., Yu, T. L., Lin, H. L., & Yeh, S. H. (2008). Nafion/PTFE and zirconium phosphate modified Nafion/PTFE composite membranes for direct methanol fuel cells. *Journal of Membrane Science, 307*(1), 10-20.

Chen, R., Zhao, T. S., & Liu, J. G. (2006). Effect of cell orientation on the performance of passive direct methanol fuel cells. *Journal of Power Sources, 157*(1), 351-357.

Chien, H. C., Tsai, L. D., Huang, C. P., Kang, C. Y., Lin, J. N., & Chang, F. C. (2013). Sulfonated graphene oxide/Nafion composite membranes for high-performance direct methanol fuel cells. *International Journal of Hydrogen Energy, 38*(31), 13792-13801.

Cho, J. H., Kim, J. M., Prabhuram, J., Hwang, S. Y., Ahn, D. J., Ha, H. Y., & Kim, S. K. (2009). Fabrication and evaluation of membrane electrode assemblies by low-temperature decal methods for direct methanol fuel cells. *Journal of Power Sources*, *187*(2), 378-386.

Chu, D., & Jiang, R. (2006). Effect of operating conditions on energy efficiency for a small passive direct methanol fuel cell. *Electrochimica Acta*, *51*(26), 5829-5835.

Chu, Y. Y., Cao, J., Dai, Z., & Tan, X. Y. (2014). A novel Pt/CeO_2 catalyst coated with nitrogen-doped carbon with excellent performance for DMFCs. *Journal of Materials Chemistry A*, *2*(11), 4038-4044.

Coats, A. W., & Redfern, J. P. (1963). Thermogravimetric analysis. A review. *Analyst*, *88*(1053), 906-924.

Costamagna, P., Yang, C., Bocarsly, A. B., & Srinivasan, S. (2002). Nafion® 115/zirconium phosphate composite membranes for operation of PEMFCs above 100 C. *Electrochimica Acta*, *47*(7), 1023-1033.

Cui, X., Zhu, Y., Hua, Z., Feng, J., Liu, Z., Chen, L., & Shi, J. (2015). SnO_2 nanocrystal-decorated mesoporous ZSM-5 as a precious metal-free electrode catalyst for methanol oxidation. *Energy & Environmental Science*, *8*(4), 1261-1266.

Cullity, B. D. (1978). Answers to problems: Elements of X-ray Diffraction. USA, Addison-Wesley Publishing Company.

Das, S., Dutta, K., & Kundu, P. P. (2015). Nickel nanocatalysts supported on sulfonated polyaniline: potential toward methanol oxidation and as anode materials for DMFCs. *Journal of Materials Chemistry A*, *3*(21), 11349-11357.

Dawoud, B., Amer, E. H., & Gross, D. M. (2007). Experimental investigation of an adsorptive thermal energy storage. *International Journal of Energy Research*, *31*(2), 135-147.

Devrim, Y., Erkan, S., Baç, N., & Eroglu, I. (2012). Improvement of PEMFC performance with Nafion/inorganic nanocomposite membrane electrode assembly prepared by ultrasonic coating technique. *International Journal of Hydrogen Energy, 37*(21), 16748-16758.

Devrim, Y. (2014). Preparation and testing of Nafion/titanium dioxide nanocomposite membrane electrode assembly by ultrasonic coating technique. *Journal of Applied Polymer Science, 131*(15).

DeLuca, N. W., & Elabd, Y. A. (2006). Polymer electrolyte membranes for the direct methanol fuel cell: a review. Journal of Polymer Science Part B: Polymer Physics, 44(16), 2201-2225.

Drew, K., Girishkumar, G., Vinodgopal, K., & Kamat, P. V. (2005). Boosting fuel cell performance with a semiconductor photocatalyst: TiO_2/Pt−Ru hybrid catalyst for methanol oxidation. *The Journal of Physical Chemistry B, 109*(24), 11851-11857.

Ercelik, M., Ozden, A., Devrim, Y., & Colpan, C. O. (2017). Investigation of Nafion based composite membranes on the performance of DMFCs. *International Journal of Hydrogen Energy*, *42*(4), 2658-2668.

Ercelik, M., Ozden, A., Seker, E., & Colpan, C. O. (2016). Characterization and performance evaluation of Pt-Ru/C-TiO_2 anode electrocatalyst for DMFC applications. *International Journal of Hydrogen Energy*. Doi: 10.1016/j.ijhydene.2016.12.020

Gago, A. S., Esquivel, J. P., Sabaté, N., Santander, J., & Alonso-Vante, N. (2015). Comprehensive characterization and understanding of micro-fuel cells operating at high methanol concentrations. *Beilstein Journal of Nanotechnology, 6*(1), 2000-2006.

Ghouri, Z. K., Barakat, N. A., Park, M., Kim, B. S., & Kim, H. Y. (2015). Synthesis and characterization of Co/$SrCO_3$ nanorods-decorated carbon nanofibers as novel electrocatalyst for methanol oxidation in alkaline medium. *Ceramics International*, *41*(5), 6575-6582.

Hasegawa, T., Béléké, A. B., & Mizuhata, M. (2013). Membrane modification by liquid phase deposition using small amount of TiO_2 for high-temperature operation of polymer electrolyte fuel cells. *Journal of Power Sources, 233*, 148-156.

He, R., Li, Q., Xiao, G., & Bjerrum, N. J. (2003). Proton conductivity of phosphoric acid doped polybenzimidazole and its composites with inorganic proton conductors. *Journal of Membrane Science, 226*(1), 169-184.

Hobson, L. J., Nakano, Y., Ozu, H., & Hayase, S. (2002). Targeting improved DMFC performance. *Journal of Power Sources, 104*(1), 79-84.

Hogarth, W. H., Da Costa, J. D., & Lu, G. M. (2005). Solid acid membranes for high temperature (140°C) proton exchange membrane fuel cells. Journal of Power Sources, 142(1), 223-237.

Hu, Y., Zhu, J., Lv, Q., Liu, C., Li, Q., & Xing, W. (2015). Promotional effect of phosphorus doping on the activity of the Fe-N/C catalyst for the oxygen reduction reaction. *Electrochimica Acta, 155*, 335-340.

Huang, H., & Wang, X. (2014). Recent progress on carbon-based support materials for electrocatalysts of direct methanol fuel cells. *Journal of Materials Chemistry A, 2*(18), 6266-6291.

Jalani, N. H., Dunn, K., & Datta, R. (2005). Synthesis and characterization of Nafion®-MO_2 (M= Zr, Si, Ti) nanocomposite membranes for higher temperature PEM fuel cells. *Electrochimica Acta, 51*(3), 553-560.

Jiang, R., & Chu, D. (2004). Comparative studies of methanol crossover and cell performance for a DMFC. *Journal of The Electrochemical Society, 151*(1), A69-A76.

Jian-hua, T., Peng-fei, G., Zhi-yuan, Z., Wen-hui, L., & Zhong-qiang, S. (2008). Preparation and performance evaluation of a Nafion-TiO_2 composite membrane for PEMFCs. *International Journal of Hydrogen Energy, 33*(20), 5686-5690.

Jiang, R., Kunz, H. R., & Fenton, J. M. (2006). Influence of temperature and relative humidity on performance and CO tolerance of PEM fuel cells with Nafion®–Teflon®–Zr $(HPO_4)_2$ higher temperature composite membranes. *Electrochimica Acta*, *51*(26), 5596-5605.

Joint Committee on Powder Diffraction Standards (JCPDS)-International Centre for Diffraction Data (ICDD), (2014). Pennsylvania, *Powder Diffraction File (PDF)* database.

Justin, P., & Rao, G. R. (2011). Methanol oxidation on MoO_3 promoted Pt/C electrocatalyst. *International Journal of Hydrogen Energy, 36*(10), 5875-5884.

Kamarudin, S. K., & Hashim, N. (2012). Materials, morphologies and structures of MEAs in DMFCs. *Renewable and Sustainable Energy Reviews*, *16*(5), 2494-2515.

Karim, N. A., & Kamarudin, S. K. (2013). An overview on non-platinum cathode catalysts for direct methanol fuel cell. *Applied Energy*, *103*, 212-220.

Ke, C. C., Li, X. J., Qu, S. G., Shao, Z. G., & Yi, B. L. (2012). Preparation and properties of Nafion/SiO_2 composite membrane derived via in situ sol–gel reaction: size controlling and size effects of SiO_2 nano-particles. *Polymers for Advanced Technologies, 23*(1), 92-98.

Khotseng, L., Bangisa, A., Modibedi, R. M., & Linkov, V. (2016). Electrochemical evaluation of Pt-Based binary catalysts on various supports for the direct methanol fuel cell. *Electrocatalysis, 7*(1), 1-12.

Kim, B. C., Spinks, G. M., Too, C. O., Wallace, G. G., Bae, Y. H., & Ogata, N. (2000). Incorporation of novel polyelectrolyte dopants into conducting polymers. *Reactive and Functional Polymers, 44*(3), 245-258.

Kim, Y. S., Wang, F., Hickner, M., Zawodzinski, T. A., & McGrath, J. E. (2003). Fabrication and characterization of heteropolyacid ($H_3PW_{12}O_{40}$)/directly polymerized sulfonated poly (arylene ether sulfone) copolymer composite membranes for higher temperature fuel cell applications. *Journal of Membrane Science*, *212*(1), 263-282.

Kuan, H. C., Wu, C. S., Chen, C. Y., Yu, Z. Z., Dasari, A., & Mai, Y. W. (2006). Preparation of exfoliated zirconium phosphate/Nafion organic-inorganic hybrid proton exchange membranes. *Electrochemical and Solid-State Letters*, *9*(2), A76-A79.

Kumar, P., Dutta, K., & Kundu, P. P. (2014). Enhanced performance of direct methanol fuel cells: a study on the combined effect of various supporting electrolytes, flow channel designs and operating temperatures. *International Journal of Energy Research*, *38*(1), 41-50.

Li, W., Liang, C., Zhou, W., Qiu, J., Zhou, Z., Sun, G., & Xin, Q. (2003). Preparation and characterization of multiwalled carbon nanotube-supported platinum for cathode catalysts of direct methanol fuel cells. *The Journal of Physical Chemistry B*, *107*(26), 6292-6299.

Liang, H., Xu, R., Chen, K., Shen, C., & Yin, S. (2016). Self-humidifying membrane electrode assembly with dual cathode catalyst layer structure prepared by introducing polyvinyl alcohol into the inner layer. *RSC Advances*, *6*(2), 1333-1338.

Liang, Z. X., Zhao, T. S., & Prabhuram, J. (2006). Diphenylsilicate-incorporated Nafion® membranes for reduction of methanol crossover in direct methanol fuel cells. *Journal of Membrane Science*, *283*(1), 219-224.

Lim, C., & Wang, C. Y. (2003). Development of high-power electrodes for a liquid-feed direct methanol fuel cell. *Journal of Power Sources*, *113*(1), 145-150.

Lin, H. L., Yeh, S. H., Yu, T. L., & Chen, L. C. (2009). Silicate and zirconium phosphate modified Nafion/PTFE composite membranes for high temperature PEMFC. *Journal of Polymer Research*, *16*(5), 519-527.

Lin, H. L., Yu, T. L., Huang, L. N., Chen, L. C., Shen, K. S., & Jung, G. B. (2005). Nafion/PTFE composite membranes for direct methanol fuel cell applications. *Journal of Power Sources*, *150*, 11-19.

Lin, J. C., Kunz, H. R., & Fenton, J. M. (2003). Membrane/electrode additives for low–humidification operation. *Handbook of Fuel Cells*. Doi: 10.1002/9780470974001.f303040

Liu, F., Yi, B., Xing, D., Yu, J., & Zhang, H. (2003). Nafion/PTFE composite membranes for fuel cell applications. *Journal of Membrane Science, 212*(1), 213-223.

Liu, G., Wang, M., Wang, Y., Tian, Z., & Wang, X. (2013). A novel anode catalyst layer with multilayer and pore structure for improving the performance of a direct methanol fuel cell. *International Journal of Energy Research, 37*(11), 1313-1317.

Liu, H., Song, C., Zhang, L., Zhang, J., Wang, H., & Wilkinson, D. P. (2006). A review of anode catalysis in the direct methanol fuel cell. *Journal of Power Sources, 155*(2), 95-110.

Liu, J., Zhao, T. S., Chen, R., & Wong, C. W. (2005). Effect of methanol concentration on passive DMFC performance. *Fuel Cells Bulletin, 2005*(2), 12-17.

Liu, J. , Zhao, T. S., Liang, Z. X., & Chen, R. (2006). Effect of membrane thickness on the performance and efficiency of passive direct methanol fuel cells. *Journal of Power Sources, 153*(1), 61-67.

Long, J. W., Stroud, R. M., Swider-Lyons, K. E., & Rolison, D. R. (2000). How to make electrocatalysts more active for direct methanol oxidation avoid PtRu bimetallic alloys!. *The Journal of Physical Chemistry B, 104*(42), 9772-9776.

Macak, J. M., Barczuk, P. J., Tsuchiya, H., Nowakowska, M. Z., Ghicov, A., Chojak, et al. (2005). Self-organized nanotubular TiO_2 matrix as support for dispersed Pt/Ru nanoparticles: enhancement of the electrocatalytic oxidation of methanol. *Electrochemistry Communications, 7*(12), 1417-1422.

Maiyalagan, T., & Khan, F. N. (2009). Electrochemical oxidation of methanol on Pt/V_2O_5–C composite catalysts. *Catalysis Communications, 10*(5), 433-436

Mauritz, K. A., & Moore, R. B. (2004). State of understanding of Nafion. *Chemical Reviews, 104*(10), 4535-4586.

Micoud, F., Maillard, F., Gourgaud, A., & Chatenet, M. (2009). Unique CO-tolerance of Pt–WO_x materials. *Electrochemistry Communications, 11*(3), 651-654.

Mokhtaruddin, S. R., Mohamad, A. B., Shyuan, L. K., Kadhum, A. A. H., & Akhmad, M. (2011). Preparation and characterization of nafion-zirconia composite membrane for PEMFC. *In Advanced Materials Research, 239*, 263-268.

Mollá, S., & Compañ, V. (2011). Performance of composite Nafion/PVA membranes for direct methanol fuel cells. *Journal of Power Sources, 196*(5), 2699-2708.

Narischat, N., Takeguchi, T., Tsuchiya, T., Mori, T., Ogino, I., Mukai, S. R., & Ueda, W. (2014). Effect of Activation Degree of Resorcinol–Formaldehyde Carbon Gels on Carbon monoxide Tolerance of Platinum–Ruthenium Polymer Electrolyte Fuel Cell Anode Catalyst. *The Journal of Physical Chemistry C, 118*(40), 23003-23010.

Ouellette D. (2015) Multiphase modeling of a flowing electrolyte direct methanol fuel cell. Ph.D. thesis. Carleton University, Ottawa.

Osmieri, L., Escudero-Cid, R., Videla, A. H. M., Ocón, P., & Specchia, S. (2017). Performance of a Fe-NC catalyst for the oxygen reduction reaction in direct methanol fuel cell: Cathode formulation optimization and short-term durability. *Applied Catalysis B: Environmental, 201*, 253-265.

Ozden, A., Ercelik, M., Ouellette, D., Colpan, C. O., Ganjehsarabi, H., & Hamdullahpur, F. (2017). Designing, modeling and performance investigation of bio-inspired flow field based DMFCs. *International Journal of Hydrogen Energy*. Doi: 10.1002/9780470974001.f303040.

Ozden, A., Ercelik, M., Ozdemir, Y., Devrim, Y., & Colpan, C. O. (2017). Enhancement of direct methanol fuel cell performance through the inclusion of zirconium phosphate. *International Journal of Hydrogen Energy*. Doi: 10.1016/j.ijhydene.2017.01.188

Park, J., Wang, L., Advani, S. G., & Prasad, A. K. (2012). Durability analysis of Nafion/hydrophilic pretreated PTFE membranes for PEMFCs. Journal of *The Electrochemical Society, 159*(12), F864-F870.

Park, Y. I., Kim, J. D., & Nagai, M. (2000). Increase of proton conductivity in amorphous phosphate–Nafion membranes. *Journal of Materials Science Letters, 19*(18), 1621-1623.

Park, Y. S., & Yamazaki, Y. (2004). High proton conducting and low methanol crossover Nafion/Hydroxyapatite (HA) composite membrane. *Fall Meeting of The Electrochemical Society of Japan*, Hawaii.

Patel, P. P., Datta, M. K., Jampani, P. H., Hong, D., Poston, J. A., Manivannan, A., et al. (2015). High performance and durable nanostructured TiN supported Pt_{50}–Ru_{50} anode catalyst for direct methanol fuel cell (DMFC). *Journal of Power Sources*, 293, 437-446.

Peighambardoust, S. J., Rowshanzamir, S., & Amjadi, M. (2010). Review of the proton exchange membranes for fuel cell applications. International Journal of Hydrogen Energy, 35(17), 9349-9384.

Ravikumar, M. K., & Shukla, A. K. (1996). Effect of Methanol Crossover in a Liquid-Feed Polymer-Electrolyte Direct Methanol Fuel Cell. *Journal of the Electrochemical Society*, 143(8), 2601-2606.

Rodgers, M. P., Shi, Z., & Holdcroft, S. (2009). Ex situ characterisation of composite Nafion membranes containing zirconium hydrogen phosphate. *Fuel Cells, 9*(5), 534-546.

Rosenthal, N. S., Vilekar, S. A., & Datta, R. (2012). A comprehensive yet comprehensible analytical model for the direct methanol fuel cell. *Journal of Power Sources*, *206*, 129-143.

Sabet-Sharghi, N., Cruickshank, C. A., Matida, E., & Hamdullahpur, F. (2013). Performance measurements of a single cell flowing electrolyte-direct methanol fuel cell (FE-DMFC). *Journal of Power Sources*, *230*, 194-200.

Sahu, A. K., Bhat, S. D., Pitchumani, S., Sridhar, P., Vimalan, V., George, C., et al. (2009). Novel organic–inorganic composite polymer-electrolyte membranes for DMFCs. *Journal of Membrane Science, 345*(1), 305-314.

Salarizadeh, P., Javanbakht, M., Abdollahi, M., & Naji, L. (2013). Preparation, characterization and properties of proton exchange nanocomposite membranes based on poly (vinyl alcohol) and poly (sulfonic acid)-grafted silica nanoparticles. *International Journal of Hydrogen Energy*, *38*(13), 5473-5479.

Scibioh, M. A., Kim, S. K., Cho, E. A., Lim, T. H., Hong, S. A., & Ha, H. Y. (2008). Pt-CeO_2/C anode catalyst for direct methanol fuel cells. *Applied Catalysis B: Environmental*, *84*(3), 773-782.

Sebastián, D., Serov, A., Artyushkova, K., Atanassov, P., Aricò, A. S., & Baglio, V. (2016). Performance, methanol tolerance and stability of Fe-aminobenzimidazole derived catalyst for direct methanol fuel cells. *Journal of Power Sources*, *319*, 235-246.

Sebastián, D., Serov, A., Artyushkova, K., Gordon, J., Atanassov, P., Aricò, A. S., et al. (2016). High Performance and Cost-Effective Direct Methanol Fuel Cells: Fe-N-C Methanol-Tolerant Oxygen Reduction Reaction Catalysts. *ChemSusChem*, *9(*15), 1986-1995.

Selvarani, G., Selvaganesh, S. V., Krishnamurthy, S., Kiruthika, G. V. M., Sridhar, P., Pitchumani, S., & Shukla, A. K. (2009). A methanol-tolerant carbon-supported Pt−Au alloy cathode catalyst for direct methanol fuel cells and its evaluation by DFT. *The Journal of Physical Chemistry C, 113*(17), 7461-7468.

Shao, Z. G., Joghee, P., & Hsing, I. M. (2004). Preparation and characterization of hybrid Nafion–silica membrane doped with phosphotungstic acid for high temperature operation of proton exchange membrane fuel cells. *Journal of Membrane Science, 229*(1), 43-51.

Shao, Z. G., Xu, H., Li, M., & Hsing, I. M. (2006). Hybrid Nafion–inorganic oxides membrane doped with heteropolyacids for high temperature operation of proton exchange membrane fuel cell. *Solid State Ionics*, *177*(7), 779-785.

Shan, C. C., Tsai, D. S., Huang, Y. S., Jian, S. H., & Cheng, C. L. (2007). Pt− Ir− IrO_2NT Thin-Wall Electrocatalysts Derived from IrO_2 Nanotubes and Their Catalytic Activities in Methanol Oxidation. *Chemistry of Materials*, *19*(3), 424-431.

Shu, C., Yang, X., Chen, Y., Fang, Y., Zhou, Y., & Liu, Y. (2016). Nano-Fe_3O_4 grown on porous carbon and its effect on the oxygen reduction reaction for DMFCs with a polymer fiber membrane. *RSC Advances*, *6*(43), 37012-37017.

Shukla, A. K., & Raman, R. K. (2003). Methanol-resistant oxygen-reduction catalysts for direct methanol fuel cells. *Annual Review of Materials Research, 33*(1), 155-168.

Singha, S., & Jana, T. (2014). Structure and properties of polybenzimidazole/silica nanocomposite electrolyte membrane: influence of organic/inorganic interface. *ACS Applied Materials & Interfaces*, *6*(23), 21286-21296.

Sridhar, P., Perumal, R., Rajalakshmi, N., Raja, M., & Dhathathreyan, K. S. (2001). Humidification studies on polymer electrolyte membrane fuel cell. *Journal of Power Sources*, *101*(1), 72-78.

Staiti, P., Arico, A. S., Baglio, V., Lufrano, F., Passalacqua, E., & Antonucci, V. (2001). Hybrid Nafion–silica membranes doped with heteropolyacids for application in direct methanol fuel cells. *Solid State Ionics*, *145*(1), 101-107.

Surampudi, S., Narayanan, S. R., Vamos, E., Frank, H., Halpert, G., LaConti, A., et al. (1994). Advances in direct oxidation methanol fuel cells. *Journal of Power Sources*, *47*(3), 377-385.

Tamaki, T., Yamauchi, A., Ito, T., Ohashi, H., & Yamaguchi, T. (2011). The effect of methanol crossover on the cathode overpotential of DMFCs. *Fuel Cells*, *11*(3), 394-403.

Tang, H., Wang, S., Pan, M., Jiang, S. P., & Ruan, Y. (2007). Performance of direct methanol fuel cells prepared by hot-pressed MEA and catalyst-coated membrane (CCM). *Electrochimica Acta*, *52*(11), 3714-3718.

Tang, Y., Zhang, J., Song, C., Liu, H., Zhang, J., Wang, H., et al. (2006). Temperature dependent performance and in situ AC impedance of high-temperature PEM fuel cells using the Nafion-112 membrane. *Journal of The Electrochemical Society*, *153*(11), A2036-A2043.

Thiam, H. S., Daud, W. R. W., Kamarudin, S. K., Mohammad, A. B., Kadhum, A. A. H., Loh, K. S., & Majlan, E. H. (2011). Overview on nanostructured membrane in fuel cell applications. International *Journal of Hydrogen Energy*, *36*(4), 3187-3205.

Tokarz, W., Lota, G., Frackowiak, E., Czerwiński, A., & Piela, P. (2013). Fuel cell testing of Pt–Ru catalysts supported on differently prepared and pretreated carbon nanotubes. *Electrochimica Acta*, *98*, 94-103.

User instructions for DMFC electrodes & MEAs prior to installation. (n.d.). Retrieved April 18, 2016, from http://www.jmfuelcells.com/page.aspx.

Vaivars, G., Maxakato, N. W., Mokrani, T., Petrik, L., Klavins, J., Gericke, G., & Linkov, V. (2004). Zirconium phosphate based inorganic direct methanol fuel cell. *Materials Science*, *10*, 162-165.

Veizaga, N. S., Paganin, V. A., Rocha, T. A., Scelza, O. A., de Miguel, S. R., & Gonzalez, E. R. (2014). Development of PtGe and PtIn anodic catalysts supported on carbonaceous materials for DMFC. *International Journal of Hydrogen Energy*, 39(16), 8728-8737.

Wang, H., Xu, C., Cheng, F., Zhang, M., Wang, S., & Jiang, S. P. (2008). Pd/Pt core–shell nanowire arrays as highly effective electrocatalysts for methanol electrooxidation in direct methanol fuel cells. *Electrochemistry Communications*, *10*(10), 1575-1578.

Wang, S., Sun, G., Wang, G., Zhou, Z., Zhao, X., Sun, H., et al. (2005). Improvement of direct methanol fuel cell performance by modifying catalyst coated membrane structure. *Electrochemistry Communications*, *7*(10), 1007-1012.

Wang, W., Wang, H., Key, J., Linkov, V., Ji, S., & Wang, R. (2013). Nanoparticulate TiO_2-promoted PtRu/C catalyst for methanol oxidation. *Ionics*, *19*(3), 529-534.

Wang, Z., Chen, G., Xia, D., & Zhang, L. (2008). Studies on the electrocatalytic properties of PtRu/C-TiO_2 toward the oxidation of methanol. *Journal of Alloys and Compounds*, *450*(1), 148-151.

Wannek, C., Glüsen, A., & Stolten, D. (2010). Materials, manufacturing technology and costs of fuel cell membranes. *Desalination*, *250*(3), 1038-1041.

Wei, Z., Wang, S., Yi, B., Liu, J., Chen, L., Zhou, W., et al. (2002). Influence of electrode structure on the performance of a direct methanol fuel cell. *Journal of Power Sources*, *106*(1), 364-369.

Wu, J., Yuan, X. Z., Martin, J. J., Wang, H., Zhang, J., Shen, J., et al. (2008). A review of PEM fuel cell durability: Degradation mechanisms and mitigation strategies. *Journal of Power Sources, 184*(1), 104-119.

Xie, Z., Navessin, T., Shi, Z., Chow, R., & Holdcroft, S. (2006). Gas diffusion electrodes containing ZHP/Nafion for PEMFC operation at 120 C. *Journal of Electroanalytical Chemistry, 596*(1), 38-46.

Xiong, B., Zhou, Y., Zhao, Y., Wang, J., Chen, X., O'Hayre, R., & Shao, Z. (2013). The use of nitrogen-doped graphene supporting Pt nanoparticles as a catalyst for methanol electrocatalytic oxidation. *Carbon, 52*, 181-192.

Xu, J., Ni, H., Wang, S., Wang, Z., & Zhang, H. (2015). Direct polymerization of a novel sulfonated poly (arylene ether ketone sulfone)/sulfonated poly (vinylalcohol) crosslinked membrane for direct methanol fuel cell applications. *Journal of Membrane Science, 492,* 505-517.

Xu, J. B., Zhao, T. S., Yang, W. W., & Shen, S. Y. (2010). Effect of surface composition of Pt-Au alloy cathode catalyst on the performance of direct methanol fuel cells. *International Journal of Hydrogen Energy, 35*(16), 8699-8706.

Yang, B., & Manthiram, A. (2003). Sulfonated poly (ether ether ketone) membranes for direct methanol fuel cells. *Electrochemical and Solid-State Letters, 6*(11), A229-A231.

Yang, C., Costamagna, P., Srinivasan, S., Benziger, J., & Bocarsly, A. B. (2001). Approaches and technical challenges to high temperature operation of proton exchange membrane fuel cells. *Journal of Power Sources, 103*(1), 1-9.

Yang, C., Srinivasan, S., Arico, A. S., Cretı, P., Baglio, V., & Antonucci, V. (2001). Composite Nafion/zirconium phosphate membranes for direct methanol fuel cell operation at high temperature. *Electrochemical and Solid-State Letters, 4*(4), A31-A34.

Ye, G., Hayden, C. A., & Goward, G. R. (2007). Proton dynamics of Nafion and Nafion/SiO_2 composites by solid state NMR and pulse field gradient NMR. *Macromolecules, 40*(5), 1529-1537.

Yu, T. L., Lin, H. L., Shen, K. S., Huang, L. N., Chang, Y. C., Jung, G. B., & Huang, J. C. (2004). Nafion/PTFE composite membranes for fuel cell applications. *Journal of Polymer Research, 11*(3), 217-224.

Yuan, T., Pu, L., Huang, Q., Zhang, H., Li, X., & Yang, H. (2014). An effective methanol-blocking membrane modified with graphene oxide nanosheets for passive direct methanol fuel cells. *Electrochimica Acta, 117,* 393-397.

Zhang, J., Xie, Z., Zhang, J., Tang, Y., Song, C., Navessin, T., et al. (2006). High temperature PEM fuel cells. *Journal of Power Sources*, *160*(2), 872-891.

Zhang, Y., Zhang, H., Ma, Y., Cheng, J., Zhong, H., Song, S., & Ma, H. (2010). A novel bifunctional electrocatalyst for unitized regenerative fuel cell. *Journal of Power Sources*, *195*(1), 142-145.

Zhang, Z., Désilets, F., Felice, V., Mecheri, B., Licoccia, S., & Tavares, A. C. (2011). On the proton conductivity of Nafion–Faujasite composite membranes for low temperature direct methanol fuel cells. *Journal of Power Sources*, *196*(22), 9176-9187.

Zhao, T. S., & Xu, C. (2009). Fuel cells–Direct alcohol fuel cells| direct methanol fuel cells: Overview performance and operational conditions. *Encycl Electrochem Power Sour*, 381-9.

Zhao, X., Fan, X., Wang, S., Yang, S., Yi, B., Xin, Q., & Sun, G. (2005). Determination of ionic resistance and optimal composition in the anodic catalyst layers of DMFC using AC impedance. *International Journal of Hydrogen Energy*, *30*(9), 1003-1010.